ISBN-13: 9781502454546
ISBN-10: 1502454548

Biophysics and Computations of the Cerebellar Purkinje Neuron

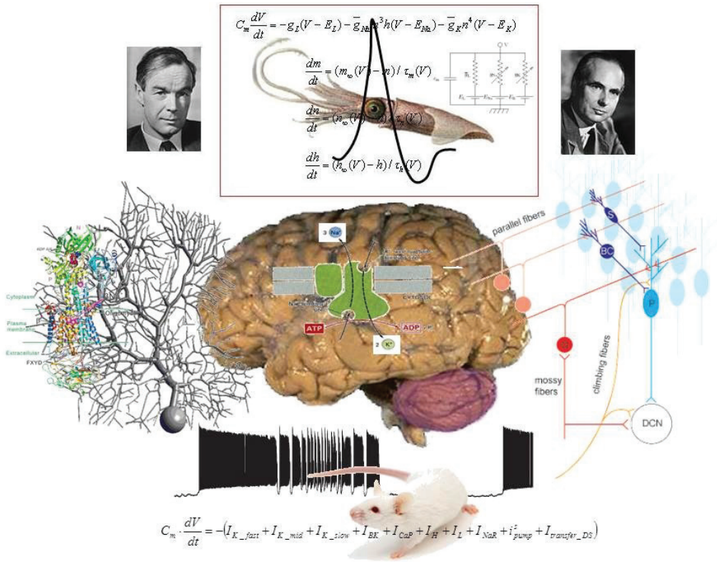

Dr. Michael D. Forrest BA (Cantab), MA (Cantab), MSc, Ph.D.

Contents

List of figures

List of tables

Abbreviations

I_{Na-p}	Persistent Na^+ current
I_{Na-f}	Fast Na^+ current
I_{Na-r}	Resurgent Na^+ current
I_h	Hyperpolarisation activated cation current
P/Q	P-type voltage-gated Ca^{2+} current
H-H	Hodgkin-Huxley
$[Na^+]_i$	Intracellular Na^+ concentration
$[K^+]_o$	Extracellular K^+ concentration
Na^+/K^+ pump	Sodium-potassium pump
K_{Na}	Sodium affinity constant of the sodium-potassium pump
K_K	Potassium affinity constant of the sodium-potassium pump
TTX	Tetrodotoxin
DCN	Deep cerebellar nuclei

The Author

Dr. Forrest holds a BA and MA in Natural Sciences (Part II: Biochemistry and Molecular Biology) from Cambridge University, an MSc in Neuroscience from Edinburgh Univesity and a Ph.D. in Computer Science from Warwick University.

This book is a replication of Dr. Forrest's Ph.D. thesis, submitted in August 2008: Forrest MD (2008) The Biophysics of Purkinje Computation. Ph.D. Thesis. University of Warwick: UK.

Innovatively this book suggests that the sodium-potassium pump may not simply be a homeostatic, "housekeeping" molecule for ionic gradients; but might be a computation element in the cerebellum and the brain. This was a bold idea in 2008, when Dr. Forrest submitted his PhD, and remains so today in 2014. It runs contrary to conventional, entrenched viewpoints on brain function. The *in vitro* Purkinje cell recordings in Chapters 2 & 5 were performed by Dr. Mark Wall at the School of Life Sciences, University of Warwick, UK. This book will please those curious about brain computation, especially the computational capability of single neurons, and Ph.D. candidates that want to study the template and standard of a successful thesis. This book presents both computational and experimental approaches to neuroscience research.

Introduction

The quantitative tact afforded by computational neuroscience is most distinguished from classical neurobiology by an explicit investigative focus on how the nervous system computes (Feng, 2003). In this study, we employ this approach to advance our understanding of the cerebellum.

The hindbrain's cerebellum region is a beautifully two-dimensional and convolved structure with close to 80% of the neurons in the nervous system (Kandel et al, 2000). It is primarily a motor/sensory integration system, pivotal to motor coordination and motor learning, but it is also implicated in "higher" cognition e.g. the processing of language and music. We hope that an understanding of the cerebellum's computations can prime clinical solutions to its pathologies and improve the quality of life for millions of patients worldwide.

In contrast to the complexity of other brain regions, the cerebellum has a single repeating connectivity motif (Ito, 1984). This motif consists of parallel, climbing, basket and stellate inputs feeding into a central Purkinje cell, which transforms these inputs into an output. The relative simplicity of the cerebellar motif makes it a good focal point for trying to understand how a brain circuit actually computes. Ultimately its computation collapses to one question, how does the Purkinje cell compute? In particular, how does its morphology and conductances transform/encode its inputs into an output?

Summary

Although others have reported and characterised different patterns of Purkinje firing (Womack and Khodakhah, 2002, 2003, 2004; McKay and Turner, 2005) this thesis is the first study that moves beyond their description and investigates the actual basis of their generation. Purkinje cells can intrinsically fire action potentials in a repeating trimodal or bimodal pattern. The trimodal pattern consists of tonic spiking, bursting and quiescence. The bimodal pattern consists of tonic spiking and quiescence. How these firing patterns are generated, and what ascertains which firing pattern is selected, has not been determined to date. We have constructed a detailed biophysical Purkinje cell model that can replicate these patterns and which shows that Na^+/K^+ pump activity sets the model's operating mode. We propose that Na^+/K^+ pump modulation switches the Purkinje cell between different firing modes in a physiological setting and so innovatively hypothesise the Na^+/K^+ pump to be a computational element in Purkinje information coding. We present supporting *in vitro* Purkinje cell recordings in the presence of ouabain, which irreversibly blocks the Na^+/K^+ pump.

Climbing fiber (CF) input has been shown experimentally to *toggle* a Purkinje cell between an up (firing) and down (quiescent) state and set the *gain* of its response to parallel fiber (PF) input (Mckay et al., 2007). Our Purkinje cell model captures these *toggle* and *gain* computations with a novel intracellular calcium computation that we hypothesise to be applicable in real Purkinje cells. So notably, our Purkinje cell model can compute, and importantly, relates biophysics to biological information processing.

Our Purkinje cell model is biophysically detailed and as a result is very computationally intensive. This means that, whilst it is appropriate for studying properties of the individual Purkinje cell (e.g. relating channel densities to firing properties), it is unsuitable for incorporation into network simulations. We have overcome this by deploying mathematical transforms to produce a simpler, surrogate version of our model that has the same electrical properties, but a lower computational overhead. Our hope is that this model, of intermediate biological fidelity and medium computational complexity, will be used in the future to bridge cellular and network studies and identify how distinctive Purkinje behaviours are important to network and system function.

Chapter 1
Background

The highest activities of consciousness have their origins in physical occurrences of the brain, just as the loveliest melodies are not too sublime to be expressed by notes.
W. Somerset Maugham

1.1 The cerebellum

1.1.1 History

Around the beginning of the 19th century, Gall and Spurzheim noticed that the size of the cerebellum is large in bulls and so concluded that it must have a sexual function (Thach, 1996; Glickstein, 1997; Barlow, 2002). This is poor rationale of course and is now considered incorrect. Thomas Willis was much closer to the mark when, in the 17th century, he proposed that the cerebellum presides over the body's movements. Indeed, lesion studies in the 19th century by Rolando, Fluorens and Luciani, clearly indicated that the cerebellum was involved in the control of posture and the coordination of movements. Later studies (early 20th century) of human cerebellar ablation by Babinsky and by Holmes confirmed these observations (Holmes, 1939; Thach, 1996; Glickstein, 1997; Barlow, 2002).

The notion that the cerebellum might be more than just a motor organ goes back to the studies of Sherrington (1857-1952), Jelgersma (1859-1942) and Lewandowsky (1880-1953) (Walker et al., 2000). Although largely forgotten during the latter half of the 20th century, this hypothesis has been resurrected in more contemporary times with the deployment of new imaging technologies. For example, recent fMRI studies suggest that that the cerebellum is involved in the discrimination of sensory data (Bower, 1997; Blakemore et al., 1998; Devor, 2000). Imaging studies have also shown a marked increase of cerebellar activity during various cognitive tasks and, coupled with the fact that cerebellar patients often suffer various cognitive deficits, there is growing evidence that the cerebellum is involved in some higher brain functions (Thach, 1996; Schmahmann and Sherman, 1998).

1.1.2 Anatomy

(Eccles et al., 1967; Palay and Chan-Palay, 1982; Nauta and Feirtag, 1986; Kandel et al., 2000)

Figure 1.1 shows the position of the cerebellum in the brain. In humans the cerebellum makes up approximately 10% of the brain volume and contains the majority of its neurons.

The cerebellum has an outer surface of grey matter, called the cerebellar cortex, and underneath it is the white matter (*figure 1.2*). The cerebellar cortex contains 5 different cell types (Purkinje, Golgi, granule, stellate, basket) and the white matter contains all their afferent/efferent fibers and the deep cerebellar nuclei (DCN). The 5 cell types of the cerebellar cortex are arranged in 3 different layers (*figure 1.3*). The number of granule cells in the granular layer is estimated to be in the order of 10^{11}, more than the total number of neurons in the whole cerebral cortex.

The cerebellum is a very special part of the brain because, in contrast to the complexity of other brain regions, its neurons are organised in an extremely regular and repetitive way. Its architecture is effectively just repeats of an anatomically well defined connectivity motif. This motif consists of parallel, climbing, basket and stellate inputs feeding into a central Purkinje cell, which integrates them into an output that is then relayed to the deep cerebellar nuclei (DCN) (*figure 1.4*). The DCN projects out of the cerebellum to other brain regions.

Parallel and climbing fiber inputs are excitatory (glutamatergic); basket and stellate inputs are inhibitory (GABAergic). The Purkinje cell therefore has two excitatory inputs and two inhibitory inputs. The Purkinje cell output is inhibitory to the DCN.

In striking contrast, each Purkinje cell is innervated by over 10^5 parallel fibers but only a *single* climbing fiber axon. Although this single climbing fiber axon branches to make hundreds/thousands of synaptic contacts upon this single Purkinje cell.

The regularity of the cerebellar structure contrasts with other brain regions, for instance the cerebral cortex, where the circuit structure is still unclear and, indeed, it is uncertain if it even has a canonical circuit (Nauta & Feirtag, 1986). The cerebellum's regularity, which founds its crystalline histology, makes it perhaps the best point of study for deciphering basic neural principles.

1.1.3 Structure to function

The beautiful, crystalline structure of the cerebellum is the basis for a number of theories of its function. For example, Braitenberg and Atwood (1958) weaved the structure into their theory of the cerebellar cortex as a *timing device*, and Eccles et al. (1967) used it to describe the cerebellum as a computer-like structure and proposed the *beam theory* of parallel fibre effects. Later on, the seminal Marr (1969) and Albus (1971) theory of motor learning was founded upon the cerebellum's crystalline form. So influential is the Marr-Albus theory that subsequent concepts of motor learning have tended to be simply developments of it (for example, Gilbert, 1974, 1975; Ito, 1984).

However, these theories have considered the cerebellum's component neurons to be linear summing devices (integrate and fire), ignoring their complexity, nonlinearity and computations. This is perhaps too abstractive because there is evidence that the richness of biophysical properties on the single neuron scale can supply mechanisms that serve as building blocks for network dynamics (Getting, 1989).

1.1.4 Synaptic plasticity in the cerebellum

Activity dependent synaptic modifications represent a mechanism for storing information in the brain (Hebb, 1949). In the Marr-Albus theory of motor learning, information is stored in the long-term depression (LTD) of synapses between parallel fibers (PFs) and Purkinje cells (Marr, 1969; Albus, 1971). And indeed, this has now been experimentally shown: PF LTD can be induced by repeated coincident PF and climbing fiber (CF) input to the Purkinje cell (Ito et al., 1982; Ito et al., 2001). Thus, a PF activity pattern that is paired repeatedly with CF input will lead to LTD of the PF synapses activated by the pattern. This results in reduced firing in the Purkinje cell when the PF activity pattern is presented again and thus leads to reduced inhibitory input to neurons in the deep cerebellar nuclei (DCN) and increased output from the cerebellum (Ito, 1984; Ito, 1989; Ito et al., 2001).

1.2 The Purkinje cell

A striking feature of the cerebellar cortex is that the Purkinje neuron is the only cell type with an axon projecting out of the cortex. It follows that all computations taking place in the cerebellar cortex must be represented in the firing pattern of the Purkinje neurons - Purkinje neurons are the final integrator of cerebellar cortical activity. Thus, if we are to fathom the cerebellum, it is absolutely imperative that we acquire an understanding of the Purkinje cell. We must understand how the Purkinje cell computes - how its morphology and conductances transform/encode its inputs into an output. We hope to further the understanding of this process with the research we present in this thesis.

1.2.1 Purkinje cell morphology

The cerebellar Purkinje cell is large and complex with an intricately elaborate, isoplanar, spine studded dendritic arbour. It has the most branched dendritic tree in the central nervous system and the fact that its morphological characteristics are highly conserved across species suggests them to have strong functional significance (Vetter et al., 2001).

The Purkinje cell soma can fire sodium spikes and its dendrites, by contrast, can fire calcium spikes (Llinas and Sugimori, 1980a, 1980b).

1.2.2 Purkinje cell activity *in vivo*

Purkinje cells can spontaneously fire single action potentials (**simple spikes)** in the absence of synaptic innervation but this firing can also be driven/modulated by parallel fiber input. A parallel fiber input is weak; approximately 50 parallel fibers are required to generate a simple spike in a Purkinje cell (Barbour, 1993). By contrast, the single climbing fiber input is very strong and it can induce a burst of several spikes in a row (a **complex spike**). *In vivo*, inferior olivary neurons (the origin of climbing fibers) are spontaneously active, at a frequency of 1-2 Hz, and so Purkinje cells fire complex spikes

at a frequency of 1-2 Hz. These complex spikes punctuate the Purkinje cell firing of simple spikes, which Purkinje cells can perform intrinsically and/or with drive/modulation from parallel fibers (which originate from spontaneously active granule cells).

It has been shown *in vivo* shown that climbing fiber activation of the Purkinje cell (which induces a complex spike) can shift its activity from a quiescent "down" state to a spontaneously active "up" state (in which it fires simple spikes), and vice-versa, serving as a type of toggle switch (Lowenstein et al., 2005) (*Figure 1.5*). These findings have been challenged by a study suggesting that such toggling by climbing fiber inputs occurs predominantly in anaesthetized animals, and that Purkinje cells in awake behaving animals, in general, operate almost continuously in the up state (Schonewille et al., 2006). However, this challenge has been aggressively refuted (Loewenstein et al., 2006).

1.2.3 Purkinje cell activity *in vitro*

Given the slicing plane of parasagittal cerebellar slices, climbing fiber and parallel fiber inputs tend to be cut and so very little excitatory input remains. By contrast, much of the inhibitory connectivity to the Purkinje cells (stellate and basket connections) is maintained (Daniel Press and Mark Wall, personal communication).

Purkinje cells can fire spontaneously and so they can be active within parasagittal cerebellar slices, despite their lack of excitatory input in this context. Indeed, a number of spontaneous Purkinje cell firing patterns have been observed *in vitro*. Some report a repeating trimodal pattern that consists of tonic spiking, bursting and quiescence (Womack and Khodakhah, 2002, 2003, 2004; McKay and Turner, 2005) (*figure 1.6*). The repeat length of the trimodal pattern is fixed for a single Purkinje cell but can vary among different Purkinje cells, in a range from 20 seconds to 20 minutes (Womack and Khodakhah, 2002). This trimodal firing pattern has been observed in slices with no pharmacological application, but it is more commonly observed after the inhibitory connections (GABA) are blocked (Womack and Khodakhah, 2002). As far as we know, the trimodal firing pattern has not been observed *in vivo*. For the *in vitro* Purkinje cell, others have reported a repeating bimodal pattern of tonic firing and quiescence (McKay et al., 2005), continuous tonic firing (Hausser and Clark, 1997) or continuous quiescence (Llinas and Sugimori, 1980a). Although, in our interpretation, the latter two might not be operating modes in their own right, but rather components of the trimodal or bimodal patterns and the recording period was not of sufficient duration to show this.

In summary, previous work has reported and characterised different patterns of Purkinje activity (*in vivo* and *in vitro*). This thesis is the first study that moves beyond description and tries to ascertain the mechanisms of Purkinje activity generation. To do this we employ a modelling methodology.

1.3 Computational modelling of neurons

1.3.1 The membrane potential equation

At the heart of many neuron models lies the membrane potential equation, which is derived by treating the neuron as an electrical circuit comprising:

1) *A resistor* - The resistance of the membrane to current flow (R)
2) *A capacitor* – The capacitance of the membrane (C)
3) *A current source* – The current source can be:
   a) Current through channels in the membrane. I^{ionic}
   b) Current through channels located at a synapse (which have their opening and closing controlled by another neuron) I^{syn}
   c) An external current injected by the experimenter I^{ext}

These components are in parallel. From Kirchoff's first law (conservation of electric charge) we obtain the fundamental equation of neural membranes:

$$C\frac{dV}{dt} = -I^{ionic} - I^{syn} - I^{ext} \qquad (1.1)$$

Where V is the membrane potential and t is time.

Hodgkin and Huxley (1952) described how I^{ionic} can be ruled by voltage, detailing how neurons can contain voltage-dependent currents that are opened and closed by the membrane potential. And just as Hodgkin and Huxley have provided a model for I^{ionic}, there are also models for I^{syn}.

A neuron that contains no voltage-dependent components can have its spatiotemporal distribution of membrane potential described by linear cable theory. This theory can be coupled with the Hodgkin-Huxley model to yield nonlinear cable theory.

1.3.2 The Hodgkin-Huxley (H-H) model

Hodgkin and Huxley (1952) revolutionised electrophysiology with their quantitative characterisation of how ionic currents are driven by voltage, and how this dependence can account for action potential generation. They ingeniously deployed the voltage clamp technique (Cole, 1939) to dissect the excitability of the squid giant axon. Two voltage dependent currents, depolarising sodium and repolarising potassium, are the basis for squid giant axon action potentials.

The starting point of the Hodgkin-Huxley model is that the membrane current (I_m) is the sum of the ionic (I_{ionic}) and capacitive $(C_m(dV/dt))$ currents:

$$C_m\frac{dV}{dt} = -I_{Ionic} \qquad (1.2)$$

Where C_m is the membrane capacitance, V is the membrane potential and t is time.

The ionic current in turn can be subdivided into the sodium current (I_{Na}), the potassium current (I_K) and the leak current (I_{leak}). The latter is due to chloride and other ions.

$$I_{ionic} = I_{Na} + I_K + I_{leak} \tag{1.3}$$

Ohm's law linearly relates these currents to the driving potential. For example, for the potassium current:

$$I_K = g_K (V - E_K) \tag{1.4}$$

g_K is related to the potassium permeability of the membrane and has units of conductance per unit area. E_K is the equilibrium potential for potassium. The equilibrium potential (reversal potential) of an ion across a membrane follows the Nernst formulation. For example, for potassium:

$$E_K = \frac{RT}{zF} \ln \frac{[K]_O}{[K]_I} \tag{1.5}$$

Where R is the gas constant, T is the absolute temperature, F is the Faraday constant, z is the valence of potassium (1), $[K]_O$ and $[K]_I$ are the potassium concentrations outside and inside the cell respectively.

The information embodied in the above equations can be represented as a membrane circuit diagram (*Figure 1.7*) and can be summarised in the H-H membrane equation, which describes a capacitance and three ionic currents in an isopotential patch of membrane:

$$I_m = C_m \frac{dV}{dt} + g_L (V - E_L) + g_{Na} (V - E_{Na}) + g_K (V - E_K) \tag{1.6}$$

The potassium and sodium conductances (g_K and g_{Na}) are voltage-dependent:

$$g_K = \bar{g}_K n^4 \tag{1.7}$$

$$g_{Na} = \bar{g}_{Na} m^3 h \tag{1.8}$$

Where $\bar{g}_K$ and $\bar{g}_{Na}$ are constants (with dimensions of conductance per unit area of membrane) and *n*, *m*, *h* are dimensionless variables that obey first order kinetics, with voltage-dependent forward (α) and backward (β) rate constants. Hodgkin and Huxley estimated these by fitting empirical functions of voltage to the experimental data. Hodgkin and Huxley's α and β functions for the *n*, *m* and *h* variables are displayed in Box 1.

A first order kinetic scheme is described by a corresponding first order differential equation. For example, for the *n* variable:

$$\frac{dn}{dt} = \alpha_n (V)(1 - n) - \beta_n (V) n \tag{1.9}$$

An alternative to using the rate constants, α_n and β_n, is to use the derived voltage dependent time constant τ_n and steady state value n_∞

$$\tau_n = \frac{1}{\alpha_n + \beta_n} \tag{1.10}$$

$$n_\infty = \frac{\alpha_n}{\alpha_n + \beta_n} \tag{1.11}$$

With these new definitions, we can rewrite equation 1.9:

$$\frac{dn}{dt} = \frac{n_\infty (V) - n}{\tau_n (V)} \tag{1.12}$$

The solution of this equation predicts that when the membrane potential is stepped to a new value, and held there, n relaxes exponentially, at a rate τ_n, to its new value n_∞, where n_0 is the value of n at t = 0.

$$n(t) = n_\infty - (n_\infty - n_0) \exp(-\frac{t}{\tau_m}) \tag{1.13}$$

To summarize, the membrane HH model, for the squid giant axon:

$$C_m \frac{dV}{dt} = -g_L (V - E_L) - \bar{g}_{Na} m^3 h (V - E_{Na}) - \bar{g}_K n^4 (V - E_K) \tag{1.14}$$

$$\frac{dm}{dt} = (m_\infty (V) - m) / \tau_m (V) \tag{1.15}$$

$$\frac{dn}{dt} = (n_\infty (V) - n) / \tau_n (V) \tag{1.16}$$

$$\frac{dh}{dt} = (h_\infty (V) - h) / \tau_h (V) \tag{1.17}$$

This four dimensional system of differential equations constitutes the H-H model for a small membrane patch, where spatial differential in voltage along the axon length is not significant. This model reproduces the stereotyped sequence of membrane events that give rise to the initiation and propagation of all-or-none action potentials.

n	$\alpha_n = \frac{-0.01(V - V_r + 10)}{\exp[-(V - V_r + 10)/10] - 1}$	$\beta_n = 0.125\exp[-(V - V_r)/80]$
m	$\alpha_m = \frac{-0.1(V - V_r - 25)}{\exp[-(V - V_r - 25)/4] - 1}$	$\beta_m = 4\exp[-\{V - V_r)/18]$
h	$\alpha_h = 0.007\exp[-(V - V_r)/20]$	$\beta_h = \frac{1}{1 + \exp[-(V - V_r + 30)/10]}$

Box 1: Rate constants estimated by Hodgkin-Huxley for the squid giant axon at 6°C. V and V_r represent the membrane potential and resting membrane potential respectively, in mV, as dimensionless quantities.

1.3.3 The Hodgkin-Huxley model is a generic paradigm

The Hodgkin-Huxley model describes the electro-activity of the squid giant axon, which has just two voltage-dependent conductances (sodium and potassium). Other neurons can have other voltage-dependent sodium and potassium conductances (differing in their voltage and time dependence) and can have conductances for other ions e.g. calcium. In fact, other neurons can be much more complex than the squid giant axon, with dozens of different voltage-dependent conductances. However, in remarkable testimony to the power of the Hodgkin-Huxley approach, it can accurately describe the majority of these conductances.

Some conductances have been found that are not gated by voltage, but by the intracellular calcium concentration. And the Hodgkin-Huxley method can describe these with α and β terms that are empirical functions of the intracellular calcium concentration as opposed to voltage.

1.3.4 Markov models

An alternative to Hodgkin-Huxley descriptions are Markov models of currents.

Voltage gated currents flow through voltage-gated ion channels, which are transmembrane protein complexes containing a pore permeable to one or more ions, gated in an all-or-none fashion, according to the membrane potential (Hille, 1992; Kandel et al, 2000; Alberts et al, 1994; Koch 1999; Johnston and Wu, 1995). A voltage-gated ion channel, like other proteins, can exist in an infinite number of conformations, only a subset of which are stable. During channel opening, the S4 segments of the voltage-gated channel move and induce wider conformational changes that result in pore opening (Keynes and Elinder, 1999; Bezanilla 2000; Jiang et al., 2003). Probabilistic Markov models capture the conformations moved through in a finite number of model states (Patlak, 1991; Vandenberg and Bezanilla, 1991; Hille, 1992; Destexhe and Huguenard,

2000; Irvine et al, 1999). They assume that the transition probability between states depends only on the present state. Consider the state diagram:

$$S_1 \Leftrightarrow S_2 \Leftrightarrow S_n \tag{1.18}$$

Where $S_1 ... S_n$ represent distinct conformational states of the ion channel. Defining $P(S_i, t)$ as the probability of being in state S_i at time t, and $P(S_i \to S_j)$, as the transition probability from state S_i to state S_j, allows a master equation depicting the time evolution of $P(S_i, t)$ to be built

$$S_i \underset{P(S_j \to S_i)}{\overset{P(S_i \to S_j)}{\rightleftarrows}} S_j \tag{1.19}$$

$$\frac{dP(S_i,t)}{dt} = \sum_{j=1}^{n} P(S_j,t)P(S_j \to S_i) - \sum_{j=1}^{n} P(S_i,t)P(S_i \to S_j) \tag{1.20}$$

On the left is a 'source' term detailing all transitions entering state S_i. On the right is a 'sink' term detailing all transitions leaving state S_i. The time evolution depends only on the current state and is defined completely by the transition probabilities.

In the giga seal experimental preparation (Sakmann and Neher, 1995), single voltage-gated channels can be observed opening and closing stochastically, with their probability of opening being dictated by the membrane potential (Johnston and Wu, 1995; Koch 1999). Probabilistic Markov models are adept at reproducing such behaviour (Meunier and Segev, 2002). Markov models tend to be more accurate and powerful than Hodgkin-Huxley models, although it is much more difficult to derive their parameters from experimental data (Destexhe and Huguenard, 2000). Also, given their added complexity, they tend to be more computationally intensive.

In the modelling research of this thesis, our general approach is to model membrane currents with Hodgkin-Huxley descriptions (*as detailed in Appendices A1 & A2*). However, in one case – with the Purkinje cell's resurgent sodium current – we employ a Markov description to capture its distinctive "resurgent" character (reactivation during repolarisation from positive potentials; Khaliq et al., 2003) (*Appendix A2*).

1.3.5 Models of synaptic current

With a synapse, transmitter released from presynaptic terminals binds to postsynaptic receptors and temporarily opens a conductance for one or more ions. The synaptic current (i) flowing through this conductance (g) is given by:

$$i = g(V - E) \tag{1.21}$$

Where V is the voltage, E is the reversal potential of the synaptic current. The value of E depends on what ions the conductance passes. For instance, if it passes

only/predominantly potassium ions then E will be E_K (the reversal potential for potassium) at -80 mV. In this case the synapse is inhibitory because it opens a hyperpolarising current.

The change in conductance (g) can be represented mathematically by an alpha function (Rall, 1967).

$$g = g_{\max}\left(\frac{t - t_{onset}}{\tau}\right)\exp\left(-\frac{t - t_{onset}}{\tau}\right) \quad \text{For } t > t_{onset} \tag{1.22}$$

Where $g_{\max}$ is the maximal conductance, t is time, t_{onset} is the time that the change in postsynaptic conductance begins and τ is the time constant of the synapse (the time taken for g to change to $g_{\max}$).

Alternatively, the change in conductance (g) can be represented mathematically by a double exponential function:

$$g = kg_{\max}\left(\exp\left(-\frac{t - t_{onset}}{\tau_D}\right) - \exp\left(-\frac{t - t_{onset}}{\tau_R}\right)\right) \quad \text{For } t > t_{onset} \tag{1.23}$$

Where g is the conductance, k is a normalisation coefficient, $g_{\max}$ is the maximal conductance, t is time, t_{onset} is the time that the change in postsynaptic conductance begins, τ_D is the decay time constant, τ_R is the rise time constant and $\tau_R < \tau_D$.

The alpha and double exponential formalisms can approximate most synaptic currents with a small number of parameters, at low computation and storage requirements (Destexhe et al., 1995). However, the disadvantage of these approaches is that they lack correspondence to the biophysics of synapses. A more fundamental way to model synaptic currents would be based on the kinetic properties of the underlying synaptic ion channels (Destexhe et al., 1995). However, this is of course much more computationally expensive and not a methodology that we, ourselves, have used.

1.3.6 Neuronal cable theory

In 1855, Lord Kelvin theoretically described the attenuation of signals in the submerged, transatlantic telephone cable – cable theory. A nerve fibre is quite similar to an undersea cable – both have a conducting core, covered with an insulating sheath, surrounded by salty water. And as the insulation is not perfect, there will be a finite leakage through the insulation. Cable theory can be, in a modified form, applied to neural processes (Rall, 1989; Segev et al., 1995).

The cable equation, describing the spatiotemporal distribution of membrane potential along a passive neural cylinder is:

$$\lambda^2 \frac{\partial^2 V_m}{\partial x^2} = \tau_m \frac{\partial V_m}{\partial t} + V_m \tag{1.24}$$

Where t is time, x is the distance along the cylinder, V_m is the voltage across the membrane and:

$$\lambda = \sqrt{\frac{R_m}{R_i}} \quad \text{The space constant} \tag{1.25}$$

$$\tau_m = R_m C_m \quad \text{The time constant} \tag{1.26}$$

Where R_i is the specific intracellular resistance, R_m is the specific membrane resistance and C_m is the specific membrane capacitance.

Note that this description only holds if the membrane is passive/linear i.e. if its resistance/conductance is voltage-independent. In addition, this description has other sizable assumptions. Please refer to Rall (1989) and/or Segev et al. (1995) for a discussion of these.

The cable formula is a partial differential equation, first order in time and second order in space. Interestingly, this type of parabolic differential equation is quite similar to the heat and diffusion equations.

Starting in the late 1950s and early 1960s, the linear cable equation was solved by Rall and others to study the dynamics of the membrane potential and synaptic integration in passive, branching dendritic trees (Rall, 1989; Segev et al., 1995). This work considered active, voltage-dependent membrane conductances to be confined to the soma. However, what has subsequently emerged is that most, if not all, dendritic trees contain substantial voltage-dependent, nonlinear components (Koch and Segev, 1998). Despite this, Rall's work is still very important because before we can understand active trees we should probably have an understanding of passive trees. Furthermore, under certain conditions (e.g. for small synaptic inputs), voltage-dependent nonlinearities do not come into play and dendrites act as if they are passive (Koch and Segev, 1998).

When linear cable theory is coupled with formalisms for voltage-dependent nonlinearity (such as the Hodgkin-Huxley model) we have nonlinear cable theory. This is what we use in this work to model the cerebellar Purkinje cell. And we use it within the framework of compartmental modelling.

1.3.7 Compartmental modelling

In compartmental modelling, instead of solving the continuous partial differential cable equation (linear or nonlinear) it is discretized into a system of ordinary differential equations that correspond to small patches of neuronal membrane which are isopotential (Koch and Segev, 1998). These "compartments" are then coupled by sparse matrices. This is discretization in space. There is also discretization in time.

This is a numerical method and a fundamental aim of any numerical method is that its solution should be as close to the exact solution as possible. This requirement places constraints on how sparsely space and time can be discretized in order to arrive at an – approximately – correct solution. Compartments must not be too few and the time step must not be too large.

1.3.8 NEURON

We built our Purkinje cell model in the NEURON simulation environment, which is a suite specifically designed for the modelling of individual neurons and networks of neurons (Hines and Carnevale, 1997). NEURON programming is done with hoc, an interpreted language with C-like syntax, and with NMODL, a high-level programming language for expressing kinetic schemes and sets of simultaneous algebraic and/or differential equations. NEURON offers several different numerical integration methods and its computational engine achieves high efficiency by employing special algorithms that take advantage of the structure of the equations that describe neuronal properties. We used the NEURON suite, as opposed to the others available (e.g. GENESIS; Wilson et al., 1989; for review of options see De Schutter, 1992) because it is the most active in development (new standard releases appear about twice a year, supplemented by bug fixes as needed) and in use (hundreds of scientific papers have been published using it as a research methodology).

NEURON can import morphology files created in Neurolucida (mbf bioscience), which is a program that can trace a real neuron and assemble a computational representation of its anatomy. NEURON splits morphologies into isopotential compartments. The number of compartments determines the spatial resolution of the model. If the number of compartments is too low, simulation results will be inaccurate. If the number is too high, simulations will take longer than is necessary. The optimal number of compartments is empirical and found by trial and error.

1.4 Previous Purkinje cell models

There are a number of previously published Purkinje cell models. The principal attainments/conclusions of these different models are:

1) The model of De Schutter and Bower (1994a), as with real Purkinje cells, can generate two different types of spiking behaviour. With small current injections, its soma fires Na^+ spikes. With larger current injections, its dendrites fire Ca^{2+} spikes. This model has been seminal and it is the basis of all subsequent models, including our own. And it is still in use today, as De Schutter and Bower (among others) have been publishing papers from 1994 to date exploring this model's emergent properties. In De Schutter and Bower (1994b) they showed that the model could fire somatic Na^+ spikes in response to simulated parallel fiber input and could fire complex spikes in response to simulated climbing fiber input. They showed that asynchronous inhibitory inputs could block dendritic Ca^{2+} spikes and added noise to the Purkinje firing response. In De Schutter and Bower (1994c) they used the model to show that dendritic calcium channels amplify small, synchronous synaptic inputs; that distal inputs get amplified more than proximal ones, resulting in a similar amplitude of the somatic response. Staub et al. (1994) used the

model to show that voltage attenuation from soma to dendrites increased under conditions where membrane conductance is increased by depolarization or by activation of inhibitory inputs, respectively. Jaeger et al. (1997) used the model to show that intrinsic dendritic currents strongly influenced the time course of the dendritic membrane potential and as a consequence, the timing of somatic spikes did not reflect the timing of particular synaptic inputs. De Schutter (1998) used the model to study the interaction between dendritic channels and synaptic background input, showing that they increase the somatic membrane potential fluctuations generated by the background input. Santamaria et al. (2002) used the model to show that background inputs from parallel fibers and molecular layer interneurons can have a substantial effect on the response of Purkinje cells to the ascending segment of granule cell axons. A temporal rank order code uses the temporal order of spikes, disregarding their precise timing, and Steuber and De Schutter (2002) used the model to show that Purkinje cells can implement rank order decoding of temporal parallel fiber input patterns. Solinas et al. (2006) used the model to show that voltage-gated ion channels in the dendrites amplify inhibitory postsynaptic potentials (IPSPs) so that their recorded amplitude and time course at the soma is not as dependent on the synaptic distance from the soma as predicted by passive cable theory. Steuber et al. (2007) used the model to investigate how Purkinje cells may learn to recognise parallel fiber activity patterns.

2) The Purkinje cell model of Miyasho et al. (2001), which is a development of the De Schutter and Bower model (1994a), shows that the D-type K^+ channel and the class-E Ca^{2+} channel regulate the onset of depolarization-induced Ca^{2+} spikes in Purkinje neurons.

3) The Purkinje cell model of Chono et al. (2003), which is a development of the Miyasho et al. model (2001), suggested that the opening of Ca^{2+}-dependent K^+ channels by Ca^{2+} influx through voltage-gated Ca^{2+} channels hyperpolarizes the membrane potential and deactivates these Ca^{2+} channels in a negative feedback manner, resulting in local, weak Ca^{2+} responses in spiny dendrites of Purkinje cells.

None of these models however can reproduce the aforementioned spontaneous firing patterns (trimodal, bimodal). In fact, these models are intrinsically quiescent and cannot fire without external stimulation. The validity of these models must be questioned if they cannot replicate one of the most distinctive, and perhaps most important, electrophysiological features of purkinje cells. They also cannot replicate one of the most interesting behaviours of the Purkinje cell - the aforementioned "toggling" by climbing fiber input, which is a computation thought integral to cerebellar function.

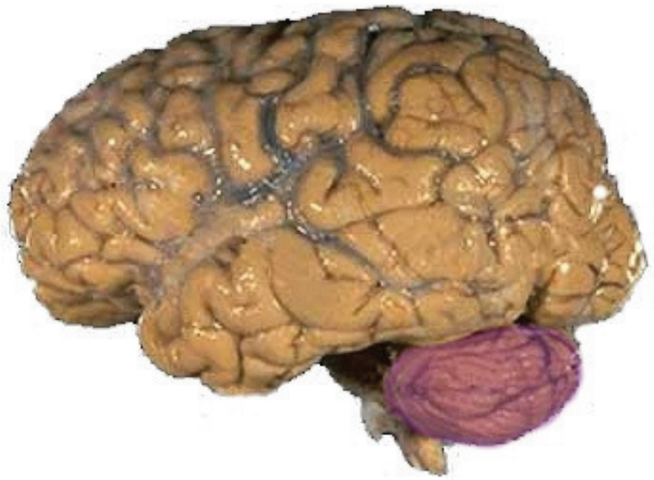

Figure 1.1 A human brain with the cerebellum highlighted in purple.
(*Figure presented with permission, courtesy of the National Institute of Health, NIH)*

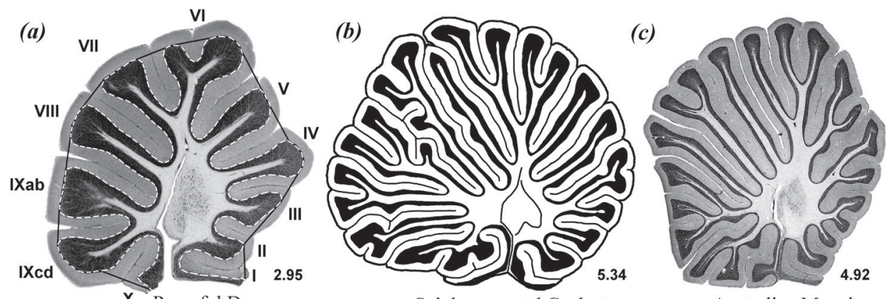

Figure 1.2 Photographs (and a drawing, *b*) of midsagittal sections taken through the cerebellum of 3 species. The outer surface of the cerebellum is a thin sheet of repeatedly folded grey matter, called the cerebellar cortex. Underneath this grey matter lies the white matter. There are a number of deep fissures which divide the cerebellum into ten lobes (labelled I to X in panel *a*). (*Figure presented with permission, courtesy of David Wylie at the University of Alberta*)

(C)

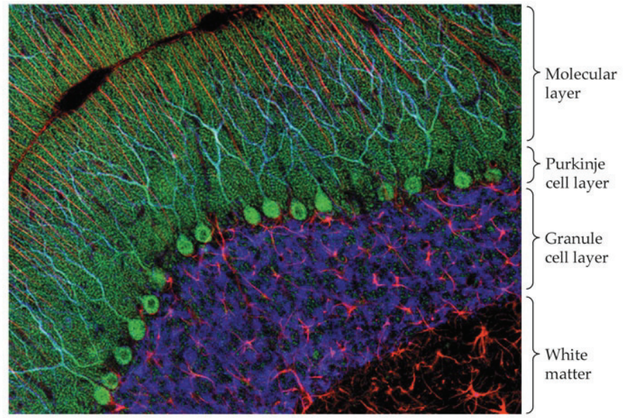

Figure 1.3 The cell bodies of the 5 different cell types of the cerebellar cortex are arranged in 3 different layers:

Molecular layer (stellate cells, basket cells)
Purkinje cell layer (Purkinje cells)
Granule cell layer (Golgi cells, granule cells)

The molecular layer is the outermost; the granule cell layer is the innermost. *(Figure presented with permission, courtesy of Tom Deerinck and Mark Ellisman at the National Center for Microscopy and Imaging Research, NCMIR)*

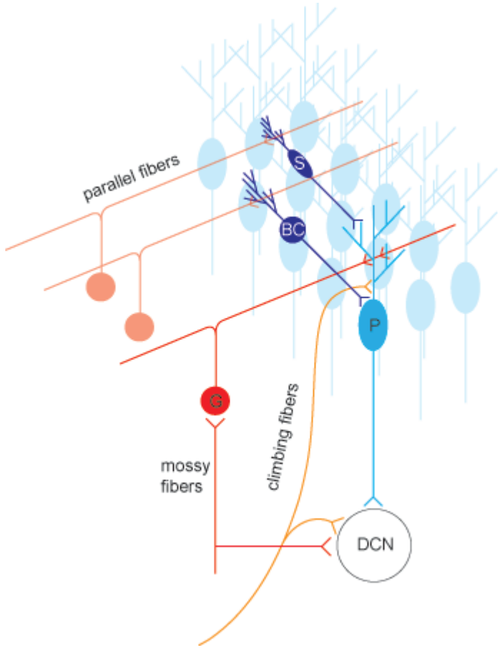

Figure 1.4 The **cerebellar connectivity motif**. The Purkinje cell (**P**) receives inhibitory input from stellate (**S**) and basket cells (**BC**); excitatory input from parallel fibers (*which originate from granule cells*, **G**) and climbing fibers. The Purkinje cell integrates and computes with these inputs to form an output, which it then relays to the deep cerebellar nuclei (**DCN**). This Purkinje cell output is inhibitory to the DCN. *(Figure presented with permission, courtesy of Peer Wulff at the University of Aberdeen)*

Figure 1.4 Further/Supplementary detail to the figure. Climbing fiber inputs originate outside the cerebellum, in the inferior olivary nucleus of the medulla (in the brainstem). Parallel fiber inputs originate from granule cells in the cerebellar cortex. Mossy fibers excite these granule cells. Mossy fibers originate from outside the cerebellum, in many nuclei throughout the brainstem (such as the pontine nucleus).

The figure shows the Purkinje cell to have just four inputs: stellate, basket, parallel, climbing. However, two others have been found: 1) Inhibitory input from recurrent collaterals of the Purkinje cell axons. 2) Excitatory input from the ascending portion of the granule cell axons.

The cerebellar circuit also has golgi cells, not shown in the figure, which are inhibitory interneurons to the granule cells. They receive excitatory input from parallel fibers, mossy fibers, climbing fibers and are inhibited by axon collaterals from Purkinje cells.

The synapses between mossy fibres and granule cells are located in the cerebellar glomeruli, isolated structures that also contain two other types of synapses: excitatory synapses between mossy fibres and Golgi cells, and inhibitory synapses between Golgi cells and granule cells.

Basket cells receive input from parallel fibers, climbing fibers and Purkinje cell axon collaterals. Stellate cells receive input from parallel fibers. The DCN receives input from mossy fibers and climbing fibers.

The DCN consists of the dentate, the fastigial and the interpositus nuclei. Each of the three nuclei sends projections to different brain areas.

In addition, the cerebellar cortex contains glial cells (not shown), which are not conventionally thought of as circuit components but as support elements (Kandel et al., 2000)

Parallel fibers connect to the most terminal dendrites of the Purkinje cell; the climbing fiber connects to the more proximal, main dendrites of the Purkinje cell. Basket cells project to the Purkinje cell bodies and stellate cells to the Purkinje dendrites.

Parallel fibers pass through the cerebellar cortex orthogonal to the plane of Purkinje cell dendrites and a single parallel fiber will make a synaptic contact onto one in every 3-5 Purkinje cells it passes. Parallel fibers tend to run for several mm. They also contact the four other cell types in the cortex – granule, golgi, stellate, basket.

Stellate and basket cells are activated in a feed-forward manner by parallel fibres making direct contact with the Purkinje cell being recorded from (known as “onbeam” inhibition) as well as by parallel fibres adjacent to the Purkinje cell (“offbeam” inhibition (Eccles et al. 1967).

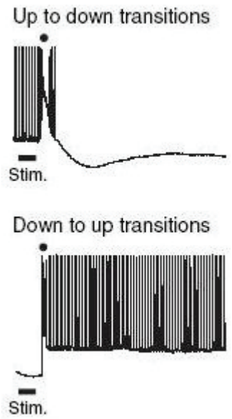

Figure 1.5 (in vivo data from Lowenstein et al., 2005; presented with permission) An air puff (40 ms) to the ipsilateral vibrissae (in the figure, this is "Stim") activates a climbing fiber and evokes a complex spike (marked by the filled circle) in this Purkinje cell.

Sensory evoked complex spikes can toggle the Purkinje cell from up to down (upper panel) or down to up (lower panel)

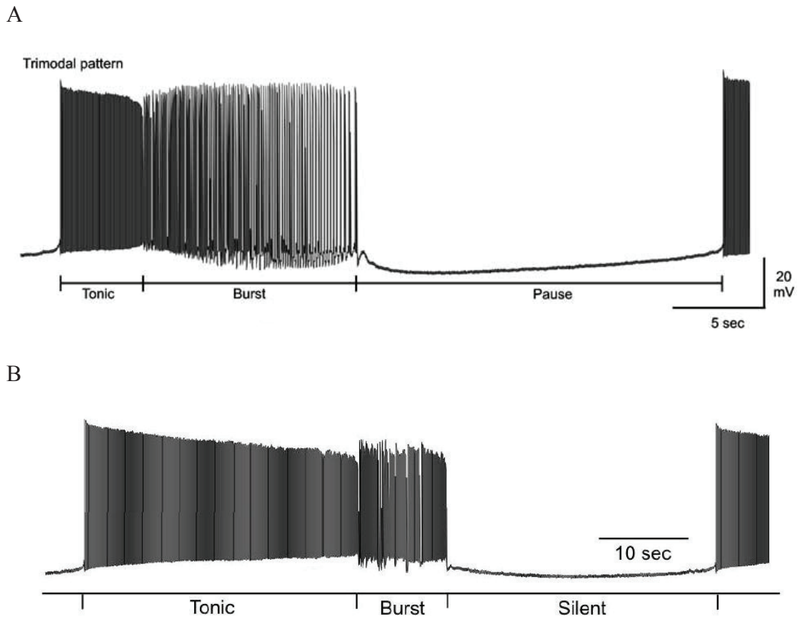

Figure 1.6 The trimodal firing pattern consists of tonic, burst and quiescent modes. Panels *A* and *B* show the trimodal firing pattern for two different Purkinje cells.

(Panel A from McKay and Turner, 2005; Panel B from McKay et al., 2007. Both presented with permission)

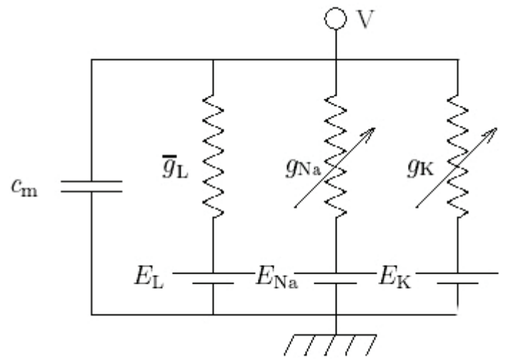

Figure 1.7 (*Figure presented with permission, courtesy of David Sterrat at the University of Edinburgh*) The membrane circuit is modelled with four parallel branches: 1) the capacitance, $C_{m;}$ 2) the leak conductance, $\overline{g}_L$, which chloride ions (mostly) are driven through by $(V - E_L)$; 3) the sodium conductance, g_{Na}, which sodium ions are driven through by $(V - E_{Na})$; 4) the potassium conductance, g_K, which potassium ions are driven through by $(V - E_K)$. The arrows for, g_{Na} and g_K, denote the voltage dependence of these conductances.

Chapter 2

The sodium-potassium pump controls the spontaneous firing of the cerebellar Purkinje neuron

2.1 Introduction

The cerebellum coordinates the execution and adaptation of motor behaviours (Ito, 1984). Cerebellar architecture is based on repeats of a well defined connectivity motif, at the centre of which is the Purkinje cell. Physiologically, the intrinsic firing of Purkinje cells is modulated by synaptic inputs but to understand the cerebellar circuit it is important to first understand the properties of each component in isolation. In this chapter we investigate the isolated cerebellar Purkinje cell.

Purkinje cells can intrinsically fire action potentials in a repeating trimodal or bimodal pattern. The trimodal pattern consists of tonic spiking, bursting and quiescence (Womack and Khodakhah, 2002, 2003, 2004; McKay and Turner, 2005). The bimodal pattern consists of tonic spiking and quiescence (McKay et al., 2005). It is unclear how these firing patterns are generated and what determines which firing pattern is selected. We have constructed a detailed biophysical Purkinje cell model that can replicate these patterns and which shows that Na+/K+ pump activity sets the model's operating mode. This model has experimental validation in its ability to replicate presented *in vitro* Purkinje cell recordings in the presence of ouabain, which irreversibly blocks the Na^+/K^+ pump.

The Na^+/K^+ pump is an enzyme that uses the energy of one ATP molecule to exchange three intracellular Na^+ ions for two extracellular K^+ ions (Glitsch, 2001). Thus the pump is electrogenic, extruding one net charge per cycle to hyperpolarize the membrane potential.

The repeat length of the trimodal pattern is fixed for a single Purkinje cell but can vary among different Purkinje cells, in a range from 20 seconds to 20 minutes (Womack and Khodakhah, 2002). This second to minute duration of the trimodal behaviour is problematic to account for with the Hodgkin-Huxley paradigm because it is decoupled from the millisecond timeframe of ion channel kinetics (Hille, 2001). However, changes in intra-and-extra-cellular ion concentrations can span seconds to minutes (Frohlich et al., 2006) and thus could drive the transition of modes in the trimodal pattern. Our biophysically detailed Purkinje cell model is a test of this hypothesis. In the model, the Na^+/K^+ pump controls the transition from tonic to burst firing by regulating the extracellular K^+ concentration ($[K^+]_o$), which controls a Kv1.2 K^+ channel "gate" to bursting. And the Na^+/K^+ pump's electrogenicity generates the quiescent mode, upon regulation by the intracellular Na^+ concentration ($[Na^+]_i$). During quiescence the ionic concentrations reset and the trimodal cycle starts again from the tonic phase. The Na^+/K^+ pump's affinity for external K^+ (K_K) sets the duration of tonic firing and its affinity for

internal Na^+ (K_{Na}) sets the total duration of firing (tonic + bursting). If these affinities are modulated to make the total firing duration shorter than the tonic, then the model cell fires in the experimentally observed bimodal pattern repeat of tonic spiking and quiescence (McKay et al., 2005). If K_{Na} is set equal to (or lower than) the basal $[Na^+]_i$, then the model cell becomes locked in quiescence (a behaviour reported for Purkinje cells; Llinas and Sugimori, 1980a; De Schutter and Bower, 1994a).

Motor coordination is achieved with precise timing signals for augmentation and inhibition of appropriate agonist and antagonist muscles, and this timing information is believed to be encoded in the rate of firing and pattern of activity of cerebellar Purkinje cells (Ito, 1984). In this chapter, we show that the Na^+/K^+ pump controls intrinsic Purkinje firing and propose that signalling cascades, which have been shown to modulate K_{Na} and K_K (Therien and Blostein, 2000), switch the Purkinje cell between different operating modes in the physiological setting. On this basis, we hypothesise that the Na^+/K^+ pump is a computational element in Purkinje information coding.

2.2 Materials and Methods

*Numerical simulations. S*imulations were performed with the NEURON 5.6 simulator (Hines and Carnevale, 1997), using its backward Euler integration method and 25 μs time steps. The model's morphology is a detailed reconstruction of a Golgi-stained Purkinje cell (Fig. 2.1*a*), sourced from an adult rat (Shelton, 1985) and discretized into 1089 compartments (soma: 1 compartment, smooth dendrites: 85 compartments, and spiny dendrites: 1003 compartments). A specific membrane capacitance of 0.8 μF/cm^2 was used for the soma and smooth dendrites whilst 1.5 μF/cm^2 was used for the spiny dendrites (Miyasho et al., 2001). Specific intracellular resistivity was set to 250 Ω/cm (Miyasho et al., 2001). The model was also run with a different experimentally reconstructed Purkinje cell morphology from guinea pig (Fig. 2.1*b*) (Rapp et al., 1994). This morphology was discretized into 946 compartments (soma: 1 compartment, dendrites: 945 compartments) and no distinction was made in regard to smooth and spiny dendrites. Global specific membrane capacitance was 0.8 μF/cm^2 and global specific intracellular resistivity was 200 Ω/cm (Rapp et al., 1994).

The model incorporates twenty-one gated ion channels with descriptions established from the literature (descriptions reproduced in Appendix A.2). The soma has highly TEA sensitive (I_{K_fast}), moderately TEA sensitive (I_{K_mid}) and TEA insensitive (I_{K_slow}) voltage-gated K^+ currents, a BK voltage-and-Ca^{2+}-gated K^+ current (I_{BK}), a resurgent Na^+ current ($I_{Na\text{-}R}$), a P-type Ca^{2+} current (I_{CaP}) , a hyperpolarisation activated cation current (I_H), a leak current (I_L) and an intracellular Ca^{2+} dynamics abstraction - all sourced from Khaliq et al. (2003). In addition, the soma has an SK Ca^{2+}-gated K^+ current (I_{SK}) (Komendantov et al., 2004). The dendrites have T-type (I_{CaT}), E-type (I_{CaE}) and P-type (I_{CaP}) voltage-gated Ca^{2+} currents; a leak current (I_L); A-type (I_{KA}), D-type (I_{KD}), M-type (I_{KM}), and delayed rectifier (I_{DR}) voltage-gated K^+ currents; BK (I_{BK}) and K2 (I_{K2}) type voltage-and-Ca^{2+}-gated K^+ currents and an intracellular Ca^{2+} dynamics abstraction - all sourced from

Miyasho et al. (2001). In addition, the dendrites have a hyperpolarisation activated cation current (I_H) (Saraga et al., 2003) and a Kv1 voltage-gated K^+ current (I_{Kv1}) (Akemann and Knopfel, 2006). The latter is incorporated as a Kv1.2 description because it replicates Kv1.2 kinetic data from a Purkinje neuron (McKay et al., 2005). The model currents have equations and kinetic parameters as described in their source literature, but with the modification of current density values to those shown in table 2.1. Current densities were assumed to be uniform over the dendrites (as in many other modelling studies e.g. De Schutter and Bower, 1994; Miyasho et al., 2001; Chono et al., 2003) because there are not data to suggest otherwise and in this absence we were ruled by parsimony. This assumption makes for a smaller and more manageable number of model parameters. The simulations were all run with a model temperature of 36 °C.

The somatic Na^+/K^+ pump (density = d^s_{pump}, 1 mA/cm^2) transports 3 Na^+ out ($i^s_{pump\_Na}$) for every 2 K^+ in ($i^s_{pump\_K}$) (Glitsch, 2001). It has a fixed voltage dependency (Lindblad et al., 1996) and an exponential relation (Baccus, 1998) to intracellular Na^+ concentration ($[Na^+]_i$). The Na^+ affinity constant (K_{Na}) is 40 mM (Glitsch, 2001) and $[Na]_{is}$ is 1 mM (Baccus, 1998). *V* represents the membrane potential in mV as a dimensionless quantity.

$$\begin{cases} i^s_{pump} = d^s_{pump}(V+70)/[(V+80)(1+\exp(\dfrac{K_{Na} - [Na^+]_i}{[Na]_{is}}))] \\ i^s_{pump\_Na} = 3i^s_{pump} \\ i^s_{pump\_K} = -2\,i^s_{pump} \end{cases} \quad (2.1)$$

The dendritic Na^+/K^+ pump (density = d^d_{pump}, 0.001 mA/cm^2) has the same $3Na^+$:$2K^+$ stoichiometry but no voltage dependency and a hyperbolic relation to extracellular K^+ concentration ($[K^+]_o$) (Courtemanche et al., 1998). The K^+ affinity constant (K_K) is 2.245 mM (Glitsch, 2001).

$$\begin{cases} i^d_{pump} = d^d_{pump}/(1+(K_K/[K^+]_o)) \\ i^d_{pump\_Na} = 3i^d_{pump} \\ i^d_{pump\_K} = -2\,i^d_{pump} \end{cases} \quad (2.2)$$

Somatic intracellular Na^+ concentration ($[Na^+]_i$) is initiated at 10 mM (Baccus, 1998) and then changes in time *t* according to the relationship:

$$\frac{d[Na^+]_i}{dt} = \frac{I_{Na\_net}}{[d \cdot F]/4} \quad \text{(Canavier, 1999)} \quad (2.3)$$

$$(I_{Na\_net})_{[t]} = (I_{Na\_in} - I_{Na\_out})_{[t-\tau]}, \quad \tau = 5\text{s} \quad (2.4)$$

$$I_{Na\_in} = I_{Na-R} + I^{s}_{ex\_Na} \quad (2.5)$$

$$I_{Na\_out} = i^{s}_{pump\_Na} + I^{s}_{pump\_Na} \quad (2.6)$$

Where $i^{s}_{pump\_Na}$ and $I^{s}_{pump\_Na}$ are Na^+/K^+ pump Na^+ currents at the soma, set by eq. [2.1] and eq. [2.16] respectively. I_{Na-R} is the voltage-gated Resurgent Na^+ current (description in Appendix A.2), $I^{s}_{ex\_Na}$ is the Na^+/Ca^{2+} exchanger Na^+ current (set by eq. [2.15]), F is the Faraday constant and d is the somatic diameter. I_{Na_net} (eq. [2.4]) is the difference between Na^+ current flowing into the soma (I_{Na_in}; eq. [2.5]) (Na^+ ions flowing through the voltage-gated Resurgent Na^+ conductance and the Na^+/Ca^{2+} exchanger) and Na^+ current pumped out of the soma by the Na^+/K^+ pump (I_{Na_out}; eq. [2.6]), lagged by parameter $\tau = 5s$. Tau (τ) is a factor that we have introduced and is not found in the original Canavier (1999) description. Intracellular Na^+ stimulates the Na^+/K^+ pump and this empirical lag τ accounts for the duration of sodium's diffusion from channels to pumps. It aligns with the concept of a "fuzzy space" under the pump where the Na^+ concentration differs from other parts of the cell (Semb and Sejersted, 1996; for a further justification refer to section 2.4, the Discussion component of this chapter). The model represents Na^+ diffusion empirically, with this τ parameter, because a more explicit account would be ill constrained by the literature and too computationally expensive; intracellular diffusion processes have a much shorter spatial scale than electrical signalling and so their modelling requires a higher *nseg* value (the number of internal points at which NEURON computes solutions in each compartment; Hines and Carnevale, 1997) to attain spatial accuracy.

Extracellular K^+ concentration ($[K^+]_o$) to the dendritic compartments is initiated at 2 mM and then changes in time t according to the relationship:

$$\frac{d[K^+]_o}{dt} = [Q \cdot I_{K\_net}] \Big/ F \cdot wid \quad (2.7)$$

$$I_{K\_net} = I_{K\_out} - I_{K\_in} \quad (2.8)$$

$$I_{K\_out} = I_{KD} + I_{KA} + I_{KM} + I_{DR} + I_{BK} + I_{K2} + I_{Kv1} \quad (2.9)$$

$$I_{K\_in} = i^{d}_{pump\_K} + I^{d}_{pump\_K} \quad (2.10)$$

Where F is the Faraday constant, *wid* is the thickness of an extracellular region around the compartment that K^+ accumulates in ($70*10^{-3}$ µm), Q is a K^+ accumulation factor (0.143) and I_{K_net} (eq. [2.8]) is the difference between K^+ current flowing out of the compartment [I_{K_out}] (through gated K^+ conductances, eq. [2.9]) and K^+ current pumped into the compartment [I_{K_in}] (by the Na^+/K^+ pump, eq. [2.10]). K^+ ions flow out of the model dendrites through the D-type (I_{KD}), A-type (I_{KA}), M-type (I_{KM}), delayer rectifier (I_{DR}), BK (I_{BK}), K2 (I_{K2}) and Kv1 (I_{Kv1}) K^+ currents (current descriptions in Appendix

A.2). The Na^+/K^+ pump K^+ current in the dendrites: $i^{d}_{pump\_K}$ is set by eq. [2.2] and $I^{d}_{pump\_K}$ is set by eq. [2.13].

A "ceiling" for extracellular K^+ accumulation is set physiologically by the glial buffer system (Heinemann and Lux, 1977; Kager et al., 2007) and accordingly the model $[K^+]_o$ is not permitted to exceed 3.03 mM (Bazhenov et al., 2004) through code of the form: if ($[K^+]_o$>3.03) [$[K^+]_o$= 3.03].

Formula [2.7] is a modification of the extracellular K^+ accumulation equation employed by Durstewitz et al. (2000) which is reproduced below:

$$\frac{d[K^+]_o}{dt} = \frac{Q \cdot I_{K\_out}}{F \cdot wid} + \frac{[K^+]_{eq} - [K^+]_o}{\tau_K} \quad (2.11)$$

Their *wid* setting is the same ($70*10^{-3}$ µm) but Durstewitz et al. (2000) utilise a Q value of 2 as opposed to our employed 0.143. We adjusted Q as a free parameter in our model tuning because this arbitrary factor is not constrained by the experimental literature. Durstewitz et al. (2000) have no Na^+/K^+ pump mechanism in their model and hence no I_{K_in} parameter, only having an I_{K_out} parameter. Their formulation has an additional term on the right hand side (RHS), setting a decay to the extracellular K^+ accumulation, where $[K^+]_{eq}$ is the equilibrium/resting value of $[K^+]_o$ and τ_K is the time constant with which it approaches this resting value. This term is an abstractive capture of cellular processes acting against extracellular K^+ accumulation, primarily the action of the Na^+/K^+ pump (I_{K_in}). In our work, we model the Na^+/K^+ pump explicitly and so this term is redundant and dropped from our description of extracellular K^+ dynamics.

The model dendrites have two different Na^+/K^+ pump mechanisms. One has already been described (eq. [2.2]). The other is more abstractive (eq. [2.13]). It is included in the model to capture our hypothesis (which is founded in the experimental work of Genet and Kado, 1997; refer section 2.3.7 of this Chapter) that the hyperpolarising Na^+/K^+ pump current electrically balances a depolarising Na^+/Ca^{2+} exchange current. A simple Na^+/Ca^{2+} exchanger mechanism is included in the model dendrites (eq. [2.12]). The use of an additional, simple Na^+/K^+ pump formalism, to offset the inclusion of a simple Na^+/Ca^{2+} exchanger formalism, facilitated tuning the model such that the Na^+/Ca^{2+} exchanger current was fully counter-balanced.

Convention permits inward (depolarising) currents to be denoted negative and outward (repolarising) currents to be denoted positive (Johnston and Wu, 1995). The Na^+/Ca^{2+} exchanger current ($I^{d}_{ex\_net}$; eq. [2.12]) is *net* depolarising (-1), inwardly passing 3 singly positive Na^+ ions (3*[+1]) for the extrusion of every doubly positive Ca^{2+} ion (1*[+2]) (Philipson, 1985). By contrast, the Na^+/K^+ pump current ($I^{d}_{pump\_net}$; eq. [2.13]) is *net* hyperpolarising (+1) in its transport of 3 Na^+ out (3*[+1]) for every 2 K^+ in (2*[+1]).

$$\begin{cases} I^{d}_{ex\_Na} = -3 \cdot [+1] \cdot g^{d}_{ex} \\ I^{d}_{ex\_Ca} = 1 \cdot [+2] \cdot g^{d}_{ex} \\ I^{d}_{ex\_net} = (I^{d}_{ex\_Ca} - I^{d}_{ex\_Na}) \Rightarrow g^{d}_{ex} \cdot [-1] \Rightarrow -g^{d}_{ex} \end{cases} \quad (2.12)$$

$$\begin{cases} I^{d}_{pump\_Na} = 3 \cdot [+1] \cdot g^{d}_{pump} \\ I^{d}_{pump\_K} = -2 \cdot [+1] \cdot g^{d}_{pump} \\ I^{d}_{pump\_net} = (I^{d}_{pump\_Na} - I^{d}_{pump\_K}) \Rightarrow g^{d}_{pump} \cdot [+1] \Rightarrow +g^{d}_{pump} \end{cases} \quad (2.13)$$

g^{d}_{ex} and g^{d}_{pump} are Na^+/Ca^{2+} exchanger and Na^+/K^+ pump membrane current densities (respectively) in the dendrites and their equality at 0.0021 mA/cm^2 ensures an electrical counterbalance So, the model dendrites have a Na^+/Ca^{2+} exchanger current and an electrically counterbalancing Na^+/K^+ pump current:

$$[-g^{d}_{ex} = +g^{d}_{pump}] \Rightarrow [-I^{d}_{ex\_net} = +I^{d}_{pump\_net}] \quad (2.14)$$

The model's soma compartment also has a simple Na^+/Ca^{2+} exchanger mechanism (eq. [2.15]; exchanger density = g^{s}_{ex}) and a counterbalancing, simple Na^+/K^+ pump mechanism (eq. [2.16]; pump density = g^{s}_{pump}). Thus, the soma compartment, like those of the dendrites, has both a detailed Na^+/K^+ pump description (eq. [2.1]) and a simpler Na^+/K^+ pump description (eq. [2.16]) in parallel.

$$\begin{cases} I^{s}_{ex\_Na} = -3 \cdot [+1] \cdot g^{s}_{ex} \\ I^{s}_{ex\_Ca} = 1 \cdot [+2] \cdot g^{s}_{ex} \\ I^{s}_{ex\_net} = (I^{s}_{ex\_Ca} - I^{s}_{ex\_Na}) \Rightarrow g^{s}_{ex} \cdot [-1] \Rightarrow -g^{s}_{ex} \end{cases} \quad (2.15)$$

$$\begin{cases} I^{s}_{pump\_Na} = 3 \cdot [+1] \cdot g^{s}_{pump} \\ I^{s}_{pump\_K} = -2 \cdot [+1] \cdot g^{s}_{pump} \\ I^{s}_{pump\_net} = (I^{s}_{pump\_Na} - I^{s}_{pump\_K}) \Rightarrow g^{s}_{pump} \cdot [+1] \Rightarrow +g^{s}_{pump} \end{cases} \quad (2.16)$$

In the soma compartment, the Na^+/K^+ pump current of equation [2.16] largely, but incompletely, counterbalances the Na^+/Ca^{2+} exchanger current of equation [2.15] – there is a *slight* mismatch [g^{s}_{ex} = 0.511 mA/cm^2, g^{s}_{pump} = 0.5 mA/cm^2] (eq. [2.17]) which permits a small *net* influx of Na^+ ions and a continued Na^+ influx into the soma when the Resurgent Na^+ conductance is removed to simulate TTX block of voltage-gated Na^+ currents; this mismatch permits the model to replicate the Purkinje cell behaviour observed upon TTX application (refer section 2.3.5 of this Chapter).

$$[g^{s}_{ex} = g^{s}_{pump} + 0.011] \Rightarrow [-I^{s}_{ex\_net} \approx +I^{s}_{pump\_net}] \quad (2.17)$$

The Purkinje cell model has four Na^+/K^+ pump equations ([2.1], [2.2], [2.13], [2.16]) and so four Na^+/K^+ pump densities ($d^{s}_{pump}, d^{d}_{pump}, g^{d}_{pump}, g^{s}_{pump}$) which we can represent as ($d^{x}_{pump}, g^{x}_{pump}; x = s,d$) where superscript [*s*] denotes a density at the soma and superscript [*d*] denotes a density in the dendrites. d_{pump} represents the density of a detailed Na^+/K^+ pump formalism (eq. [2.1], [2.2]) as opposed to g_{pump}, which represents the density of a more simplified Na^+/K^+ pump description (eq. [2.13], [2.16]). So, the soma has a detailed and simplified Na^+/K^+ pump formalism (with densities [d^{s}_{pump}] and [g^{s}_{pump}] respectively) and the dendrites have a detailed and simplified Na^+/K^+ pump formalism (with densities [d^{d}_{pump}] and [g^{d}_{pump}] respectively).

The model's four different Na^+/K^+ pump equations are each valid and founded in previously published Na^+/K^+ pump descriptions. They capture different aspects of Na^+/K^+ pumping. The first captures $[Na^+]_i$ and voltage dependency (eq. [2.1]), the second captures $[K^+]_o$ dependency (eq. [2.2]), the third and fourth (eq. [2.13], [2.16]) are essentially equivalent and capture the electrical counterbalance to the Na^+/Ca^{2+} exchanger current. It would be preferable to have these pump aspects in a single formalism. However, this would have greatly increased the complexity of tuning the model, which was methodologically unacceptable.

Ouabain irreversibly blocks the Na^+/K^+ pump (Glitsch, 2001). An increasing proportion of Na^+/K^+ pump molecules being blocked by ouabain is replicated in the model by decreasing the model's four Na^+/K^+ pump densities (d^{x}_{pump}, g^{x}_{pump}, x = s,d) by empirical functions of time t (in seconds):

(Ouabain simulation is arbitrarily initiated at t = 3 s)

$$d^{x}_{pump}(t) = \begin{cases} d^{x}_{pump}(0) & t < 3\,s \\ d^{x}_{pump}(0) - Yt & t > 3\,s \end{cases} \qquad g^{x}_{pump}(t) = \begin{cases} g^{x}_{pump}(0) & t < 3\,s \\ g^{x}_{pump}(0) - c_1^{x}\, t & 3\,s \le t < 8.5\,s \\ g^{x}_{pump}(0) - Mt - c_2^{x} & t > 8.5\,s \end{cases}$$

Where x=s,d; Y=0.1 mA cm^{-2} s^{-1}; c_1^{s}=0.002 mA cm^{-2} s^{-1}; c_1^{d}=0.01 mA cm^{-2} s^{-1}; M=0.1 mA cm^{-2} s^{-1}; c_2^{s}=0.011 mA cm^{-2} s^{-1}; c_2^{d}=0.055 mA cm^{-2} s^{-1} (2.18)

Catch coding, which is code of the form: if (x<0) [x=0], is used to prevent negative values of (d^{x}_{pump}, g^{x}_{pump}, x = s,d) from occurring.

To illustrate the sensitivity of the model to the K_{Na}, K_K and τ parameters a variant of the model was constructed in which they were modified. K_{Na} was changed from 40 mM to 10.5mM, K_K from 2.245 mM to 50 mM and τ from 5s to 1s.

GABAergic Stellate inputs make inhibitory synaptic contacts upon the model dendrites; two inputs to every smooth dendrite compartment and one input to every spiny dendrite compartment (De Schutter and Bower, 1994b). They fire asynchronously, following a Poisson distribution around a mean frequency of input (1 Hz). Their reversal potential is -80mV, with a synaptic weight of 0.001 μS and their amplitude upon activation follows a dual exponential time course (τ_1 = 0.9 ms; τ_2 = 26.5 ms) (De Schutter and Bower, 1994b). These model inputs can be removed to simulate pharmacological blocking of GABAergic synapses.

All parameters were established by prior literature (as referenced) except the twenty-one current densities, the Na^+/K^+ pump and Na^+/Ca^{2+} exchanger densities, the synaptic weight, Q, τ and the functions of Na^+/K^+ pump density decline used in the simulation of ouabain application. These were all ill constrained by the literature and tuned manually.

Preparation of cerebellar slices. Parasagittal slices of cerebellum (250 μm) were prepared from male Wistar rats, at postnatal days 28-35 (P28-35), with methods based on (Llinas and Sugimori, 1980). As described previously (Wall and Usowicz, 1997) and in accordance with the U.K. Animals (Scientific Procedures) Act (1986), male rats were killed by cervical dislocation and decapitated. The cerebellum was rapidly removed and slices were cut on a Microm HM 650V microslicer in cold (2-4ºC) high Mg^{2+}, low Ca^{2+} aCSF, composed of (mM): 127 NaCl, 1.9 KCl, 7 $MgCl_2$, 0.5 $CaCl_2$, 1.2 KH_2PO_4, 26 $NaHCO_3$, 10 D-glucose (pH 7.4 when bubbled with 95% O2 and 5% CO_2). Slices were stored in normal aCSF (1.3 mM $MgCl_2$, 2.4 mM $CaCl_2$) at room temperature for 1-6 hours before recording.

Electrophysiological recording. Individual slices were viewed on a Zeiss FS Axioskop microscope with a 40× water immersion objective and Nomarski differential interference optics, at a total magnification of 640×. Slices were maintained at 30-32°C and continuously perfused (1-5 ml min^{-1}) with aCSF, which was bubbled with 95% O_2 and 5% CO_2. Whole-cell patch-clamp recordings were made from visualized Purkinje cells using an EPC 8 amplifier (Heka, Digitimer, Welwyn Garden City, UK) controlled via a Digidata 1322a interface (Axon Instruments INC, Foster City CA, USA) using Clampex (v 9, Axon Instruments). Patch-pipettes (thick-walled borosilicate glass, Harvard Apparatus, Edenbridge, UK) were fire-polished, and had resistances of 1.5-4 MΩ when filled with an intracellular solution containing (mM): 135 K gluconate, 7 NaCl, 10 HEPES, 0.5 EGTA, 2 Na_2-ATP 0.3 Na_2-GTP and 10 mM Na phosphocreatine (adjusted to pH 7.2 with KOH and osmolarity adjusted to 300 mOSM with sucrose). Aliquots of intracellular solution were stored frozen at -20ºC and thawed on the day of recording.

Drugs. Drugs were dissolved at 1-100 mM in deionised water: bicuculline methiodide (Sigma), TTX (tetrodotoxin, Advent Scientific) and ouabain (Sigma). Aliquots of these stock solutions were stored frozen at -20°C, thawed and diluted in perfusion *medium* on the day of recording. All drugs were bath applied.

2.3 Results

2.3.1 The Purkinje cell model can replicate the trimodal pattern of spontaneous firing

In the absence of synaptic input, the model Purkinje cell fires spontaneously in a repeating trimodal pattern that consists of tonic spiking (*t*), bursting (*b*) and silence/quiescence (*s*) (Fig. 2.1). Significantly, the model captures the long timescale reported for Purkinje cell trimodality (Womack and Khodakhah, 2002), with a pattern repeat length of ~20 seconds.

There is some uncertainty as to whether the trimodal firing pattern is intrinsically generated or a function of neuromodulatory input (Womack and Khodakhah, 2002). This replication of trimodal firing in an experimentally constrained and detailed model of an isolated Purkinje cell adds significantly to the case for intrinsic generation.

The model soma can fire sodium spikes (Fig. 2.1*c*) and the model dendrites can fire calcium spikes (Fig. 2.1*d*), which is in alignment with experimental findings (Llinas and Sugimori, 1980a, 1980b). A comparison of figures 2.1*c* and 2.1*d* shows that the model's tonic mode (*t*) is somatic spiking in the absence of dendritic spiking. Whilst the model's burst mode (*b*) is produced by dendritic spikes propagating to the soma to drive somatic bursting.

A single dendritic calcium spike initiates and terminates each somatic burst, producing a stereotypical burst waveform (Fig 2.1*e*). The leading foot of the dendritic calcium spike (Fig. 2.1*e iii,* denoted by #) causes the slow progressive depolarisation during the burst (Fig. 2.1*e iv,* denoted by &). The peak of the dendritic calcium spike (Fig. 2.1*e iii,* denoted by *) causes the sudden and rapid depolarisation that ends the burst (Fig. 2.1*e iv*).

The model's relationship between dendritic spikes and trimodal bursting is in alignment with experimental data, where a similar stereotypical burst waveform has been observed (Womack and Khodakhah, 2004). The frequency of dendritic spiking sets the model's burst parameters. For example, the Kv1.2 K^+ channel limits the frequency of dendritic calcium spikes and its removal from the model permits a higher frequency of dendritic firing (Fig. 2.1*h i*), which decreases the number of spikes per burst (Fig. 2.1*h ii*). This replicates experimental data recorded when Kv1.2 channels were pharmacologically blocked (McKay et al., 2005).

2.3.2 In the model, the Kv1.2 channel gates the trimodal pattern's tonic to burst transition

The model dendrites have an intrinsic capacity to fire Ca^{2+} spikes. Their low-threshold T-type and E-type voltage-gated Ca^{2+} channels open near the resting potential and they depolarise the membrane potential to activate high-threshold P-type voltage-gated calcium channels. These P-type Ca^{2+} channels then produce Ca^{2+} spikes, which are repolarised by K^+ flow through BK-type K^+ channels (in alignment with Miyasho et al., 2001).

This system is gated by dendritic Kv1.2 voltage-gated K^+ channels. Kv1.2 channels generate hyperpolarizing current which clamps dendritic excitability and prevents Ca^{2+} spike generation, thus allowing the tonic mode of firing. However, the power of this excitability clamp diminishes with time because extracellular K^+ accumulates and this reduces the electrochemical driving force for potassium flow. Eventually the hyperpolarizing current produced by Kv1.2 channel activity is insufficient to prevent dendritic spiking and the model is switched from the tonic to the burst mode.

The control of the tonic to burst transition by Kv1.2 channels enables the model to replicate an experimental investigation in which Kv1.2 channel block dramatically shortened the tonic phase within the trimodal pattern (fig. 2.1*f*) (McKay et al., 2005).

2.3.3 In the model, the Na^+/K^+ pump generates the trimodal pattern's quiescent phase

The Na^+/K^+ pump hyperpolarizes the membrane potential with a stoichiometry of three internal Na^+ ions exchanged for every two external K^+ ions (*methods*). The Na^+ concentration in a "fuzzy space" underneath the pump ($[Na^+]_i$) rises during the tonic and burst firing modes, as a function of voltage-gated Na^+ entry, and this intracellular Na^+ enzymatically increases pump activity (*methods*). Eventually, during the bursting mode, the pump generates such a hyperpolarising current that firing stops and the model cell is driven to quiescence. In this case, without any spike associated Na^+ entry, $[Na^+]_i$ would be expected to stop rising. However, $[Na^+]_i$ continues to increase as the Na^+ influx is lagged by an empirical parameter τ (*methods*), which phenomenologically encodes the long duration of Na^+ diffusion from the Na^+ channel to Na^+/K^+ pump (*discussion*). When τ expires, Na^+ influx stops whilst the pump maintains Na^+ efflux. This decreases $[Na^+]_i$, which reduces hyperpolarising pump activity and eventually permits the model's spontaneous firing to resume. Firing resumes in the tonic spiking mode, rather than in the bursting mode which preceded the quiescence, as during the quiescence the Na^+/K^+ pump resets the extracellular K^+ concentration and the Kv1.2 channels block to bursting. Thus, the trimodal pattern is reset for another cycle.

2.3.4 The model can account for the heterogeneity in trimodal repeat length between different Purkinje cells

The trimodal repeat length is the duration of a single repeat of the trimodal pattern. It is a constant for an individual Purkinje cell but can vary from 20 seconds to 20 minutes between different cells (Womack and Khodakhah, 2002). The model reproduces the fixed repeat length for a single cell and identifies the mechanistic basis of the cell-to-cell heterogeneity.

The Na^+/K^+ pump's affinity for internal Na^+ (K_{Na} model parameter) sets the "firing length", which is the combined duration of the tonic and bursting modes. The lower K_{Na}, the less intracellular Na^+ required for stimulating the Na^+/K^+ pump to produce a hyperpolarisation that can silence firing, which equates to a shorter period of Na^+ entry i.e. a shorter "firing length" (Fig. 2.2*b*). Reported K_{Na} values vary in the literature (Glitsch, 2001) and thus it is feasible that K_{Na} could vary between Purkinje cells.

The Na^+/K^+ pump's affinity for external K^+ (K_K model parameter) sets the duration of tonic firing. The higher K_K, the shorter the tonic mode (Fig. 2.2*c*). K_K exerts this control by regulating the rate of extracellular K^+ accumulation. Reported K_K values vary in the literature (Glitsch, 2001) and thus it is feasible that K_K could vary between Purkinje cells.

Intracellular Na^+ dynamics (encoded by the τ model parameter) set the duration of the quiescent mode. The smaller τ, the shorter the quiescent phase (Fig. 2.2*d*). Na^+ dynamics are complex and embrace many constituent parameters, some of which could feasibly vary between different Purkinje cells.

K_{Na}, K_K and τ are hypothesised to be fixed constants for a single cell but with the potential to vary between different cells. A model variant was constructed in which these three parameters were modified. K_{Na} was changed from 40 mM to 10.5mM, K_K from 2.245 mM to 50 mM and τ from 5 s to 1 s. This variant had a trimodal repeat length of ~3 seconds (Fig. 2.2*e*, Fig 2.4*a*) as compared to the ~20 seconds of the standard model (Fig. 2.2*a*). This shorter repeat length is not within the experimentally reported range (Womack and Khodakhah, 2002). However, this model variant will now be the standard model preparation for the remainder of this report as the shorter repeat length is more practical for simulations of multiple trimodal repeats. Our Purkinje cell model is computationally expensive to run, with 22 minutes of CPU time required for 1 second of simulation (on an Intel Pentium PC). This shorter repeat variant has enabled faster rates of investigation, whilst its length is still sizeable and has a proven relation to a longer, realistic pattern length.

The model cell has a morphology reconstructed from a Purkinje cell in an adult rat cerebellum (fig. 2.1*a*) (Shelton, 1985). When the model was re-run with the same parameters, but with a different reconstructed morphology (fig. 2.1*b*) (from guinea pig,

Rapp et al., 1994), the trimodal repeat length was not greatly changed (Fig. 2.2*f*). This is despite the second morphology being visually distinct. This suggests that morphology is not a primary dictator of the trimodal repeat length. Although it does appear to dictate the number of spikes per burst, with the second morphology having more spikes per burst than the first (15 as compared to 11).

2.3.5 The model's soma and dendrites can both fire spontaneously

The model has a soma capable of spontaneously firing sodium spikes and a dendritic tree capable of spontaneously firing calcium spikes. Thus, the model's dendritic spiking is not reliant upon an excitatory drive from the soma. This enables the model to replicate the persistence of dendritic Ca^{2+} spikes (Fig. 2.3*b*) when Na^+ channels are blocked (by TTX; Womack and Khodakhah, 2004) (TTX block is simulated in the model by setting the resurgent sodium current density to 0). These dendritic spikes propagate to the soma where they produce small deflections in the membrane potential (Fig. 2.3*a*). In the model dendrites, the hyperpolarisation activated cation current, I_h, is essential to the model's dendritic spontaneity. Without I_h the dendrites cannot fire Ca^{2+} spikes spontaneously, only in the presence of somatic drive (data not shown). The importance of I_h in the Purkinje cell's electrical response to TTX has been shown experimentally (Chang et al., 1993).

In the presence of TTX, somatic activity is bimodal with periods of Ca^{2+} spike firing alternating with periods of quiescence (Womack and Khodakhah, 2004). The model can replicate this pattern (Fig. 2.3*a*), with the quiescent periods generated by the electrogenic action of the Na^+/K^+ pump (as with the trimodal pattern). In this TTX simulation, though there is no resurgent Na^+ entry, stimulatory Na^+ to the Na^+/K^+ pump can still enter through the Na^+/Ca^{2+} exchanger.

2.3.6 The model can replicate other patterns of Purkinje cell firing

Some Purkinje cells express the trimodal firing pattern without pharmacological manipulation while others express it only upon the condition that GABAergic synaptic inputs are blocked (Womack and Khodakhah, 2002). In our experimental Purkinje cell recordings, we observed a repeating bimodal pattern of tonic spiking and quiescence when GABAergic connectivity is intact and only observed the trimodal firing pattern upon pharmacological block of GABA synapses.

GABAergic stellate cells make inhibitory synaptic contacts upon the dendrites of Purkinje cells (De Schutter and Bower, 1994b). When these inputs are introduced into the Purkinje cell model they clamp the dendritic excitability and prevent Ca^{2+} spike generation. Thus, they prevent the tonic to bursting transition and switch the model from firing in a trimodal pattern to firing in a repeating bimodal pattern of tonic spiking and quiescence (fig. 2.4*b*).

Some Purkinje cells intrinsically fire in this repeating bimodal pattern, in the absence of synaptic input (McKay et al., 2005), and with adjustment the model can reproduce this behavior. For the model, we shall term the length of firing (tonic and/or bursting) that can happen before the pump gains enough strength to overcome it, and cause quiescence, as the "pump repeat length". This is dictated by K_{Na}. And we shall term the length of tonic spiking that can happen before the onset of bursting as the "tonic repeat length". This is dictated by K_K, which sets the loss rate of the Kv1.2 channel gate to bursting. These two lengths are fixed for a particular model cell but can vary between different model cells. If [pump repeat length > tonic repeat length] then the model cell fires in a trimodal pattern (Fig. 2.4*a*). If [tonic repeat length > pump repeat length] then the model cell fires in a bimodal pattern (Fig. 2.4*c*) - no bursting is observed because the pump drives the model cell to quiescence before it can occur. A model cell can be switched from bimodal to trimodal firing, or vice-versa, by changing the K_{Na} or K_K values to modify the relation of "pump repeat length" to "tonic repeat length".

An intrinsically bimodal model cell can be switched to trimodal firing by blocking the Kv1.2 current (setting Kv1.2 channel density to 0) (Fig. 2.4*d*). This has experimental support with McKay et al. (2005) observing that pharmacological block of Kv1 channels can switch a bimodal Purkinje cell into bursting; with the pertinent Kv1 channel reasoned by the authors to be Kv1.2. Physiologically, we can speculate that Kv1.2, with its acute phosphorylation control (Huang et al., 1993; Winklhofer et al., 2003; Colley et al., 2004), might be an "online" molecular switch between the bimodal and trimodal firing modes.

A model cell firing in the trimodal pattern can be switched into the bimodal pattern by removing its dendritic P-type Ca^{2+} channel complement (Fig. 2.4*e*) such that it can no longer fire dendritic Ca^{2+} spikes. This replicates Purkinje data recorded when the dendritic P-type Ca^{2+} channels were pharmacologically blocked (Womack and Khodakhah, 2004).

Without synaptic input, not all Purkinje cells fire spontaneously - some are quiescent (Llinas and Sugimori, 1980a; De Schutter and Bower, 1994a). The model's basal intracellular Na^+ concentration is 10mM (*methods*) and setting K_{Na} to 10 mM, which is a realistic value (Glitsch, 2001), locks the model cell in continuous quiescence (data not shown). It is worth mentioning that the persistently quiescent Purkinje state might be erroneous and that when quiescence is experimentally observed (Llinas and Sugimori, 1980a) it is not a continuous operating mode in its own right, but just a component of the trimodal or bimodal patterns. Our model is neutral to this debate, being able to replicate either scenario.

2.3.7 The model replicates the response of Purkinje cells to Na^+/K^+ pump block by ouabain

As an objective assay of the model's validity we investigated whether it could predict the Purkinje cell response to the application of ouabain. This is an experimental test that the

model has not been specifically tuned to capture and the ability of a model to predict/fit data not used in determining its parameters is an independent measure of how well the model approximates reality. Ouabain inhibits the Na^+/K^+ pump irreversibly (Glitsch, 2001) and thus, after ouabain application, the proportion of pump molecules blocked increases in time until eventually all pump activity is abolished. Ouabain application was simulated in the Purkinje cell model by decreasing the Na^+/K^+ pump densities by arbitrary functions of time (*methods*), which switched the model's trimodal firing pattern into a continuous burst mode that converged upon depolarization block. This same transition was observed experimentally in whole cell patch clamp recordings from Purkinje cells (firing in the trimodal pattern) following the application of 2.5 μM ouabain (with 10 μM bicuculline present to block GABAergic inputs) (*n = 4*). After noting that the model and experimental response to ouabain matched, validating the model, we then tuned the model's pump density decline functions to generate a best fit between model (Fig. 2.6) and data (Fig. 2.5).

In the Purkinje cell response to ouabain (real or simulated), the duration of the trimodal pattern's quiescent periods became shorter until firing was continuous (Fig. 2.5*a*) (Fig. 2.6*a*). The duration of the trimodal pattern's tonic mode also decreased, leading to an increased proportion of burst firing (compare Fig. 2.5*b* and 2.5*c*) (compare Figs. 6*b*, 6*c* and 6*d)*. Indeed, by the time cells were continuously active the firing only consisted of bursts, with no tonic mode remaining (Fig. 2.5*d*) (Fig. 2.6*e*). An experimental hyperpolarisation of the membrane potential could not prompt the re-emergence of the tonic or quiescent modes (*n* = 3). After a time, this continuous bursting attained a shallow gradient of depolarisation that eventually converged upon somatic depolarisation block (Fig. 2.5*a*) (Fig. 2.6*a*). This block was furrowed with small deflections in the membrane potential (Fig. 2.5*e*) (Fig. 2.6*f*), which are attributable to Ca^{2+} spikes that have travelled from the dendrites. So, although the soma was in depolarisation block the dendrites were not and continued to fire. In some cells these deflections got smaller and smaller until there was complete quiescence, which suggests that in these cases the dendrites entered depolarisation block as well (data not shown). During the progression to somatic depolarisation block, the number of Na^+ spikes per burst decreased (Figs. 2.5*f*, 2.5*g*, 2.5*h*) (Figs. 2.6*g*, 2.6*h*, *2.6i*) until there were none and only Ca^{2+} spikes (from the dendritic arborisation) were observed (Fig. 5*i*) (Fig. 6*j*). During the somatic depolarisation block, an experimental hyperpolarisation of the membrane potential brought re-emergent Na^+ spiking and showed this block to be a function of Na^+ channel inactivation. However, this recovery could not occur if the hyperpolarisation was introduced too long after the onset of depolarisation block, perhaps because these Na^+ channels become irreversibly inactivated in time.

With this matching experimental and model response to ouabain, the loss of the quiescent mode shows the Na^+/K^+ pump to generate trimodal quiescence. The loss of the tonic mode shows that the Na^+/K^+ pump controls the tonic to burst transition through its setting of extracellular $[K^+]$, which controls a Kv1.2 channel "gate" to bursting. The depolarisation block demonstrates that the Na^+/K^+ pump is required to counterbalance a strong and depolarising force. Indeed, the pump has been reported to offset a depolarising tetrodotoxin (TTX) resistant Na^+ entry in the Purkinje cell (Genet and Kado, 1997). The

model incorporates a hypothesis that this Na^+ entry is through the Na^+/Ca^{2+} exchanger, which has been to be shown present in Purkinje cells (Fierro et al., 1998). The Na^+/Ca^{2+} exchanger is *net* depolarising (-1), inwardly passing 3 Na^+ ions for the extrusion of every Ca^{2+} ion (Philipson, 1985). By contrast, the Na^+/K^+ pump is *net* hyperpolarising (+1) with a stoichiometry of [3 Na^+ out: 2 K^+ in] (Glitsch, 2001). The model soma and dendrites have a Na^+/Ca^{2+} exchanger and an electrically counterbalancing Na^+/K^+ pump mechanism (*methods*). With pump loss the counterbalance to the depolarising force of the Na^+/Ca^{2+} exchanger is lost and depolarisation ensues. The sizable exchanger density at the soma, when not counterbalanced by the pump, puts the soma into depolarisation block. However, the lesser exchange density in the dendrites, when not counterbalanced by the pump, cannot put the dendrites into depolarisation block. We predict that the somatic depolarisation block in the Purkinje response to ouabain would be abolished by pharmacological block of the Na^+/Ca^{2+} exchanger.

The reader must be aware that Na^+/K^+ pump block might eradicate quiescence, not because the Na^+/K^+ pump generates quiescence (per se), but because this block causes depolarisation which compromises the activity of the true entity responsible. This is actually a problem inherent to many pharmacological block experiments that seek to parse the function of individual neuronal currents. By knocking out a current, the voltage trajectory is changed and in interpretation one is then unsure as to whether functional changes are due to that loss or due to changes in (an)other current(s), which is regulated by the membrane potential. We did control experiments where we injected hyperpolarising current to counter the depolarisation (*n=3*) and in which we still observed the loss of the quiescent mode. However, this injection was at the soma and it probably didn't prevent depolarisation in the entirety of the elaborate dendritic tree. So, it is with this caveat that we propose the Na^+/K^+ pump as the generative mechanism to trimodal quiescence.

Before we considered the Na^+/K^+ pump as the drive to trimodal quiescence, we entertained the possibility that a Ca^{2+}-activated K^+ current might be responsible. However, we discounted the SK K^+ current because the trimodal pattern's quiescent mode can still occur when this current is blocked by apamin (Womack and Khodakhah, 2003). And we discounted the BK K^+ current because the trimodal pattern's quiescent mode can still occur when this current is pharmacologically blocked by IBTX (Womack and Khodakhah, 2004) or when it is genetically knocked out (Sausbier et al., 2004). And our Na^+/K^+ pump block experiment indicates that Ca^{2+}-activated K^+ currents are not involved - Na^+/K^+ pump block has been shown to cause intracellular Ca^{2+} accumulation in a number of cell types because it compromises the Na^+ electrochemical gradient, which the Na^+/Ca^{2+} exchanger requires to pump Ca^{2+} out of the cell (Gustafsson and Wigstom, 1983; Wit et al., 1981). So, if the trimodal pattern's quiescent mode is not generated by the Na^+/K^+ pump, but instead by a Ca^{2+}-activated hyperpolarising current, we would expect Na^+/K^+ pump block to promote quiescence rather than shorten and eradicate it. Indeed, Na^+/K^+ pump block has been shown to cause quiescent periods, via Ca^{2+}-activated K^+ currents, in canine coronary sinus fibers (Wit et al., 1981).

Unfortunately, the ouabain response of the real and model Purkinje cell was not in complete alignment. The model's deflections in the membrane potential, furrowing the depolarisation block, are smaller than those observed experimentally. Also, the model's timescale of response to ouabain (~10 seconds, fig. 2.6*a*) does not match that observed *in vitro* (1000 seconds, fig. 2.5*a*). Although, to address the latter we propose that the model might be modified to operate over the longer experimental timescale by 1) changing K_{Na^+}, K_{K^+} and τ to yield a longer trimodal repeat length and 2) using slower functions of decline for the model's Na^+/K^+ densities.

In experiments with a lower ouabain concentration (1.5 μM) the same sequence of events occurred but took longer ($n = 3$), presumably because the pump block progression was slower. And with higher ouabain concentrations (10- 20 μM), the progression to depolarisation block was rapid and the transition through the aforementioned sequence was not observed ($n = 5$).

Ouabain block of the Na^+/K^+ pump also imposes a switch in behaviour for Purkinje cells that still have intact inhibitory synaptic inputs and which fire in a repeating bimodal pattern of tonic spiking and quiescence. Ouabain (2.5 μM) initially switches their firing from bimodal to trimodal before continual bursting and an eventual depolarisation block (Fig. 2.7*a*) ($n = 3$). This shows that the pump generates the quiescent mode in the bimodal pattern of firing as well as in the trimodal pattern. The model is able to accurately reproduce this experimentally observed behaviour (Fig. 2.7*b*).

In the presence of TTX (1 μM), the Purkinje cell expresses a repeating bimodal pattern of activity and quiescence (Womack, 2004). When Ouabain (2 μM) is applied to a Purkinje cell that is in this TTX induced bimodality, it shortens the length of the quiescent periods until ultimately the cell is switched to a pattern of continuous firing (Fig. 2.8*a*) ($n = 3$). This suggests that it is the Na^+/K^+ pump that generates the quiescent periods in the Purkinje response to TTX. This experiment is well replicated by the model (Fig. 2.8*b*).

2.4 Discussion

This investigation valuably reconciles the divergent Purkinje behaviours observed in different *in vitro* studies (quiescent, Llinas and Sugimori, 1980a; trimodal, Womack and Khodakhah, 2002; bimodal, McKay et al., 2005) and establishes the biophysical basis to the operating diversity of the cerebellar Purkinje neuron. We find that at the foundation of Purkinje cell multimodality there is the working of just a single molecular species – the Na^+/K^+ pump - and we show that it sets the Purkinje cell as persistently quiescent or spontaneously firing in trimodal or bimodal patterns.

The mechanisms that we propose to drive the Purkinje cell's trimodal pattern of firing have been observed in other classes of neuron. Extracellular K^+ has been experimentally

observed to accumulate during sustained neural activity (Moody et al., 1974; Heinemann and Lux, 1977; Amzica et al., 2002) and has been modelled to drive a tonic to burst transition in the neocortical pyramidal cell (Frohlich et al., 2006). The electrogenic action of the Na^+/K^+ pump (regulated by the intracellular Na^+ concentration) has been shown experimentally to generate quiescent periods in canine coronary sinus fibers (Wit et al., 1981).

The trimodal pattern's quiescent mode can span seconds or minutes (Womack and Khodakhah, 2002) and thus its generative mechanism, which we suggest to be Na^+/K^+ pumping, must match this timescale. Na^+/K^+ pump activity is stimulated by intracellular Na^+ and for it to persist at sufficient intensity during the quiescence, to perpetuate the quiescence, there must be a maintained intracellular Na^+ accumulation. This persistence is non-intuitive as pump activity would be expected to quickly erode the Na^+ accumulation during quiescence (by continuing to pump Na^+ out of the cell in the absence of any voltage-gated Na^+ entry) and down-regulate pump activity. However, intracellular Na^+ accumulation has actually been experimentally observed to persist minutes after the end of voltage-gated Na^+ entry; a phenomenon that has been ascribed to a nonuniform cytoplasmic distribution of ions (Wendt-Gallitelli et al., 1993; Verdonck et al., 2004; Blaustein and Wier, 2007). Neurons and muscle cells have a "fuzzy space" between the endoplasmic reticulum (ER) and the plasma membrane (Henkart et al., 1976; Semb and Sejersted, 1996; Blaustein and Lederer, 1999; Delmas and Brown, 2002), termed the "PLasmERosome", where some "unknown molecular anatomy severely impedes the movement of small ions and yet allows equilibration with the cytoplasm over longer times" (Lederer et al., 1990). Thus, the soma has two spatially-distinct and weakly coupled compartments for Na^+, the fuzzy space and the bulk cytoplasm. A steep Na^+ gradient has been experimentally measured between these two spaces (Wendt-Gallitelli et al., 1993). The Na^+/K^+ pump is located in the fuzzy space whilst the voltage-gated Na^+ channels might be localised to a "third functional domain" (Verdonck et al., 2004) or they may also be in the fuzzy space but spatially segregated from the pumps, given this domain's reported microheterogeneity of high $[Na^+]$ "hot spots" alternating with areas of lower $[Na^+]$ (Wendt-Gallitelli et al., 1993). Either way, the Na^+ channel and pump appear geographically distinct. In the model, the empirical lag parameter (τ) accounts for the duration of sodium's diffusion from channel to pump. This duration can be on the order of seconds to minutes because diffusion is significantly restricted in the fuzzy space by an, as yet, uncharacterized physiochemical process (Despa and Bers, 2003). Thus, when Na^+ influx stops it takes time to feed through and reduce the Na^+ concentration underneath the pump, which is the critical concentration for pump activity. This lag could account for why the pump current decays on the "order of seconds to minutes", as reported by Su et al. (1998), rather than milliseconds. This large diffusive lag might also account for why no elevated pump activation is observed within 2 seconds of an increased Na^+ entry (Silverman et al., 2003). The model represents diffusion empirically, with the τ parameter, because an explicit account would be too computationally expensive and ill constrained by the literature.

To date, the trimodal firing pattern has only been observed *in vitro* and the length of its constituent modes (tonic, bursting, quiescent) is reported as fixed for a particular Purkinje cell (Womack and Khodakhah, 2002). However, if the trimodal pattern is physiologically relevant we propose that modulators to Na^+/K^+ pumping might act to regulate the length of modes as a signalling element to the deep cerebellar nuclei (DCN). The model shows how modifying the K_{Na} and K_K pump parameters, which have been experimentally shown as modulated elements (Therien and Blostein, 2000), can change the trimodal pattern. Indeed, the model highlights that their modulation could be an "online" molecular switch between the trimodal and bimodal patterns of firing.

The model shows that the trimodal pattern of firing is regulated by the extracellular K^+ concentration. Neighboring Purkinje cells share an immediate extracellular milieu, which raises the possibility that adjacent or nearby Purkinje cells can signal to each other through the extracellular K^+ concentration variable. Glial cells buffer K^+ *(*Kofuji and Newman, 2004*)* and they might modulate this communication and be a novel working component of the cerebellar circuit.

In vitro, repetitive climbing fiber (CF) input (at a physiological frequency, 1 Hz) switches Purkinje cells out of the trimodal firing pattern and into a nonbursting pattern of activity (McKay et al., 2007). On this basis it might be that the trimodal firing pattern is not applicable *in vivo*. However, in these experiments, although CF input blocks the trimodal pattern's bursting mode, long quiescent periods still occur (in which CF input cannot evoke a state transition into the firing state; figure 1D in McKay et al., 2007) and these have been observed *in vivo* also (Loewenstein et al., 2005). We propose that these are Na^+/K^+ pump generated silences. So, we assert that although CF input blocks the trimodal pattern's bursting mode, it does not block its quiescent mode, which we have shown to be generated by Na^+/K^+ pumping i.e. we suggest that Na^+/K^+ pump generated silences occur physiologically. And we affirm this suggestion with the research and findings presented in *Chapter 4*, where we model Purkinje activity under conditions of CF input.

Spikes are frequently taken as the basic unit of neural coding. However, silences in spiking may be just as meaningful for the Purkinje cell as its firing output is inhibitory to the downstream deep cerebellar nuclei (DCN) and so a pause in its spiking would convey disinhibition (Jaeger, 2007; Steuber et al., 2007) . We suggest that the patterning and lengths of quiescent periods might be salient to how the Purkinje cell encodes information. We propose intracellular Na^+ concentration to be a memory element in the Purkinje cell, integrating firing history and setting Na^+/K^+ pump activity to dictate quiescence length and patterning, with potential modulation by signaling cascades convergent on the pump (Therien and Blostein, 2000). In support, a mutation in the Na^+/K^+ pump causes rapid-onset dystonia-parkinsonism (RDP), which has symptoms to indicate that it is a pathology of cerebellar computation (Cannon, 2004; de Carvalho et al., 2004). A role of the Na^+/K^+ pump in neural coding has very recently been established for the T-neurons of the leech, in particular the adaptation of its code to stimulus statistics (Arganda et al., 2007). So, there is a precedent for what we propose here, that the Na^+/K^+

pump can be more than just a homeostatic mechanism for ionic gradients - it can actually be a computational element. This shift in view may change earlier estimates of the metabolic cost of neural information where ionic pumping was considered purely as cost (Laughlin et al., 1998).

Table 2.1 Maximal current conductances (mS/cm^2) (assumed uniform over the dendrites).

Current	Soma	Dendrite
Resurgent Na+	156	0
P-type Ca2+	0.52	1.6
T-type Ca2+	0	0.6
E-type Ca2+	0	3.2
A-type K+	0	32
D-type K+	0	36
M-type K+	0	0.004
Delayed rectifier K+	0	0.24
Bk K+	72.8	60
SK K+	10	0
K2 K+	0	0.16
Kv1.2 K+	0	1
Highly TEA sensitive K+	41.6	0
Moderately TEA sensitive K+	20.8	0
TEA insenstitive K+	41.6	0
hyperpolarisation activated cation, I_h	1.04	0.29
Leak	0.1	0.08

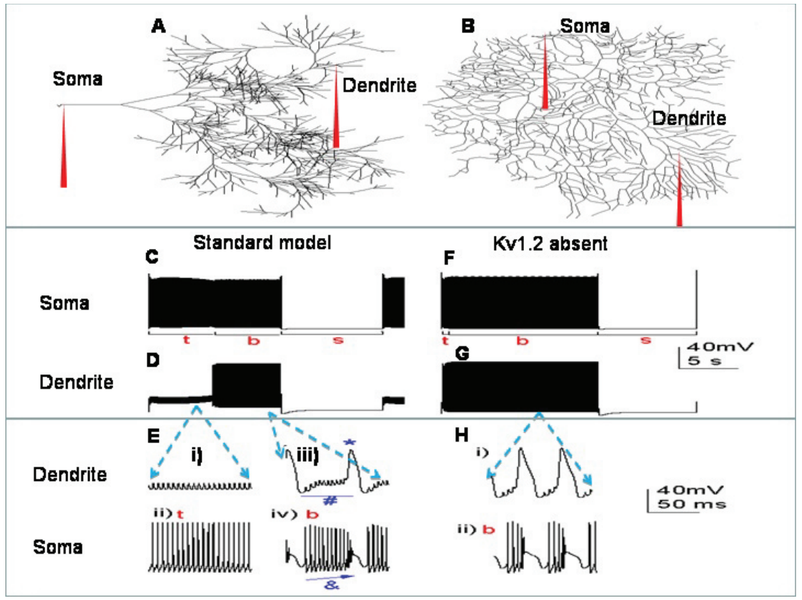

Figure 2.1 The Purkinje cell model. **In the absence of synaptic input, the Purkinje cell model fires spontaneously in a repeating trimodal pattern**. *A*, The model cell's default morphology with somatic and dendritic recording points labeled. *B*, An alternative morphology used for the model. *C,* A single trimodal repeat, recorded at the soma (A), with the constituent tonic (t), burst (b) and silent (s) modes labeled. *D,* The same trimodal repeat as (C) but recorded from a point within the dendritic tree (A). *E*, Without high-threshold dendritic spikes (i), somatic firing has a tonic (*t*) form (ii). With high-threshold dendritic spikes (iii), somatic firing has a stereotypical burst (*b*) waveform (iv). A single dendritic spike initiates and terminates each somatic burst. The leading foot of the dendritic spike (*#,* iii) causes the slow progressive depolarisation of the somatic burst (*&,* iv). The peak of the dendritic spike (**,* iii) causes the sudden and rapid depolarisation that ends the somatic burst (iv). *F*, A single trimodal repeat recorded from the soma (A) of a model variant that lacks the Kv1.2 channel. It has a markedly shorter tonic mode (t) than observed with the standard model (C). *G*, The same trimodal repeat as (F) but recorded from a point within the model's dendritic tree (A). *H*, Without Kv1.2 channels, the dendritic spike frequency is higher (i) which results in a smaller number of spikes per somatic burst (ii). *Panels C, D, F and G are scaled by the first scale bar (40 mV, 5 s) and panels E and H by the second scale bar (40 mV, 50 ms).*

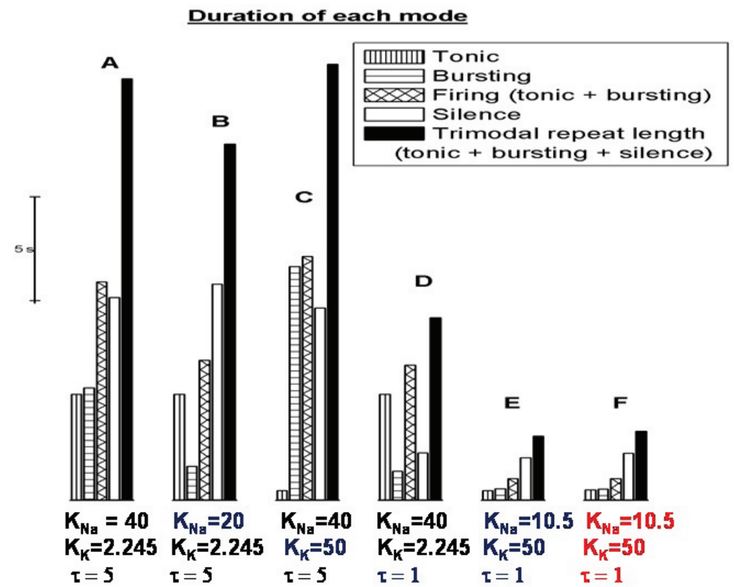

Figure 2.2 Model output. **The K_{Na}, K_K and τ model parameters set the model's trimodal repeat length.** This is shown by the presented durations of the tonic mode, bursting mode, firing mode (tonic + bursting), quiescent mode and trimodal repeat length (tonic + bursting + quiescent) for different model settings. *A*, With default settings [K_{Na} = 40mM; K_K =2.245mM; τ = 5s] the trimodal repeat length is ~20 s. *B*, Reducing K_{Na} (40 mM to 20mM) shortens the firing (tonic + burst) duration. *C*, Increasing K_K (2.245mM to 20mM) shortens the tonic duration. *D*, Reducing τ (5s to 1s) shortens the quiescent mode. *E*, With K_{Na}, K_K and τ all modified [K_{Na} = 10.5mM; K_K =50mM; τ = 1s] the trimodal repeat length is ~3 s. *F*, When the model was run with a different reconstructed Purkinje cell morphology, but with the same parameters as (E), the trimodal repeat length was not majorly changed.

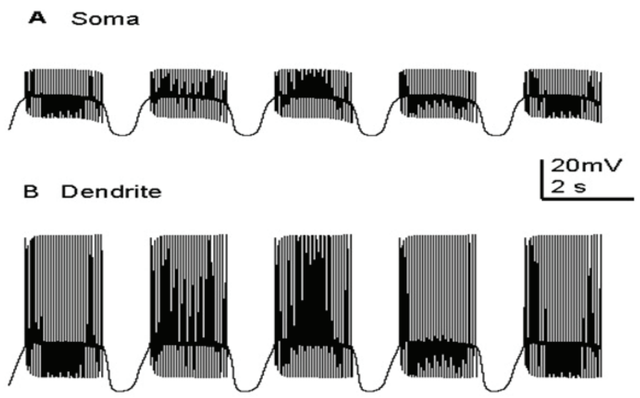

Figure 2.3 Model output. **Removal of Na^+ channels (simulation of TTX application) abolishes the model's somatic Na^+ spiking but not it's dendritic Ca^{2+} spiking**. *A*, The model's somatic membrane potential (vs. Time), when Na^+ channels are absent. There are no Na^+ spikes but periods of small deflections in the membrane potential, which alternate with quiescent periods (bimodal behaviour). *B*, The model's dendritic membrane potential (vs. Time), when Na^+ channels are absent. Ca^{2+} spikes persist in the dendrites and travel to the soma to produce the aforementioned small somatic deflections in membrane potential.

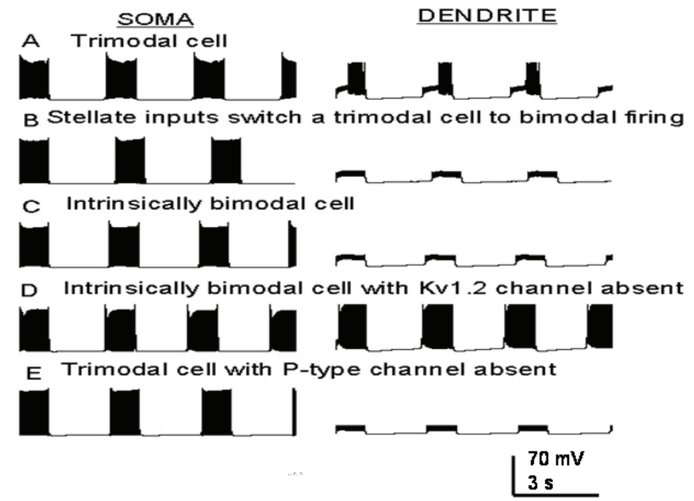

Figure 2.4 Model output. **The Purkinje cell model can replicate experimentally observed bimodal patterns of Purkinje cell firing**. Left panels are somatic membrane potential and right panels are dendritic membrane potential (vs. Time). By referring to the dendritic membrane potential one can distinguish bursting from tonic firing at the soma - because bursting, unlike tonic activity, is co-incidental with dendritic spiking. *A,* The standard Purkinje cell model fires in a repeating trimodal pattern. *B*, Addition of inhibitory input switches the standard model out of the trimodal pattern and into a repeating bimodal pattern of tonic spiking and quiescence. *C*, Modifying the K_K parameter (50 to 0.8) makes the model intrinsically bimodal - firing bimodally (tonic spiking and quiescence) in the absence of inhibitory input. *D*, Removal of Kv1.2 channels converts the model's intrinsic bimodal pattern (Panel *C*) into a trimodal pattern. *E*, Removal of P-type Ca^{2+} channels converts the model's intrinsic trimodal pattern (Panel *A*) into a bimodal pattern.

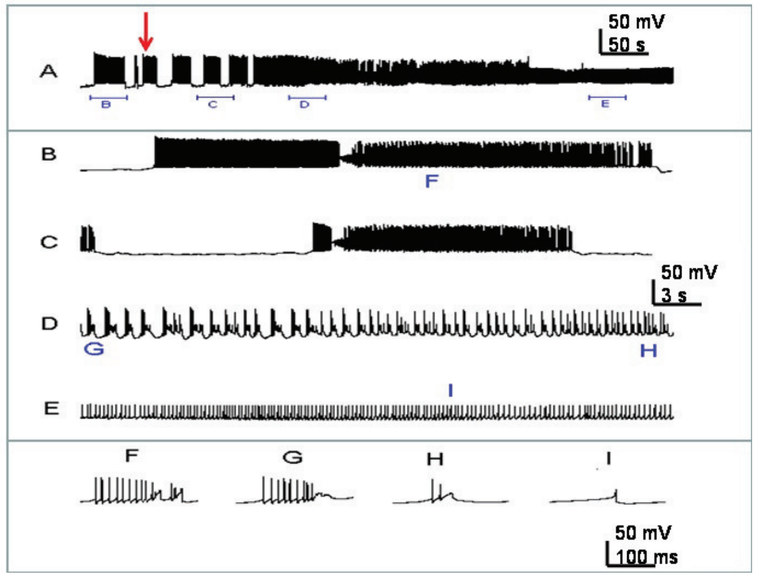

Figure 2.5 Experimental data. **Ouabain block of the Na^+/K^+ pump switches Purkinje cell activity out of the trimodal firing pattern and into a continuous burst mode that ultimately converges upon depolarisation block**. Panel *A* shows a whole cell patch clamp recording from a Purkinje cell following the application of 2.5 μM ouabain. The arrow denotes the time at which we feel that ouabain starts to modify Purkinje cell firing (recording courtesy of Mark Wall at the University of Warwick, personal communication). Panels *B*, *C*, *D*, and *E* correspond to the labelled parts of panel *A*. Panels *F*, *G*, *H* and *I* show individual bursts from *B*, *D*, *D* and *E* respectively. The initial firing mode, before any Na^+/K^+ pump block, is trimodal (panel *B*). With time, as Na^+/K^+ pumps become blocked, the trimodal pattern's quiescent periods get shorter until they are eventually abolished and the cell fires continuously (panel *A*). Over this same period the length of the trimodal pattern's tonic mode also decreases, ceding to an increasing propensity to burst (compare panels *B* and *C*). Indeed, by the time of continuous firing (panel *D*) there is only bursting and no tonic fraction at all. This continuous bursting has a gradient of depolarisation (Panel *A*) and, as it depolarises, the number of spikes per burst steadily decreases (*F*, *G*, *H*) until the soma enters depolarisation block and there are none. In this case, the only deflections observed are those of the Ca^{2+} spikes that have travelled into the soma from the dendritic arborisation (*E*, *I*). Panel *A* scaling is encoded in the first scale bar (50mV, 50s). The scaling of panels *B*, *C*, *D* and *E* is encoded in the second scale bar (50mV, 3s). The scaling of panels *F*, *G*, *H* and *I* is encoded in the third scale bar (50mV, 100ms).

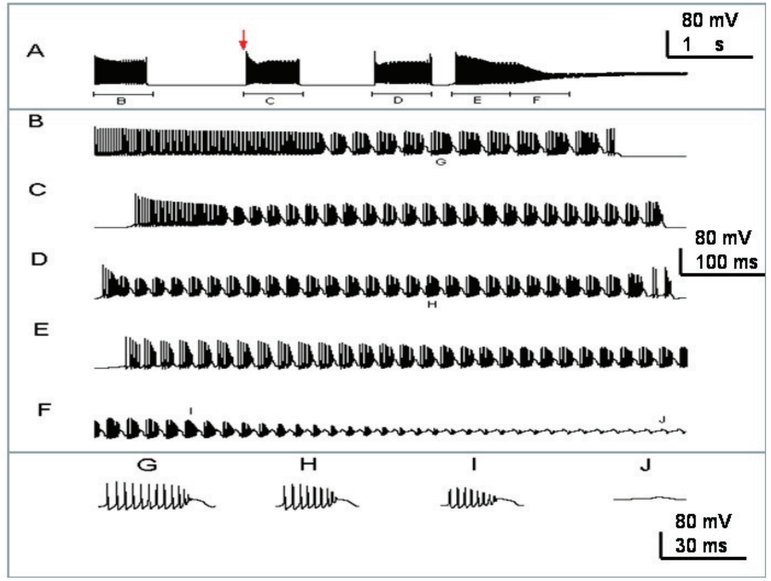

Figure 2.6 Model output. **The model can replicate the response of Purkinje cells (firing in the trimodal pattern) to Na^+/K^+ pump block by ouabain**. *A*, Somatic membrane potential (vs. Time) with the arrow denoting the onset of Na^+/K^+ pump block. Panels *B*, *C*, *D*, *E* and *F* correspond to the labelled parts of Figure *A*. Panels *G*, *H*, *I* and *J* show individual bursts from *B*, *D*, *F* and *F* respectively. The firing pattern in control, before any Na^+/K^+ pump block, is trimodal (panel *B*). Following the onset of Na^+/K^+ pump block, the trimodal pattern's quiescent periods get shorter until eventually they are abolished and the cell fires continuously (panel *A*). Over this same period the duration of the trimodal pattern's tonic mode also decreases, leading to an increased proportion of burst firing (compare panels *B*, *C* and *D*). Indeed, by the time cells are continuously active the firing only consists of bursts, with no tonic mode remaining (panel *E*). This continuous bursting has a gradient of depolarisation (Panel *A*) and, as it depolarises, the number of spikes per burst steadily decreases (*G*, *H*, *I*) until the soma enters depolarisation block and there are none. In this case, the only deflections observed are those produced by Ca^{2+} spikes that have travelled to the soma from the dendritic arborisation (*F*, *J*). Panel *A* scaling is encoded in the first scale bar (80mV, 1s). The scaling of panels *B*, *C*, *D*, *E* and *F* is encoded in the second scale bar (80mV, 100ms). The scaling of panels *G*, *H*, *I* and *J* is encoded in the third scale bar (80mV, 30ms).

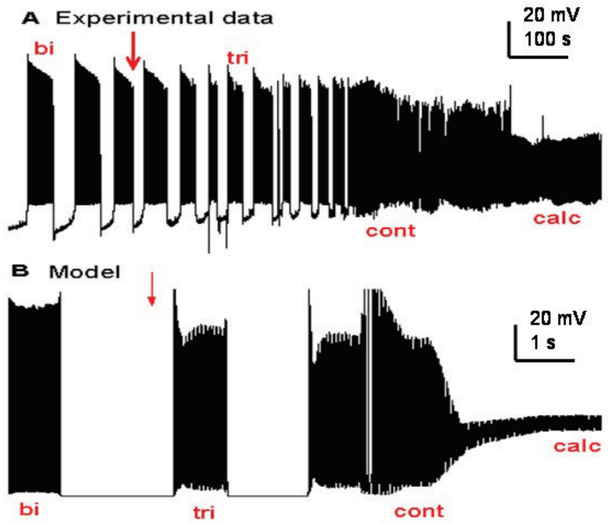

Figure 2.7 Experimental (*panel A*) and model (*panel B*) data plots. **With inhibitory synaptic inputs unblocked, some Purkinje cells fire in a repeating bimodal pattern (tonic spiking/quiescence) and the model can replicate the experimental response of these cells to Na^+/K^+ pump block by ouabain**. *A*, Whole cell patch clamp recording from a Purkinje cell (with GABA synaptic inputs unblocked) in control and following the application of 2.5 μM ouabain (recording courtesy of Mark Wall at the University of Warwick, personal communication). The arrow denotes the time at which we feel that ouabain starts to modify Purkinje cell firing. In control, the Purkinje cell activity is in the repeating bimodal pattern (*bi*). Following the addition of ouabain, the firing pattern is switched from bimodal to trimodal (*tri*) and then transitions into continuous bursting (*cont*) and somatic depolarisation block (*calc*). *B*, With GABAergic synaptic inputs, the model replicates this Purkinje cell response to ouabain. The arrow denotes the onset of simulated ouabain application.

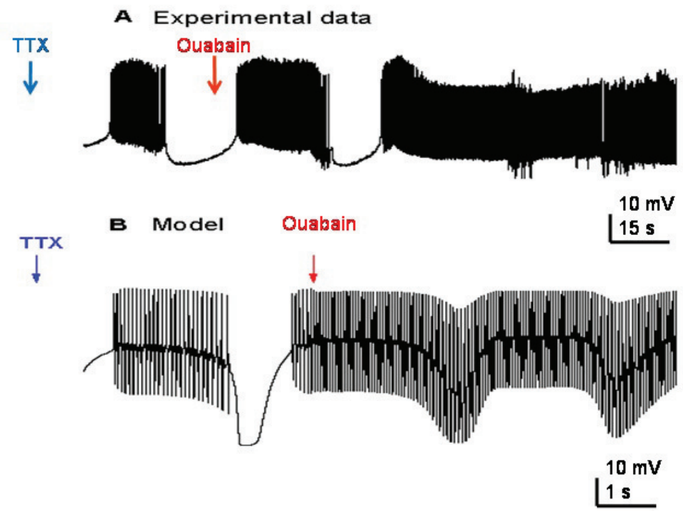

Figure 2.8 Experimental (*panel A*) and model (*panel B*) data plots. **Upon Na^+ channel block, real and model Purkinje cells express a repeating bimodal pattern (activity/quiescence) and Na^+/K^+ pump block eradicates its quiescent component**. *A*, Whole cell patch clamp recording from a Purkinje cell in the presence of 1 μM TTX (to block Na^+ channels), which sets a repeating bimodal pattern of activity and quiescence, before the introduction of 2 μM ouabain (to block the Na^+/K^+ pump) eradicates quiescence and renders continuous activity (recording courtesy of Mark Wall at the University of Warwick, personal communication). *B*, The model's somatic membrane potential (vs. Time), with arrows denoting the onset of TTX simulation (Na^+ channel density = 0) and ouabain simulation (Na^+/K^+ pump densities reduced as a function of time), replicates the experimental recording.

Chapter 3

A reduced compartmental model of the cerebellar Purkinje cell that is suitable for deployment in network models of the cerebellar cortex.

3.1 Introduction

There are presently two principal, but minimally interacting, levels of investigation in computational neuroscience. In the first, researchers use Hodgkin-Huxley models of currents (1952) and compartmental/cable modelling of dendrites (introduced by Rall, 1959) to assemble detailed single neuron descriptions. In the second, researchers study neural circuits and find it useful to represent each neuron and synapse as simply as possible, ignoring much of the biological detail. A major reason for this demarcation is that the computational complexity of the former is not conducive to the scaling of the latter. For example, the Purkinje cell model of *chapter 2* requires 22 minutes of CPU time for 1 second of simulation and so it is too computationally expensive to use in a network model of the cerebellar cortex, with its many constituent Purkinje cells. This issue is unfortunate as there is some evidence that the richness of biophysical properties on the single neuron scale can supply mechanisms that serve as the building blocks for network dynamics (Getting, 1989).

In neuromodelling there is great potential for bridging the gap between these two levels of enquiry using networks of neurons with a level of complexity and biological fidelity intermediate between highly detailed multi-compartmental models and simple network models. In this chapter, we take the detailed Purkinje cell model of *chapter 2* and use mathematical transforms to collapse its dendrites into fewer compartments, to produce a simpler, surrogate version with the same electrical properties.

3.2 Materials and Methods

To generate a simpler version of the Purkinje cell model of *chapter 2*, the dendritic arbour was collapsed into fewer compartments with a reduction algorithm that conserves axial resistance (R_a) (Bush and Sejnowski, 1993; Destexhe et al., 1998). The method consists of merging successive dendritic branches into equivalent cylinders, preserving the axial resistance of the original branches. With this method, the radius (R) of an equivalent cylinder is given by:

$$R = \sqrt{\sum_i r_i^2} \tag{3.1}$$

Where r_i are the radii of the collapsed branches for that equivalent cylinder. The length (l) of an equivalent cylinder is taken as an average of the lengths of the collapsed branches (l_i) for that cylinder, weighted by their respective radii (r_i):

$$l = \frac{\sum_i l_i r_i}{\sum_i r_i} \tag{3.2}$$

With this collapsing method, the membrane surface area of the reduced model is less than the original because, although axial resistance is conserved, surface area (and hence the membrane resistance and capacitance) is not. This is compensated for by introducing, in each equivalent cylinder, a dendritic correction factor (C_d), which rescales the current/pump/exchanger density values (g_i) and membrane capacitance (C_m) in the dendrites such that:

$$g_i^{'} = C_d g_i \tag{3.3}$$

$$C_m^{'} = C_d C_m \tag{3.4}$$

The dendritic correction factor C_d is the ratio of the total surface area of the dendritic segments to their equivalent cylinders. The model's somatic compartment is not introduced into the collapsing algorithm and so in the reduced model it has the same dimensions as in the full model, and the C_d correction factor is not applied to any of its parameters.

Following the methodology of Destexhe et al. (1998), our reduced Purkinje cell model had C_d applied to the model parameter, *depth*, which sets the depth of the sub-membrane shell that Ca^2 diffuses in within the model dendrites (the dendrite description of intracellular Ca^{2+} dynamics is sourced from Miyasho et al., 2001).

$$depth^{'} = C_d depth \tag{3.5}$$

There are a number of published mathematical transformations for collapsing dendrites into equivalent profiles (for a review, refer to Burke, 2000). We favoured this "R_a conservation" algorithm because it has been shown to produce reduced, surrogate models that capture the synaptic integration properties of their full, parent models i.e. reduced models produced by this algorithm can perform the same non-linear integration of dendritic EPSPs and IPSPs and hence have the same input-output function as their parent models (Bush and Sejnowski, 1993).

We used this "R_a conservation" algorithm to collapse the 1089 compartments of the full Purkinje cell model into the 41 compartments of a reduced model (1 soma, 40 dendritic compartments). The reduced model's 40 dendritic compartments were allocated smooth and spiny (20 smooth, 20 spiny) in an arbitrary mirroring of the full model (85 smooth, 1003 spiny). Note that in our approach, smooth and spiny dendrites are not distinguished from one another by the actual modelling of dendritic spines, but by empirical representation, with a larger specific membrane capacitance (C_m) for spiny dendrites (Miyasho et al., 2001). C_d was 3.80. The dimensions of the soma were as in the full morphology (length = 22 μm; diameter = 22 μm) and the dimensions of the 40 dendritic compartments are shown in *table 3.1*.

The *Q* parameter is a setting in the model's description of extracellular K^+ dynamics (refer *chapter 2*) and in the full model it is 0.143. In order for our reduced model to replicate full model behaviours we had to change this parameter to 0.033, which is reasonably distinct from the value of 0.543 obtained by a C_d manipulation (0.143 * C_d = 0.543, where C_d is 3.80). We utilised 0.033 as opposed to 0.543 because it conferred closer behaviour to the full model and because there is no precedence in the literature for applying C_d in this way. This parameter, Q, isn't set or constrained by any feature of the reduction algorithm used. Thus, in our reduction process there was a model parameter (*Q*) that needed manual tuning to get best fit between reduced and full model output.

We strove for a small number of compartments, but through testing we found that 41 (1 soma, 40 dendrite) was the smallest number that could behave equivalently to the full 1089 compartments. Through further testing we ascertained that this is because the collapse algorithm employed doesn't conserve dendritic length fully (*see * below*) and that Purkinje functioning requires a degree of uncoupling (distance) between somatic and dendritic events. 41 compartments is the smallest number that confers sufficient uncoupling (distance). Without this, for instance if the reduced model is the full model transposed to just 3 compartments, the tonic mode is absent in the trimodal firing pattern i.e. the reduced model of 3 compartments cannot replicate the Purkinje cell's trimodal firing pattern. By contrast, the reduced model of 41 compartments can replicate this activity motif.

* The length of the 40 dendritic compartments (collapsed from the original 1089 compartments, using the described "R_a conservation" algorithm) in the 41 compartment model is ~502 μm. With this same algorithm and substrate, the length of 22 collapsed dendritic compartments is ~359 μm and the length of 3 collapsed dendritic compartments is ~129 μm. Models with the latter two dendritic lengths are too short to replicate the trimodal firing pattern. Exhaustive testing of many different compartment numbers determined that 40 dendritic compartments is the lowest compartment number that provides the minimum dendritic length required (~502 μm).

We established that the problem with the 3 compartment model was a lack of dendritic distance, rather than a lack of dendritic load, because increasing dendritic load could not enable a compartment number lower than 41. The "rallbranch" variable is unique to the NEURON simulator (Hines and Carnevale, 1997). When a model compartment has a rallbranch number of *n* it is as though there are [*n*] mathematically identical compartments, including the entire sub-tree, connected to that compartment. This is a method of adding load to a dendritic tree without adding load to computation time. However, increasing rallbranch numbers could not decrease the compartment number requirement and thus it is not a load requirement that is limiting.

The reduced model (41 compartments) ran ~19 times faster than the full model (1089 compartments) - it requires 68 seconds of CPU time for 1 second of simulation, as compared to the full model's 22 minutes. However, this reduced model still requires 22 minutes of CPU time to replicate a single cycle of the trimodal firing pattern if its pattern

length is the shortest that has been experimentally reported - 20 seconds (Womack and Khodakhah, 2002). Longer pattern lengths (e.g. 20 minutes) take longer to simulate. Given the protracted timescale of Purkinje behaviours, simulating them is a formidable challenge even with reduced models.

Our reduced Purkinje cell model could replicate the intrinsic firing behaviour (e.g. the trimodal firing pattern) of the full model, which itself can replicate intrinsic behaviours of a real Purkinje cell. After some time researching the properties of our reduced 41 compartment model, we had a renewed appetite for further simplification. But of course this was hindered by the aforementioned problem of dendritic distance. We sidestepped this issue by collapsing the dendritic tree of the full model to just 3 compartments (using the "R_a conservation" algorithm), and linking these three to the soma through a coupling compartment that had dimensions of our setting. This coupling compartment had the same passive and conductance properties as the three dendritic compartments and, indeed, can just be thought of as component to the reduced model's dendritic tree. We manually tuned the coupling compartment's dimensions to confer the right degree of uncoupling between soma and dendrites; to ensure that this 5 compartment model could replicate the behaviours of the 41 compartment and 1089 compartment models. In the tuned and final 5 compartment model, its C_d value (the ratio of [membrane surface area upon its 4 dendritic compartments: membrane surface area upon the full model's 1088 dendritic compartments]) was 4.79. The total length of its dendritic compartments was ~529 μm. For this 5 compartment model, we had to modify the aforementioned *Q* parameter, from 0.143 (as it is in the full model) to 0.02, to replicate full model behaviour. This modification in no way approximates a C_d multiplication (0.143 * C_d = 0.68, where C_d is 4.79). The dimensions of the soma were as in the full morphology (length = 22 μm; diameter = 22 μm) and the dimensions of the 4 dendritic compartments are shown in *table 3.2*. The "coupling compartment" is compartment number 1 in this table.

Given that this 5 compartment model has some "dimensions of our setting" it does lose some line of sight to the full model and the biology. But at this cost it runs much faster, with 26 seconds of CPU time required for 1 second of simulation, which is ~51* faster than the full model, and ~3* faster than the 41 compartment model.

3.3 Results

Figure 3.1 shows that the 1089, 41 and 5 compartment models can all spontaneously fire in the trimodal pattern of activity i.e. they are qualitatively equivalent. *Figure 3.2* shows that the 1089, 41 and 5 compartment models all respond equivalently to simulated ouabain block of the Na^+/K^+ pump. The different models have matching qualitative behaviour with minor quantitative discrepancies, which could presumably be minimised further by continued manual tuning of *Q* parameters.

3.4 Discussion

Our reduced models run much faster than the full model, yet faithfully reproduce its electrical behaviour. This similarity, between the outputs of the full model and its derivatives (the 41 compartment and 5 compartment models), serves to illustrate the

reproducibility (semi-quantitative) of the computational experiments performed with the full model in *chapter 2*. So, the work in this chapter reinforces and validates the work in *chapter 2*.

Our reduced models are the first intermediate-complexity models for the cerebellar Purkinje cell. We hope that others will see the benefit of their lower computational costs and utilise them in network simulations in the future. In this way we hope that these reduced models will be a bridge between studies of the cerebellar Purkinje cell and those of the cerebellar network. At present these are largely studied independently (in experiment and computation), which may be overly reductionist as cellular features are likely to be very important in system functioning. To elucidate brain functioning we believe that ultimately we need to build bridges between the different levels of description - to relate genes to molecules, molecules to cells, cells to systems, and systems to behaviour and perception. We lay the framework for one bridge in this study, by producing a detailed Purkinje cell model that has a low computational overhead and hence suitability for inclusion in network simulations.

Our most reduced model (5 compartments) is likely *not* the most minimal biophysical/mathematical description that can account semi-quantitatively for the dynamical features of the full model. We envisage that there is still margin for this description to be further idealized while retaining enough accountability to the full formalism. For instance, although we have sought to reduce the compartment number, we have not investigated if any currents can be omitted without perturbation of the dominant qualitative mechanisms. It is likely that some can. An absolutely minimal description contains only elements thought to be essential. The pathway to this account is usually by including additional features when the model is deemed too limited. But we suggest that in the future this account can be converged upon by pruning our 5 compartment model. Of course, this pruning is to move further along the abstraction gradient, with a loss of much biological realism, which is a path that we were anxious not to take ourselves. However, we do see that the result could have value, because with fewer variables and parameters (hence less computational overhead) it will enable protocols unfeasible in fuller models. For instance, it could permit one to explore rather thoroughly the dependence on parameters, which we could not do (to the extent that we would have liked) in the fuller models. Although we do predict that the most minimal working description would still not be just a single compartment, because trimodal bursting depends on spatiotemporal interactions between the soma and dendrites that require their (incomplete) electrical decoupling, and such decoupling cannot be represented in an isopotential, single compartment.

Although our reduced models are very useful it is important to know their limits. For instance, be aware that a single IPSP/EPSP on an equivalent dendrite of a reduced model is not equivalent to a single IPSP/EPSP on a single dendrite of the full model. Rather it is equivalent to dividing this IPSP/EPSP and applying one fraction of it to each of the real dendrites represented by the equivalent dendrite. Thus, a reduced model is not appropriate for studying the effect of *single* synaptic inputs on single dendritic branches of Purkinje cells, or for studying local dendritic processing in general. For example, we

cannot use a reduced model to investigate clustering of individual synaptic inputs or the inhibitory control of specific dendrites. Such studies must use the full Purkinje cell model that represents each process of the neuron explicitly. The reduced models are however useful for studying the effect of *multiple* synaptic inputs that are diffuse over the dendritic tree. Such work is conducted in the next chapter.

Table 3.1 Dimensions of the 40 dendritic compartments in the 41 compartment model. Compartment 1 is linked to the somatic compartment.

Compartment	Length (μm)	Diameter (μm)
1	20.545455	3.3166248
2	19.4	2.236068
3	18	1.7320508
4	17.571429	2.6457513
5	8.5306122	3.3045423
6	13.344828	2.6305893
7	12.567568	2.8213472
8	16.9	3.1622777
9	11	3.3166248
10	10.352941	3.4467376
11	12.732394	3.9849718
12	12.5	3.7309516
13	10.475728	4.7791213
14	15.361446	4.3405069
15	11.986486	3.9899875
16	12.692308	5.5497748
17	10.326667	5.9665736
18	9.6402116	6.9079664
19	13.5625	6.2289646
20	9.8686831	6.5415792
21	10.347368	6.6932802
22	8.5744681	7.5232971
23	10.075188	8.2267855
24	9.5446429	7.3972968
25	8.6412429	9.1389277
26	8.8216783	8.5135187
27	8.1569732	9.4462488
28	6.1189159	8.5064444
29	7.8575581	10.055844
30	6.7650755	10.560032
31	6.892365	10.617743
32	6.5219251	11.041739
33	7.6343948	11.421714
34	7.9040284	10.478619
35	10.028048	10.878798
36	18.067147	9.2108216
37	17.821097	8.0038358
38	57.640576	7.3301444
39	24	3.5777088
40	18	4

Table 3.2 Dimensions of the 4 dendritic compartments in the 5 compartment model. Compartment 1 is linked to the somatic compartment.

Compartment	Length (μm)	Diameter (μm)
1	400	3
2	16.11816	18.5088
3	95.16785	7.947963
4	18	4

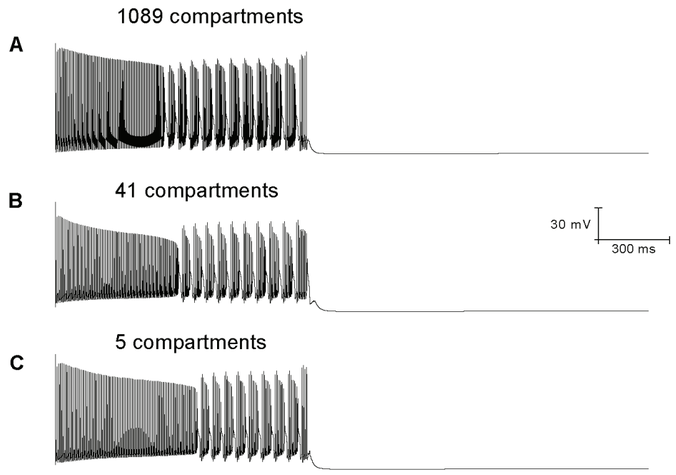

Figure3. 1 The 1089, 41 and 5 compartment models can all spontaneously fire in the trimodal pattern of activity i.e. they are qualitatively equivalent.

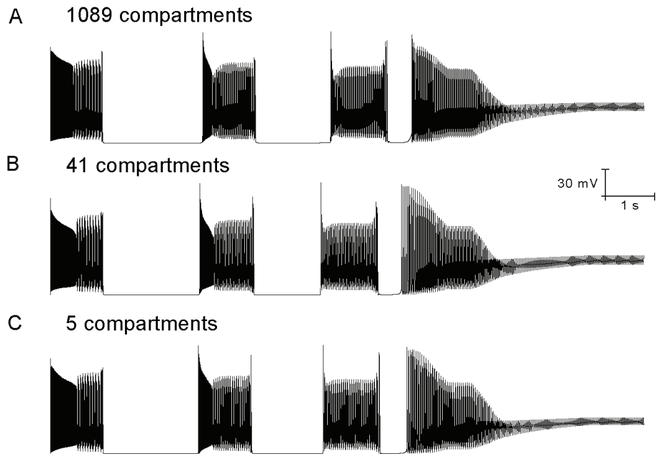

Figure 3.2 The 1089, 41 and 5 compartment models all respond equivalently to simulated ouabain block of the Na^+/K^+ pump.

Chapter 4

An intracellular calcium computation permits the Purkinje cell model to perform toggle and gain computations upon its inputs.

4.1 Introduction

In contrast to the complexity of other brain regions, the cerebellum has a single repeating connectivity motif (Ito, 1984). This motif consists of parallel, climbing, basket and stellate inputs feeding into a central Purkinje cell, which transforms them into an output. The relative simplicity of the cerebellar motif makes it a good focal point for trying to understand how a brain circuit actually computes. Ultimately its computation collapses to one question, how does the Purkinje cell compute? In particular, how does its morphology and conductances transform/encode its inputs into an output? Our work addresses this issue. In *chapter 2* we researched the intrinsic activity of the Purkinje cell, and how it is modulated by stellate cell input (*section 2.4.6*). In this chapter we investigate how this intrinsic activity is modulated by climbing and parallel fiber inputs. We show how the Purkinje cell performs computations with these inputs, to generate an output.

4.2 Materials and Methods

Numerical simulations. The Purkinje cell model for this chapter is almost identical to the 41 compartment model described in Chapter 3, with the same morphology and largely the same incorporated ion currents/channels, at the same densities. However, this model differs in having no Kv1.2 channels, no Na^+/Ca^{2+} exchanger and no Na^+/K^+ pump description in the dendrites (it does, however, have the same Na^+/K^+ pump descriptions at the soma). Also, in this model, extracellular K^+ concentration ($[K^+]_o$) is not set by a formula but is a fixed constant (2.5 mM). In short, this model doesn't have the {Kv1.2, $[K^+]_o$ accumulation, Na^+/K^+ pump, Na^+/Ca^{2+} exchanger} system in its dendrites.

The model of this chapter can fire in the trimodal pattern of activity, like the 41 compartment model of Chapter 3. The two models are conceptually equivalent, reproducing the trimodal pattern with the same incorporated ideas. The difference is that the model of this chapter is more abstractive in its implementation. The added abstraction of this model is a limitation. However, abstraction is necessarily inherent to all neuronal modelling and the additional abstraction is founded upon good rationale, it benefits the simulation speed and reduces the parameter number which greatly facilitated the manual tuning of the model to replicate the complex Purkinje cell response to climbing and parallel fiber inputs. So, the model of this chapter is a further simplification; simplified for practical reasons. It does however incorporate, and is an investigation into, the same hypotheses.

The models differ in relation to the [tonic → burst] transition in the trimodal pattern of firing. The same concept drives this transition in both models, but the models differ in the level of detail that this shared concept is represented at. The model of Chapter 3 has a {Kv1.2, $[K^+]_o$ accumulation, Na^+/K^+ pump, Na^+/Ca^{2+} exchanger} system in its dendrites controlling this transition, whereas the model of this chapter doesn't have this dendritic system. It's tonic to burst transition is instead controlled by a slowly inactivating D-type K^+ current (I_D), which is set to be a simulacrum of the {Kv1.2, $[K^+]_o$ accumulation, Na^+/K^+ pump, Na^+/Ca^{2+} exchanger} system. The D-type K^+ current is in place of Kv1.2 (which is reasonable because they are likely equivalent; Shen et al., 2004) and the decrease in this current over time, through a very slow inactivation mechanism, empirically captures a slow decrease in K^+ current through ion relaxation processes (which in the other model are modelled explicitly; set by its incorporated $[K^+]_o$ accumulation, Na^+/K^+ pump, Na^+/Ca^{2+} exchanger mechanisms). So, to reiterate, the difference between the models is not conceptual. The same intellection drives the tonic to burst transition in both models, but the model of Chapter 3 encapsulates it with a relatively detailed abstraction whilst the model of this chapter encapsulates it with a simpler abstraction. This is expanded on in following paragraphs.

The 41 compartment model in Chapter 3 can fire in the trimodal pattern of activity, with K^+ flux through Kv1.2 channels controlling its tonic to burst transition. Dendritic Ca^{2+} spikes generate the bursting mode. The Kv1.2 channels produce hyperpolarizing current which clamps dendritic excitability and prevents Ca^{2+} spike generation, thus permitting the tonic mode of firing. However, the power of this excitability clamp diminishes with time because extracellular K^+ accumulates ($[K^+]_o$ increases) and this reduces the electrochemical driving force for K^+ flow. Eventually the hyperpolarizing current produced by Kv1.2 channel activity is insufficient to prevent dendritic spiking and the model is switched from the tonic to the burst mode. During the quiescent mode of the trimodal pattern, Na^+/K^+ pump activity in the dendrites reduces the extracellular K^+ accumulation and "resets" $[K^+]_o$. The Na^+/Ca^{2+} exchanger permits Na^+ entry to the dendrites (dendrites have no voltage-gated Na^+ channels) so that the Na^+/K^+ pump can function – the Na^+/K^+ pump cannot pump K^+ into the dendrites if there is no Na^+ in the dendrites to be pumped outside. So, in this model the tonic to burst transition is controlled by a {Kv1.2, $[K^+]_o$ accumulation, Na^+/K^+ pump, Na^+/Ca^{2+} exchanger} system. The model of course has other K^+ currents/channels in its dendrites, but these are largely uninvolved in the clamping of dendritic excitation as, unlike the Kv1.2 channel which is low-voltage gated, they are high-voltage gated and not open at the relevant potentials. Although the incorporated D-type and A-type K^+ currents are low-voltage gated, they are still uninvolved as they inactivate quickly. The Kv1.2 current by contrast is non-inactivating, which is why its current persists long enough to be tempered by slow ion relaxation processes. Indeed, experiment has shown the Kv1.2 current to be non-inactivating in the Purkinje cell (McKay, 2005). We are open to the possibility that other low-voltage gated K^+ currents might be non-inactivating in the Purkinje cell, and involved in this regulation of the tonic to burst transition, but at this time Kv1.2 is the only current that has been experimentally implicated.

The model of this chapter can also fire in the trimodal pattern but it has no Kv1.2 channels. Its tonic to burst transition is instead controlled by the D-type K^+ current (I_D). This is not so distinct from the model of chapter 3, as the kinetics of the Kv1.2 and I_D currents are very similar. In fact, there is evidence that Kv1.2 is actually a channel correlate to the I_D current (Shen et al., 2004). The D-type K^+ current's inactivation formalism is modified in this model from its original form (Miyasho et al., 2001), with an added parameter ($k = 0.05$) that slows its inactivation:

$$\frac{dh}{dt} = (h_\infty - h)/\tau_h \tag{4.1}$$

$$h_\infty = \frac{\alpha_h}{\alpha_h + \beta_h} \tag{4.2}$$

$$\tau_h = \frac{1}{\alpha_h + \beta_h} \tag{4.3}$$

$$\alpha_h = k * \frac{0.0015}{1 + \exp((V + 89)/8)} \tag{4.4}$$

$$\beta_h = k * \frac{0.0055}{1 + \exp((V + 83)/-8)} \tag{4.5}$$

Where h is the Hodgkin-Huxley inactivation gate, t is time and V represents the membrane potential in mV as a dimensionless quantity.

In this model, I_D activates at simulation onset and its hyperpolarizing K^+ current clamps dendritic excitability and prevents Ca^{2+} spike generation, thus permitting the tonic mode of firing. However, I_D slowly inactivates over time, and when its current has diminished past a critical point it can no longer block dendritic Ca^{2+} spiking and the model is switched from the tonic to the burst mode. So, the rate of I_D inactivation (modulated by the k parameter) sets the tonic mode duration. To get a realistic tonic duration requires an extremely slow and unreported rate of I_D inactivation. However, we actually include this slow inactivation with the postulate that I_D, by analogy to Kv1.2, is non-inactivating and that this slow inactivation is an empirical capture of ion relaxation i.e. the slow inactivation of the I_D current empirically represents the slow decline in a non-inactivating I_D/Kv1.2 current because of ion relaxation. So, this model is conceptually equivalent to that of chapter 3, just more abstractive in its implementation.

In some model simulations, climbing fiber (CF) inputs were introduced. CF inputs make 17 excitatory synaptic contacts upon 17 of the model's proximal smooth dendrites (De Schutter and Bower, 1994b). They fire synchronously at a frequency of 1 Hz. Their reversal potential is 0 mV, with a synaptic weight of 1 μS and their amplitude upon activation follows a dual exponential time course ($\tau_1 = 0.5$ ms; $\tau_2 = 1.2$ ms) (De Schutter and Bower, 1994b).

In other model simulations, parallel fiber (PF) inputs were introduced. PF inputs make one excitatory synaptic contact upon each of the model's spiny dendrites (De Schutter and Bower, 1994b). They fire asynchronously around a mean frequency of input (100 Hz). Their reversal potential is 0 mV, with a synaptic weight of 0.005 μS and their amplitude upon activation follows a dual exponential time course ($\tau_1 = 0.5$ ms; $\tau_2 = 1.2$ ms). The Purkinje cell is known to receive ~ 200,000 parallel fiber synaptic contacts (Ito, 1984). Given computing resources, it was not possible for us include all these inputs and that is why our model has just 20 parallel fiber synaptic contacts (one on each spiny dendrite compartment) – 0.01% of the real value. Under the conditions of random, asynchronous inputs simulated here, this missing input is compensated for by an increased firing rate of each parallel fiber synapse. A similar approach has been taken by other Purkinje cell modellers (Rapp et al. 1992; De Schutter and Bower, 1994b). Assuming a linear scaling, our simulation of 0.01% of the inputs, with an asynchronous firing rate of 100 Hz, corresponds to the *realistic* average parallel fiber firing rate of ~ 0.01 Hz.

In some model simulations, both CF and PF inputs were introduced.

The intracellular Ca^{2+} dynamics abstraction, incorporated in the model dendrites, is modified from its original description in Miyasho et al. (2001). The modified form:

$$\frac{d[Ca^{2+}]_i}{dt} = \left(\frac{10000 * I_{Ca^{2+}}}{2 * F * depth}\right) + \left(\frac{-kt * [Ca^{2+}]_i}{[Ca^{2+}]_i + kd}\right) + \left(\frac{y - [Ca^{2+}]_i}{\tau_r}\right) \tag{4.6}$$

$$I_{Ca^{2+}} = I_{CaT} + I_{CaE} + I_{CaP} \tag{4.7}$$

Where $[Ca^{2+}]_i$ is the intracellular Ca^{2+} concentration in a supra-membrane shell of *depth* = 0.1 μm, F is the Faraday constant, $kt = 1*10^{-4}$ mM/ms, $kd = 1*10^{-4}$ mM, $\tau_r = 2$ ms and $I_{Ca^{2+}}$ is the Ca^{2+} membrane current which is the sum of the T-type (I_{CaT}), E-type (I_{CaE}) and P-type (I_{CaP}) voltage-gated Ca^{2+} currents (descriptions in Appendix A.2). Parameter y is the set point/equilibrium Ca^{2+} concentration that the system strives to return the Ca^{2+} concentration to after a perturbation. The equation form and all of the aforementioned parameters are as in Miyasho et al., 2001. However, whereas Miyasho et al. (2001) has y specified as a constant ($2.4*10^{-4}$ mM), in this model y is dictated by the following relationship:

$$\frac{dy}{dt} = \left(\frac{I_{Ca^{2+}} \Big/ [d \cdot F]/4}{g}\right) + \left(\frac{z - y}{m}\right) \tag{4.8}$$

Where $I_{Ca^{2+}}$ is the Ca^{2+} membrane current, F is the Faraday constant, d is the compartment diameter, $z = 2.4*10^{-4}$ mM, $g = 1*10^5$ and $m = 100$ ms. On the right hand side (RHS) of the equation, the first block is an intracellular Ca^{2+} accumulation term that

is equivalent to the intracellular Na^+ accumulation equation in Chapter 2 [eq. 2.3] (sourced from Canavier, 1999) but with the modification of an added parameter *g* (which has a role described later). The second block on the RHS has the same first order decay form as the third block on the RHS of equation [4.6], which was sourced from Miyasho et al. (2001).

Equation [4.8] dictates that *y*, the Ca^{2+} set point concentration, increases with Ca^{2+} influx into the cell. Through equation [4.6], this increase in *y* then drives increased $[Ca^{2+}]_i$. Studying equations [4.6] and [4.8], it should be clear that *y* is in essence a floating set point for $[Ca^{2+}]_I$ that adheres to a true, fixed set point: $z = 2.4*10^{-4}$ mM.

In these equations dictating $[Ca^{2+}]_i$, accumulation is applied to $[Ca^{2+}]_i$ both directly (the first block on the RHS of eq. [4.6] - the equation for $[Ca^{2+}]_i$) and indirectly (the first block on the RHS of eq. [4.8] - the equation for *y*). The former captures $[Ca^{2+}]_i$ accumulation on the scale of milliseconds, during $Ca^{2+}/[Ca^{2+}]_i$ spiking for instance, and the latter captures more gradual accumulation over seconds and minutes. Without this layered system, using the intermediary of the *y* parameter, it is not possible to have $[Ca^{2+}]_i$ accumulation over these longer time scales without disrupting the fast spiking in $[Ca^{2+}]_i$, which is relevant as this spiking is integral to the operation of the Purkinje cell model ($Ca^{2+}/[Ca^{2+}]_i$ spikes in the dendrites drive somatic bursting, refer *Chapter 2*). Anyhow, we believe that a "creeping" Ca^{2+} set point is a very realistic proposition as Ca^{2+} efflux and buffering systems are sub-linearly dependent on $[Ca^{2+}]_i$, as they rely on enzymes that have saturation (Michaelis-Menten) kinetics.

The *g* and *m* parameters control the rate of increase (and decrease) in the Ca^{2+} set point concentration (*y*). Their value is controlled by the value of parameter *w*:

Initial condition, w = 0
if ($I_{Ca^{2+}} > 0.06$ mA/cm^2) {w = 1}

$$\frac{dw}{dt} = \left(\frac{-w}{f}\right) \qquad f = 100 \text{ ms}$$

if (w > 0.1) {g = 10,000, m = 1000}
if (w < 0.1) {g = $1*10^5$, m = 100} (4.9)

The default value of *w* is 0 and so the default values of *g* and *m* are $1*10^5$ and 100 respectively. However, if $I_{Ca^{2+}}$ surpasses 0.06 mA/cm^2, as it does when there is a climbing fiber (CF) input, *w* is set to 1 and the *g* and *m* parameters are updated to 10,000 and 1000 respectably. The rational for these parameter changes are that the dramatic CF associated Ca^{2+} influx floods the Ca^{2+} regulatory systems and with their nonlinearity they cannot increase their activity to match the increasing $[Ca^{2+}]_i$, in which case the rate of increase in $[Ca^{2+}]_i$ must rise. Parameter *f* controls the lifespan of these changed *g* and *m* values, after a CF input event, by controlling a rate of attenuation to the *w* parameter. When *w* declines to below 0.1, *g* and *m* revert to default. However, if there is another CF input event before *w* falls to below 0.1, *w* is reset to 1 which prolongs the lifespan of *g* and *m* at their updated values for another cycle of *w* decline.

The model dendrites have an SK type Ca^{2+}-activated K^+ conductance (sourced from Moczydlowski and Latorre, 1983), of density g_{sk}, which is activated only upon the condition of CF input. This condition is realised by g_{sk} being 0 at default but, upon CF input, it being reassigned a positive value. The value of g_{sk} is controlled by the value of parameter *r*:

Initial condition: r = 0
if ($I_{syn} > 3$ nA) {r = 1}

$$\frac{dr}{dt} = \left(\frac{-r}{s}\right) \qquad s = 1000 \text{ ms}$$

if (r > 0.1) { $g_{sk} = 0.72$ S/cm^2}
if (r < 0.1) { $g_{sk} = 0$ S/cm^2} (4.10)

The default value of *r* is 0 and so g_{sk} at default is 0 S/cm^2. However, if there is CF input, I_{syn} (the synaptic current across the CF synapses) exceeds 3 nA and *r* is set to 1, g_{sk} is thus updated to 0.72 S/cm^2. This system captures the essence that g_{sk} is the density of an SK conductance that is *only* activated by Ca^{2+} entry generated by CF input. It is not activated by the equivalently large Ca^{2+} entries during the trimodal bursting mode. This system is an empirical representation of a postulated compartmentalisation to the intracellular Ca^{2+} dynamics in the Purkinje cell dendrite, where we hypothesise that there is an SK Ca^{2+}-activated K^+ conductance that is activated only by CF generated Ca^{2+} influx. Ca^{2+} compartmentalisation has been observed experimentally before for the Purkinje cell, but in other contexts (Womack, 2004). Parameter *s* controls the lifespan of this changed g_{sk} value, after a CF input event, by controlling a rate of attenuation to the *r* parameter. When *r* declines to below 0.1, g_{sk} reverts to default. However, if there is another CF input event before *r* falls to below 0.1, *r* is reset to 1 which prolongs the lifespan of g_{sk} at its updated value for another cycle of *r* decline.

This system of intracellular Ca^{2+} dynamics was built and incorporated in the Purkinje cell model to endow it with the ability to replicate the experimentally observed CF toggling of the Purkinje cell state (refer *Results*). And the system's free parameters (*g*, *m*, *f*, *w*, *z*, g_{sk}, *r*, *s*) were manually tuned to attain this replication. Of course it is an abstraction, but it is founded upon good rationale in the absence of good experimental data - our present understanding of intracellular Ca^{2+} dynamics is extremely limited and so there is not much to guide and constrain its modelling.

Experimentally, repetitive CF input (1 Hz) doesn't always produce Purkinje toggling. In some cases it induces a different Purkinje firing pattern in which tonic activity is punctuated, at a frequency of 1 Hz, by a complex spike and its short evoked after-pause (refer *Results*). In our model, CF input generates this pattern, as opposed to the CF driven bimodal patterning, when the raised value of g_{sk} is 0.62 S/cm^2 as opposed to 0.72 S/cm^2.

4.3 Results

4.3.1 Parallel fiber inputs change the frequency, but not the pattern, of Purkinje cell firing

In the model, with the introduction of parallel fiber inputs (refer *methods*), the frequency of firing in the trimodal pattern's tonic mode shifts from 99 to 132 Hz – a 33% increase.

4.3.2 Climbing fiber input blocks trimodal output

A climbing fiber (CF) input induces a Ca^{2+} spike event in the dendrites, which produces a *complex spike* at the soma (Kandel et al., 2000). *In vitro*, if a Purkinje cell firing in the trimodal pattern is presented with repetitive CF input, at a physiological frequency (1 Hz), then its trimodality is replaced with a more naturalistic, nonbursting pattern of tonic firing (McKay et al., 2007). This tonic firing can be in the context of a repeating bimodal pattern of tonic firing and quiescence, with tonic firing termed the up state and quiescence the down state. In which case, the CF input, via its induced complex spike, toggles the Purkinje cell between the two states at a frequency of 1 Hz. When the cell is in the up state, CF input toggles it to the down state. When the cell is in the down state, CF input toggles it to the up state. It is presently unknown how identical CF inputs can produce such contrasting transitions. Addressing this issue, we have constructed a detailed biophysical Purkinje cell model that can replicate this CF toggling and which shows its basis to be intracellular Ca^{2+} dynamics (*figures 4.1, 4.2, 4.3, 4.4*).

CF input opens AMPA ionotropic receptors (AMPAR), which pass a depolarising cation flow (McKay et al., 2007). The AMPAR variant found in the Purkinje cell has a constituent $GluR_2$ subunit, with the [gluatamine/arginine] RNA editing site set to arginine, which sets it as impermeable to Ca^{2+} (Kandel et al., 2000). So, with CF input, no Ca^{2+} enters through AMPAR directly. However, the CF induced cation flow through AMPAR causes depolarisation, which opens voltage-gated Ca^{2+} channels locally, which raises intracellular Ca^{2+} concentration ($[Ca^{2+}]_i$) and augments the activation of hyperpolarising Ca^{2+}-gated K^+ channels (McKay et al., 2007). So, CF input directly prompts depolarising cation flow but also has a parallel, indirect hyperpolarising action.

The CF induced complex spike at the soma is a burst event. With experimental and model data, comparing a complex spike to a single burst from the trimodal firing pattern reveals much similarity. This then raises the issue of why a single complex spike can toggle the Purkinje cell to quiescence and a single burst of the trimodal pattern cannot. Our model incorporates our hypothesis that there is a compartmentalisation to the intracellular Ca^{2+} system, with an SK Ca^{2+}-regulated K^+ conductance that is activated by CF associated Ca^{2+} influx, but not by bursting associated Ca^{2+} influx. Ca^{2+} compartmentalisation has been observed experimentally before for the Purkinje cell, but in other contexts (Womack, 2004).

Our model incorporates our hypotheses that the tonic firing (up) state responds differently to CF input than the quiescent (down) state, because it has a different intracellular Ca^{2+} concentration. During tonic firing, intracellular Ca^{2+} accumulates as a function of voltage-gated Ca^{2+} entry, and during quiescence it recedes as Ca^{2+} extrusion exceeds any remaining Ca^{2+} entry. A CF input during tonic firing produces an [up-to-down] transition because, with the higher basal $[Ca^{2+}]_i$, it produces a *net* hyperpolarisation. A CF input

during quiescence produces a [down-to-up] transition because, with the lower basal $[Ca^{2+}]_i$, it produces a *net* depolarisation. In this way, the same stereotypical CF input produces two very different effects, depending on the prior state of the cell i.e. the CF input acts as a toggle switch, flipping the cell from whichever of the two states it is in to the alternate state.

In vitro, repetitive CF input (1 Hz) doesn't always switch a trimodal Purkinje cell to bimodal patterning. In some cases, it switches the cell to a tonic firing pattern, which is punctuated, at a frequency of 1 Hz, by a complex spike and its short evoked after-pause (McKay et al., 2007). In our model, CF input generates this pattern, as opposed to the CF driven bimodal patterning, when the CF conferred activation of SK is present but at lower amplitude (*figure 4.3*).

So, to summarise, repetitive CF input (1 Hz) blocks the trimodal firing pattern and replaces it with a tonic firing pattern, interrupted either by short or longer pauses. No bursting mode is observed. In both these firing patterns there are very long quiescent periods, where the only deflections in somatic membrane potential are attributable to CF driven spikes at the frequency of CF input and in which CF input cannot evoke a state transition into the firing state (McKay et al., 2007). The cause of these quiescent periods is not known. We hypothesise that they are generated by the electrogenic action of the Na^+/K^+ pump. So, we suggest that although CF input blocks the trimodal pattern's bursting mode, it does not block its quiescent periods, which we have shown to be generated by Na^+/K^+ pumping (*chapter 2*). Indeed, our incorporated Na^+/K^+ pump system enables the model to replicate these long quiescent periods in the CF produced tonic firing patterns.

To collate, we suggest that there are two different classes of pause/silence in Purkinje cell activity – 1) CF conferred (via the action of Ca^{2+}-regulated K^+ conductances) and 2) Na^+/K^+ pump conferred.

The validity of the model can be assessed by comparing its output (figures 4.1, 4.2, 4.3) to the experimental data (figure 4.4).

Parallel fiber (PF) input increases tonic firing frequency. CF input decreases it. In fact, CF input decreases the frequency of firing to a range where PF input can greatly increase it, setting the gain of the PF response (McKay et al., 2007). Our model replicates this gain computation. In the model, with the introduction of just PF inputs, the frequency of tonic firing shifts from 99 to 132 Hz – a 33% increase. With the introduction of just CF input (g_{sk} = 0.62 S/cm^2), the frequency of tonic firing shifts from 99 to 54 Hz – a 55% decrease. With CF input already introduced and then with the subsequent introduction of PF inputs, the frequency of tonic firing shifts from 54 to 80 Hz – a 68% increase. So, CF input confers a 68-33 = 35% gain in the PF induced frequency change.

We have thus far described the response of Purkinje cells firing in the trimodal pattern to 1 Hz CF input. Purkinje cells firing in the bimodal firing pattern (tonic firing and quiescence) respond to 1 Hz CF input in the same manner as trimodal cells, in the

experimental data (McKay et al., 2007) and the model (not shown). They are switched to a tonic firing pattern that has 1) long or short CF induced pauses and 2) longer pauses, which we suggest are generated by Na^+/K^+ pumping.

4.4 Discussion

CF toggled bimodal patterning, unlike the trimodal firing pattern, has been observed *in vivo* (Loewenstein et al., 2005). In this chapter's modelling, we show the mechanistic relation between the trimodal firing pattern and CF toggled bimodal patterning. In this way we are reconciling *in vitro* and *in vivo* behaviour. This is useful because a lot of research is conducted on the trimodal firing pattern (Womack and Khodakhah, 2002; Womack and Khodakhah, 2003; Womack et al., 2004; Womack and Khodakhah, 2004; Mckay and Turner, 2004; McKay and Turner, 2005; Mckay et al., 2005; Mckay et al., 2007) and the pursuit of this *in vitro* study assumes a correlation between the reduced and intact behaviour. This correlation doesn't necessarily have to be complete, but there certainly needs to be a real understanding to any differences so that it can be factored into *in vitro* drawn conclusions. Our study provides such an understanding.

Our Purkinje cell model captures the biophysics of the Purkinje cell's toggle and gain computations. This has broad interest because there are not many biophysical models of single neuron computation, despite an avid interest in the computational repertoire and power available to individual neurons (Sejnowski et al., 1988; Koch, 1999; Zador, 2000; London and Hausser, 2005; Herz et al., 2006; Mel, 2006). In particular, this is the first biophysically detailed model of a toggle computation for any neuron class.

Our model incorporates the innovative hypothesis that the Purkinje cell toggle and gain computations hinge on an underlying Ca^{2+} computation. The model's intracellular Ca^{2+} concentration provides memory (information store), recording the history of firing and inputs, to dictate how the model cell responds to future inputs. For example, the model's Ca^{2+} system memorizes a CF input, which causes it to then respond differently to a PF input than it would otherwise. This Ca^{2+} memory has a lifespan, and once it has expired, the model cell then responds by default, unless of course there is another CF input along to renew the memory setting. So, we hypothesise that the membrane potential is not the Purkinje cell's only computational element, but that its intracellular Ca^{2+} concentration is a computational element as well. These two interact, with the Ca^{2+} memory being encoded and decoded by the membrane potential. Encoding is by way of CF input causing membrane depolarisation, which then opens voltage-gated Ca^{2+} channels to raise the intracellular Ca^{2+} concentration. Decoding is by way of this Ca^{2+} concentration modulating the membrane potential via Ca^{2+}-activated K^+ channels. So, again this investigation hypothesises the importance of ion concentrations to neural functioning - a major theme of our work. We suggest that neural behaviour is not simply a function of ion channel kinetics, as in the Hodgkin-Huxley paradigm, but is also set by pumps, exchangers and changing ion concentrations.

What/where is the seat of memory in the brain? The membrane potential could conceivably act as a memory element through a persistent change in its potential or firing (Durstewitz, 2000). This persistence could be endowed by reverberating activity within a

"cell assembly" - a reciprocally/recurrent wired network (Hebb, 1949). Or it could be conferred by activity circulating in connectivity loops ("synfire chains") of feedforward-connected subgroups of neurons, with no direct feedback links between successive groups (Abeles, 1991). Or it could be endowed via single cell bistability, where the cell potential can be set to the alternate state for storage of information (Marder, 1996; Lisman, 1998). Such persistence could be the basis for short-term memory, as distinct from synaptic plasticity, which might underlie long-term memory. This short-term memory can be termed "working memory" - "the ability to transiently hold and manipulate goal-related information to guide forthcoming actions" (Durstewitz, 2000).

For Purkinje cells, we boldly propose that the intracellular Ca^{2+} concentration is their fundamental short-term memory store, as opposed to the membrane potential. Ca^{2+} memory has been proposed before, for other cell classes, with models distinguished by Ca^{2+} release from stores (Teramae, 2005), by propagating Ca^{2+} wave-fronts along dendritic processes (Loewenstein, 2003; Wang, 2003), by an intracellular Ca^{2+} handling subsystem whose dynamics depend upon the level of the IP3 secondary messenger (Fall, 2006), or by the involvement of a Ca^{2+} activated K^+ channel that has two distinct states, analogous to phoshorylated and unphosphorylated (Connors, 2002; Egorov, 2002; Dudman, 2006; Fransen, 2006). So, the Ca^{2+} memory proposed in this work is very different to that proposed previously and sets a new theory of Ca^{2+}/working memory. It is also operational in a biophysically detailed setting, which is not the case for a number of these models.

Spikes are frequently taken as the basic unit of neural coding. However, silences in spiking may be just as meaningful for the Purkinje cell as its firing output is inhibitory to the downstream deep cerebellar nuclei (DCN), and so a pause in its spiking would convey disinhibition (Jaeger, 2007; Steuber et al., 2007) . We suggest that the patterning and lengths of quiescent periods might be salient to how the Purkinje cell encodes information. And we have shown that CF input, in interaction with intracellular Ca^{2+} dynamics, can dictate the timing and duration of quiescent periods. This system might be modulated in the physiological setting by signalling cascades that regulate intracellular Ca^{2+} dynamics (Falcke and Malchow, 2003).

In this chapter we propose the intracellular Ca^{2+} concentration to be a memory element, dictating the timing and duration of quiescent periods. And in *chapter 2* we proposed the intracellular Na^+ concentration to be a memory element, dictating the timing and duration of quiescent periods. Thus, we propose that the Purkinje cell has two memory systems in parallel. These may cross-talk through the action of the Na^+/Ca^{2+} exchanger. Looking at the frequency of CF prompted silences, via Ca^{2+} computation, and the lesser frequency of sodium pump conferred silences, via Na^+ computation, we could propose that these two memory systems are specialised for, and operating on, different time scales.

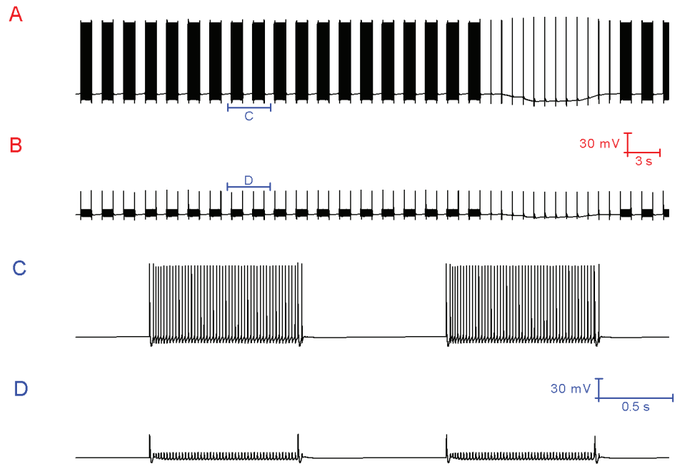

Figure 4.1 **Simulated climbing fiber (CF) input blocks the Purkinje cell model's trimodal pattern of activity.** *Panel A*, The somatic membrane potential (vs. Time). *Panel B*, The membrane potential at a dendritic location (for the same window of time). *Panel C* relates to the labelled part of panel A. *Panel D* relates to the labelled part of panel B. The scaling of panels A and B is encoded in the first scale bar (30 mV, 3 s). The scaling of panels C and D is encoded in the second scale bar (30 mV, 0.5 s).

With synaptic inputs absent, the Purkinje cell model fires in the trimodal pattern of activity. However, simulated CF input (1 Hz) can block this pattern and replace it with the activity pattern presented in panel A. Every second, CF input generates a Ca^{2+} spike in the dendrites (panel B) that drives a complex spike at the soma (panel A). These complex spikes toggle the cell between a tonic firing and a quiescent state at a frequency of 1 Hz (panel A). When the cell is firing, a CF input toggles it to quiescence. When the cell is quiescent, a CF input toggles it to firing.

With CF input, Na^+/K^+ pump generated silences still occur and one can be observed in panel A (the longer quiescent period). This Na^+/K^+ pump generated quiescence is punctuated by CF driven spikes at the frequency of CF input (1 Hz). |During this quiescent period, the CF input cannot evoke a state transition into the firing state.

Figure 4.2

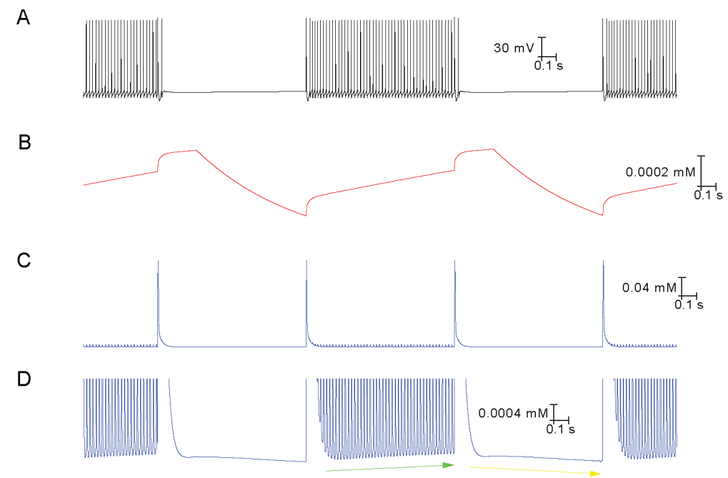

Figure 4.2 **The model's capture of toggling behaviour is made possible by its novel account of intracellular calcium dynamics.** All panels relate to the same window of time. *A*, Somatic membrane potential. *B*, Model parameter *y* (refer *methods*) at a dendritic point. *C*, Intracellular Ca^{2+} concentration, $[Ca^{2+}]_i$, at the same dendritic point. *D*, Panel C at higher resolution.

This figure shows the model cell being toggled on (tonic firing) and off (quiescence) by CF input at a frequency of 1Hz. Observe the cross-correlation between a Ca^{2+} spike event in the dendrites (panel C) and a toggle of state at the soma (panel A). Model parameter *y* rises during tonic firing, rises at a greater rate of change during a CF induced Ca^{2+} spike and decreases during quiescence (panel B). These changes in *y* drive corresponding changes in $[Ca^{2+}]_i$, as $[Ca^{2+}]_i$ is mathematically linked to *y* (refer *methods*). Thus, $[Ca^{2+}]_i$ rises during tonic firing, rises at a greater rate of change during a CF induced Ca^{2+} spike and decreases during quiescence (panels C and D). The $[Ca^{2+}]_i$ increase during tonic firing, and decrease during quiescence, is clear in the resolution of panel D where it is highlighted by green and yellow arrows respectively. During these phases, $[Ca^{2+}]_i$ rises and falls by way of it set point, the equilibrium $[Ca^{2+}]_i$ value (model parameter *y*), rising and falling. The rising set point during the tonic firing phase is apparant in panel D – the $[Ca^{2+}]_i$ value that $[Ca^{2+}]_i$ is returned to after a calcium spike event increases over time.

It is the changes in $[Ca^{2+}]_i$, that allow an identical, stereotypical CF input to produce very different effects - flipping the model cell from [quiescence to firing] or from [firing to quiescence]. CF input is both depolarising and hyperpolarising. It is depolarising because it prompts depolarising Ca^{2+} influx. Yet, at the same time it is hyperpolarising because this Ca^{2+} then activates hyperpolarising Ca^{2+}-gated SK channels. Which process is dominant dictates as to whether the CF input is *net* depolarising or hyperpolarising.

The firing state responds differently to CF input than the quiescent state because it has a higher $[Ca^{2+}]_i$, level. The CF conferred rise in $[Ca^{2+}]_i$,, added to the firing state's higher $[Ca^{2+}]_i$, level, recruits enough hyperpolarising SK activation to outweigh the depolarising force of CF input – there is *net* hyperpolarisation - and the cell is switched to quiescence. By contrast, the CF conferred rise in $[Ca^{2+}]_i$,, added to the quiescent state's lower $[Ca^{2+}]_i$, level, does not recruit enough SK activation to outweigh the depolarising force of CF input – there is *net* depolarisation and the cell is excited to the firing mode.

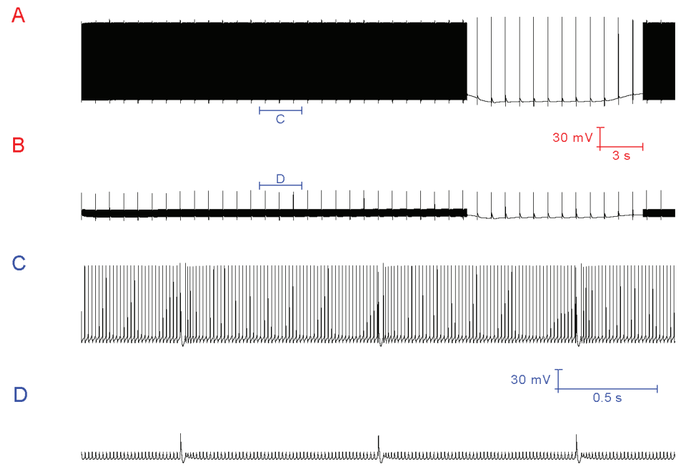

Figure 4.3 **Simulated climbing fiber (CF) input blocks the Purkinje cell model's trimodal pattern of activity (2).** *Panel A*, The somatic membrane potential (vs. Time). *Panel B*, The membrane potential at a dendritic location (for the same window of time). *Panel C* relates to the labelled part of panel A. *Panel D* relates to the labelled part of panel B. The scaling of panels A and B is encoded in the first scale bar (30 mV, 3 s). The scaling of panels C and D is encoded in the second scale bar (30 mV, 0.5 s).

Simulated CF input (1 Hz) blocks the trimodal activity pattern and replaces it with a nonbursting pattern of tonic firing interrupted, at a frequency of 1 Hz, by a complex spike and its short evoked after-pause (after-pauses can be most easily distinguished in the resolution of panel C). The model generates this pattern in response to CF input, as opposed to the toggled pattern of *figure 4.1*, when the model parameter g_{sk} (refer *methods*) is 0.62 as opposed to 0.72.

Na^+/K^+ pump generated silences still occur and one can be observed in panel A. This Na^+/K^+ pump generated quiescence is punctuated by CF driven spikes at the frequency of CF input (1 Hz). During this quiescent period, the CF input cannot evoke a state transition into the firing state.

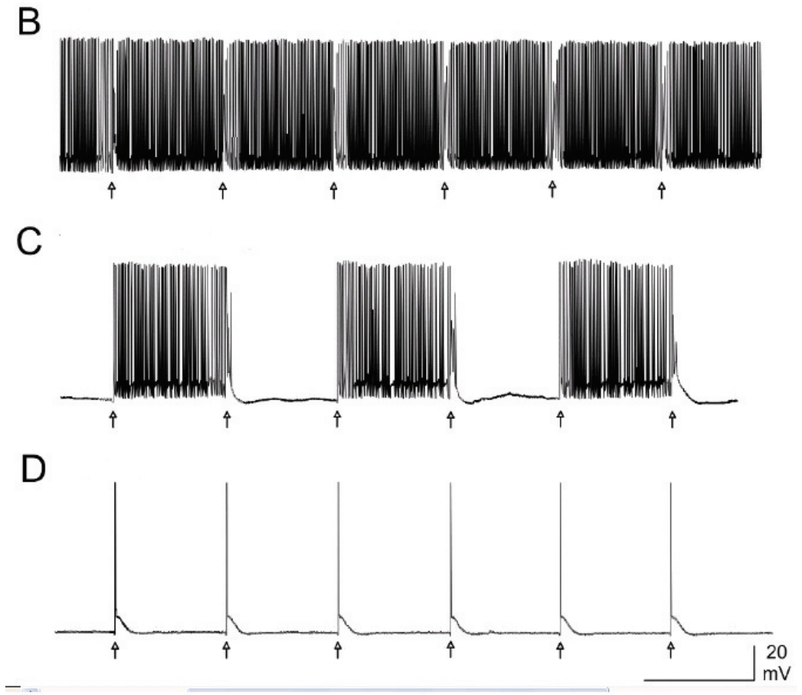

Figure 4.4 **Experimental data from McKay et al., 2007** *(presented with permission)***.** CF input (arrows) at 1 Hz abolishes the burst phase of trimodal output.

CF input switches Purkinje cells from their trimodal pattern of activity to sustained tonic firing (top panel, lettered *B*) OR periodic transitions between up and down states (middle panel, lettered *C*).

CF input abolishes the trimodal pattern's burst phase but not its quiescent phase, which it punctuates with CF driven spikes at the frequency of CF input (1 Hz) (bottom panel, lettered *D*). During this quiescent phase, the CF input cannot evoke a state transition into the firing state.

Chapter 5

The cerebellar Purkinje cell has two distinct bursting modes.

5.1 Introduction

Purkinje behaviour is often studied in a dissociated soma preparation in which the dendritic projection has been cleaved. A fraction of these dissociated somas are quiescent whilst others spontaneously fire simple spikes (Khaliq et al., 2003) or spontaneously burst (Swensen and Bean, 2003).

The mechanism of the isolated soma's spontaneous bursting is unknown. However, given its lack of dendrites, we can conclude that the drive to bursting must be of somatic origin and hence must be distinct from the somatic bursting previously described, which was shown to be dendritically driven (*chapter 2*). Indeed, their bursts have different characteristics (*figure 5.1*). Dendritically driven bursts follow a stereotypical waveform with an ongoing increase in firing rate and termination by a more rapid increase in firing rate, with a decrease in spike height. The burst rides upon a slow wave of depolarisation and ends with a rapid depolarization. This depolarization is followed by a rapid hyperpolarization that persists through the interburst interval. Somatically driven bursting is, by contrast, without any systematic change in firing rate or spike height upon burst progression. The burst's final spike height is not dramatically smaller and the burst does not ride upon a wave of depolarisation. In addition, somatically driven bursts tend to be shorter (two to four spikes per burst) than dendritically driven bursts (which can have hundreds of spikes per burst, although most typically have under ten).

We have constructed a biophysical Purkinje soma model, guided and constrained by experiments, which can replicate the somatically driven bursting pattern and which hypothesises persistent Na^+ current ($I_{Na\text{-}p}$) to be its burst initiator and SK K^+ current to be its burst terminator. This is the first time that this type of bursting ($I_{Na\text{-}p}$ vs. SK) has been reported for any neuron class and is a new bursting paradigm. The emergence of the model's bursting is regulated by the BK and SK K^+ currents in combination/redundancy.

Current abbreviations used in this chapter: Persistent Na^+ current ($I_{Na\text{-}p}$), fast Na^+ current ($I_{Na\text{-}f}$), resurgent Na^+ current ($I_{Na\text{-}r}$), hyperpolarisation activated cation current (I_h), P-type voltage-gated Ca^{2+} current (P/Q).

5.2 Materials and methods

Numerical simulations. Our aim was to build an isolated somatic model that could replicate the bursting pattern experimentally observed in some isolated Purkinje somata. As our starting point we removed the somatic compartment from the Purkinje cell model of *chapter 2*. This isolated somatic compartment spontaneously fired in a simple spiking form, as many isolated Purkinje somata do. We then set about modifying this isolated model compartment so that it spontaneously bursts instead.

The completed model soma has highly TEA sensitive, moderately TEA sensitive and TEA insensitive K^+ currents, a resurgent Na^+ current, a P-type Ca^{2+} current, a hyperpolarisation activated cation current, a BK voltage-and-Ca^{2+}-gated K^+ current, a leak current and an intracellular Ca^{2+} dynamics abstraction – all with descriptions sourced from Khaliq et al. (2003). With just these incorporated mechanisms, the model soma fires simple spikes. It can be switched to bursting (4 spikes per burst) by adding a persistent Na^+ current ($I_{Na\text{-}p}$, density = 0.004 S/cm^2; description from D'Angelo et al., 2001) and an SK Ca^{2+}-gated K^+ current (SK, density = 0.004 S/cm^2; description from Destexhe et al., 1994).

5.3 Results

5.3.1 The Purkinje soma model can replicate the somatically driven bursting pattern (*figure 5.1*).

The model's depolarising persistent Na^+ current ($I_{Na\text{-}p}$) produces the sustained depolarization that initiates and maintains a somatic burst; $I_{Na\text{-}p}$ is the "burst initiator" (*figure 5.1C*). Whilst the model's hyperpolarising Ca^{2+}-activated SK K^+ current builds in magnitude with burst progression, until it attains enough strength to terminate the burst, and produce the period of hyperpolarization before the next burst; SK is the burst "terminator" (*figure 5.1D*). So, this bursting can be described as having a [$I_{Na\text{-}p}$ vs. SK] basis and it has the following characteristics:

1) $I_{Na\text{-}p}$ alone is not sufficient for bursting, SK is also required. If $I_{Na\text{-}p}$ (0.004 S/cm^2) is introduced, without SK, then the model soma doesn't burst – it is depolarisation blocked. This is because the introduced $I_{Na\text{-}p}$ initiates a burst, but there is no SK to terminate it. So, the soma gets "stuck" mid-burst at a depolarised membrane potential (*figure 5.2A*).
2) Increasing the density of $I_{Na\text{-}p}$ (from 0.004 S/cm^2 to 0.005 S/cm^2) increases the number of spikes per burst (from 4 to 7) - increasing the density of the burst initiator increases the number of spikes per burst (*figure 5.2B*).
3) Increasing the density of SK (from 0.004 S/cm^2 to 0.008 S/cm^2) decreases the number of spikes per burst (from 4 to 2) - increasing the density of the burst terminator decreases the number of spikes per burst (*figure 5.2C*).
4) Increasing the density of resurgent Na^+ current ($I_{Na\text{-}r}$) (from 0.156 S/cm^2 to 0.3 S/cm^2) increases the number of spikes per burst (from 4 to 7). $I_{Na\text{-}r}$ is not the burst initiator and cannot generate bursting *de novo*. However, it can promote $I_{Na\text{-}p}$ established bursting (*figure 5.2D*).
5) Increasing the density of SK sufficiently (from 0.004 S/cm^2 to 0.02 S/cm^2) can switch the model out of bursting and into simple spiking (*figure 5.3A*)
6) Increasing the density of BK sufficiently (from 0.0728 S/cm^2 to 10 S/cm^2) can switch the model out of bursting and into simple spiking (*figure 5.3B*)
7) Increasing the density of both SK and BK (to 0.02 S/cm^2 and 10 S/cm^2 respectively) can switch the model out of bursting and into simple spiking (*figure 5.3C*)

So, $I_{Na\text{-}p}$ and SK can confer bursting. Raising the BK, and/or SK, density can "mask" this bursting and switch the model to simple spiking activity. So, BK and/or SK "gate" the

[$I_{Na\text{-}p}$ vs. SK] bursting. In conclusion, the soma model generates either simple spikes or bursts, the activity expressed being dependent on just two variables – the BK and SK current densities.

5.3.2 The Purkinje soma model is a product of, and can replicate, a number of pharmacological/electrophysiological experiments upon Purkinje somata.

We set SK as the model's burst terminator because its importance to somatic bursting has been shown experimentally: "SK increases progressively during bursts and plays an important role in regulating burst duration" (Swensen and Bean, 2003). SK is likely the burst terminator, and not BK, because "BK current progressively decreases during the burst, whereas SK current progressively increases" (Swensen and Bean, 2003). Our model replicates this rising SK current, and falling BK current, during burst progression (*figure 5.1 D & E*).

We set a Na^+ current, rather than a Ca^{2+} current, as the depolarising force that initiates and maintains a somatically driven Purkinje burst because Na^+ channel block, by cobalt or TTX, prevents this bursting (Swensen and Bean, 2003). By contrast, Ca^{2+} channel block actually promotes burst firing - "Blocking voltage-dependent Ca^{2+} entry by cadmium or replacement of external Ca^{2+} by Mg^{2+} enhanced burst firing" (Swensen and Bean, 2003). This promotion is likely manifested by Ca^{2+} channel block decreasing the intracellular Ca^{2+} concentration, which then results in less activation of the hypothesised burst terminator, the Ca^{2+}-activated SK channel.

So, the depolarising current that initiates and maintains somatic bursting is likely a Na^+ current. Model tuning of persistent Na^+ ($I_{Na\text{-}p}$), fast Na^+ ($I_{Na\text{-}f}$) and resurgent Na^+ ($I_{Na\text{-}r}$) current densities showed only $I_{Na\text{-}p}$ able to generate bursts. The final model version includes only $I_{Na\text{-}p}$ and $I_{Na\text{-}r}$. $I_{Na\text{-}f}$ is omitted for brevity. With this modelling result, we hypothesise that $I_{Na\text{-}p}$ is the burst initiator.

Our "$I_{Na\text{-}p}$ hypothesis" should be tested pharmacologically. Tetrodotoxin (TTX) is not ideal as it blocks not just $I_{Na\text{-}p}$, but $I_{Na\text{-}f}$ as well. The anti-epileptic drug, Phenytoin, has been shown to preferentially reduce $I_{Na\text{-}p}$ in CA1 Hippocampal Pyramidal neurons (Segal, 1997). Assuming this holds for Purkinje neurons, it would be a good tool to test the "$I_{Na\text{-}p}$ hypothesis". In addition, Protein Kinase C (PKC) activation suppresses $I_{Na\text{-}p}$ in CA1 Hippocampal Pyramidal neurons (Alroy, 1999). PDB is a phorbol ester that potently activates PKC (Castagna, 1982) and so this should likely inhibit $I_{Na\text{-}p}$ in Purkinje neurons. This would be another good tool to apply. $I_{Na\text{-}p}$ is regulated by Nitric Oxide (Hammarstrom, 1999) and external Ca^{2+} concentration (Su, 2001) - these relationships provide further leverage for investigating this "$I_{Na\text{-}p}$ hypothesis".

The hyperpolarisation activated cation current (I_h) contributes to bursting in a number of neuron types (Pape, 1996; Luthi, 1998). However, Swensen and Bean (2003) do not find it involved in Purkinje somatic bursting. The modelling concurs with this as I_h block has no consequence upon model bursting.

5.3.3 The bursting of the Purkinje soma model is gated by the BK and SK conductances.

In dissociated soma recordings, some Purkinje somata spontaneously fire simple spikes and others spontaneously burst (Khaliq et al., 2003; Swensen and Bean, 2003). The Purkinje soma model can be switched from bursting to simple spiking by raising the BK and/or SK densities (*figure 5.3*). In this way the model hypothesises that a Purkinje somata that spontaneously fires simple spikes is identical to a Purkinje somata that spontaneously bursts, save the setting of just two variables: the BK and SK current densities.

Bursting occurs when the depolarisation capacity exceeds the repolarisation capacity, and so the potential cannot be repolarised to the resting potential before the onset of the next spike. Raising BK and/or SK density, both repolarising entities, can correct this imbalance and set a simple spiking pattern. Conceivably the raising of any repolarising current can act similarly to switch bursting to simple spiking – to gate the bursting/simple spiking duality. However, we specifically hypothesise BK and SK in this role. At this point it is interesting to note that SK has a dual function, both being a gate to bursting and, upon bursting onset, the mechanism to burst termination. Higher SK densities block bursting, while lower SK densities permit bursting and act as the burst terminator.

Model bursting can be gated by BK and/or SK. Our final model version has gating by both BK and SK in combination and hence for bursting to be "unlocked", both BK and SK activation must be reduced. The reduction of just one is not sufficient because of this functional redundancy. The concept of somatic bursting having this dual, redundant BK & SK gating axis comes from a novel interpretation of experimental data. This data is not from the study of isolated Purkinje somata but from full Purkinje morphologies. If the Purkinje cell's P-type voltage-gated Ca^{2+} current (P/Q) is blocked by agatoxin then its inherent trimodal firing pattern is switched to bursting (Womack 2002 & 2004). Given the waveform of this bursting (bursts are short [2 to 4 spikes per burst] without the systematic depolarisation and stereotypical change in firing rate/spike height [upon burst progression] that characterises dendritically generated bursting), we hypothesise that it is somatically driven and corresponds to the bursting observed in some isolated Purkinje somata. Thus, we believe its study can be used to derive insight into isolated somata bursting, and vice-versa. This bursting, reasoned as somatic, occurs upon P/Q block. We hypothesise that this P/Q block translates to a combined BK and SK block, as BK and SK activation is selectively coupled to P/Q activation - experiment has shown that Ca^{2+} for activating BK and SK is provided *solely* by P/Q in the Purkinje cell (Womack, 2004) i.e. BK and SK do not "read" the global intracellular Ca^{2+} concentration but singly the Ca^{2+} flux through P/Q. So, the gate to somatic bursting is ultimately P/Q activation, exerting its control through BK and SK. Individual experimental block of BK or SK in a Purkinje cell is not observed to induce bursting (Womack 2003 & 2004). From this we hypothesise that combined BK and SK block is required, and P/Q block services this requisite.

This hypothesis has 2 dimensions that both require experimental testing: 1) The bursting of a trimodal cell, upon P/Q block, is somatic in origin and equivalent to the bursting observed in some dissociated Purkinje somata; 2) The distinction between an isolated

soma that fires simple spikes and one that bursts is the level of BK and SK activation, which is set by the level of P/Q activation. The following are some recommended experimental tests to explore this hypothesis:

1) Can P/Q block switch an isolated, simple spiking Purkinje soma to bursting?
2) Can parallel BK and SK block switch an isolated, simple spiking Purkinje soma to bursting?
3) Can parallel BK and SK block switch a full morphology Purkinje cell to bursting?

5.3.4 The Purkinje soma model can replicate Swensen and Bean's (2003) elicited burst protocol.

The focus of the bursting study of Swensen and Bean (2003) is not spontaneously bursting somata. Instead they study a rather artificial form of somatic bursting. They take an isolated soma that spontaneously fires simple spikes and hold it at a hyperpolarised silence (-90mV) with a maintained hyperpolarising current injection. This "held" cell is then driven to fire a single burst by a very short (1 ms) depolarising current injection. Although the cell intrinsically generates simple spikes it fires a burst in this protocol. Hence the studied burst is elicited rather than spontaneous. This raises the concern that the mechanisms elucidated for the generation of such an elicited burst are not relevant for spontaneous bursts. Modelling can help address this issue. Our model's bursting mechanism ($I_{Na\text{-}p}$ vs. SK) comes from an analysis of observations that Swensen and Bean (2003) made for elicited bursts. Indeed, this mechanism allows the model to replicate their elicited burst results (*figure 5.4*). But importantly, it also allows the model to fire bursts spontaneously. This demonstrates that elicited and spontaneous bursts have an equivalent basis, which vindicates the value of experiments that employ the elicited burst protocol.

In the elicited burst experiments, block of SK current (by apamin or scyllatoxin) increases the number of spikes per burst and prolongs burst duration (Swensen and Bean, 2003). However, with the model's spontaneous bursting, SK block can have a much more dramatic effect. Whilst partial SK block simply increases the number of spikes per burst and prolongs burst duration, as with the elicited burst experiment, complete SK block actually terminates bursting and renders the model cell to silence (*figure 5.2A*). When a spontaneously bursting model cell has SK completely blocked, the first initiated burst cannot be terminated as it is now missing the SK burst terminator - without SK, the membrane potential cannot be repolarised to a potential where another burst can be initiated. The cell is committed to "depolarisation block", which is a cell silence that is not at the resting potential, which would reflect a lack of depolarising capacity, but instead at a depolarised potential, indicating a lack of repolarising capacity. So, upon complete SK block in the spontaneously bursting model, just one more burst occurs that can't terminate and which reverberates into depolarisation block. The elicited burst experimental technique cannot foresee this effect upon spontaneous bursting because of its study of a single burst rather than a train of bursts.

SK block switching a spontaneously bursting soma to a depolarised silence is a model prediction that needs to be experimentally tested. And it needs to be tested directly, by applying an SK blocker (apamin or scyllatoxin) to a spontaneously bursting soma.

As stated earlier, when P/Q is blocked by agatoxin the Purkinje cell's inherent trimodal firing pattern is lost to bursting (Womack 2002 & 2004). And eventually this bursting cedes to "depolarisation block" silence, which is somewhat paradoxical given that it is a depolarising entity (P/Q) being lost. However, this outcome is well accounted for by the novel reasoning outlined above. P/Q block reduces BK and SK activation, and somatic bursting behaviour is unlocked. As BK and SK fall further, and specifically as SK falls further, these bursts cannot be terminated and depolarisation block silence ensues.

It is important to note that SK block alone cannot drive a Purkinje cell to a "depolarisation block" silence. Combined BK and SK block (as occurring upon P/Q block) is first needed to unlock somatic bursting behaviour. Then the SK block can go on to cause "depolarisation block" silence. If the cell is not in a somatic bursting state, then SK block cannot cause silence. To reiterate, combined BK and SK block is needed to unlock the somatic bursting state, from which SK block can cause silence.

5.3.5 P/Q can initiate somatic bursts in the absence of $I_{Na\text{-}p}$.

In our bursting model, omitting $I_{Na\text{-}p}$ switches it from bursting to simple spiking (*figure 5.5A*) and replacing the resurgent Na^+ current with a non-resurgent equivalent switches it from bursting to simple spiking. However, this does not correlate with experiments. Swensen and Bean (2005) studied isolated Purkinje somata of mutant mice that lack the Scn8a gene, which encodes the NaV1.6 Na^+ channel protein. These somata have transient Na^+ current reduced by 40%, with even more dramatic reductions in the persistent and resurgent Na^+ currents. However, they have a maintained bursting capability. Swensen and Bean (2005) show that this robustness of bursting is due to compensatory channel density changes that offset the lesser Na^+ current. These density changes are likely chronic, developmental adaptations. There is 1) an upregulation in T-type and P-type Ca^{2+} currents and 2) a change in the balance of Ca^{2+} current and Ca^{2+}-activated potassium currents such that their combined *net* influence shifts from being inhibitory during bursts, as with wild-type, to being excitatory. The model soma loses its bursting upon dramatic Na^+ current reduction, unlike an experimental soma, because it doesn't make these needed compensatory changes. If we afford the model these compensatory changes upon dramatic Na^+ current loss, then it can maintain its somatic bursting. For instance, $I_{Na\text{-}p}$ loss switches a spontaneously bursting model soma to simple spiking. However, a compensatory rise in P/Q density (0.00052 to 0.00092 S/cm^2) can recapture the bursting behaviour (*figure 5.5B*). P/Q is then the depolarising agent that initiates and maintains bursts rather than $I_{Na\text{-}p}$. So, we note that a large change in one conductance may produce little change in firing properties if accompanied by suitable changes in other conductances. This may be a general feature of neurons – that, where possible, they respond to a "channel density challenge" to their firing with compensatory channel density changes that maintain their characteristic firing properties. The cause of such a "channel density challenge" can be a pharmacological or genetic knockdown/knockout.

In conclusion, there may be multiple "solutions" (current density combinations) that yield a particular firing pattern or character. The model can capture this.

5.3.6 Experimental validation of the Purkinje soma model.

When P/Q is blocked in the Purkinje cell, it is switched into a phase of bursting before entering depolarisation block (Womack 2002 & 2004). Our Purkinje soma model predicts that this reaction occurs because P/Q block results in a concurrent compromise of BK and SK activation. So, we hypothesise that experimentally blocking BK and SK will produce a switch into the same series – bursting and depolarisation block. *In vitro* Purkinje cell recordings were performed by Mark Wall (University of Warwick) to test this prediction, with Charybdotoxin (100 nM) and Apamin (100 nM) applied to concurrently block the BK and SK currents respectively. These blocks switched the firing pattern into bursting and depolarisation block (*figures 5.6 and 5.7*) - validating the Purkinje soma model.

5.4 Discussion

In this chapter we establish the biophysical basis to bursting in isolated Purkinje somata. Although an isolated Purkinje soma is a severely reduced system it is used heavily for experimental Purkinje cell research and thus we sought to understand it in order to potentiate the value of these experiments.

We do not believe that the observed bursting is an artefact of the isolated soma preparation, because we hypothesise that the full Purkinje morphology exhibits the same bursting pattern upon P/Q block. Although this display is in a pharmacological reaction, we speculate that the Purkinje cell may use this bursting mode physiologically. So we propose that the Purkinje cell has two separate and distinct modes of bursting - somatically generated and dendritically generated - which have dramatically different waveforms. We venture that the Purkinje cell leverages this in information coding strategies.

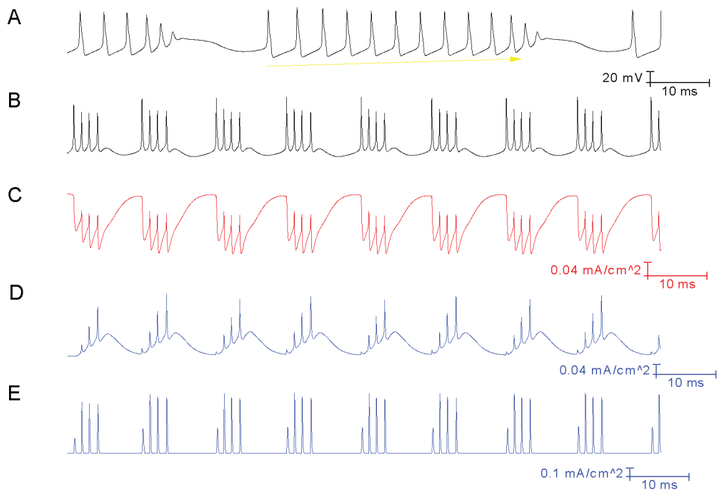

Figure 5.1 **The isolated Purkinje soma model bursts (4 spikes per burst) if the $I_{Na\text{-}p}$ and SK conductances are both set to 0.004 S/cm^2.** These somatically driven bursts have a different waveform than dendritically driven bursts. *Panel A*, Dendritically driven bursts in our full Purkinje cell model (described in *chapter 2*) have a very stereotypical waveform with an ongoing increase in firing rate and termination by a more rapid increase in firing rate, with a decrease in spike height. Each burst rides upon a slow wave of depolarisation (highlighted by the yellow arrow) and ends with a quick depolarization, followed by a rapid hyperpolarization that persists through the interburst interval. *Panel B*, Somatically driven bursts in our isolated Purkinje soma model are, by contrast, without any systematic change in firing rate or spike height upon burst progression and do not ride upon a wave of depolarisation. In addition, somatically driven bursts tend to be shorter (two to four spikes per burst) than dendritically driven bursts (which can have hundreds of spikes per burst, although more typically have under ten). *Panel C*, $I_{Na\text{-}p}$ initiates and maintains the bursts in the Purkinje soma model. The Na^+ current conducted by the somatic $I_{Na\text{-}p}$ channel (following convention $I_{Na\text{-}p}$, as an inward current, is represented as negative) is persistent and does not return to baseline after each spike in the burst. This persistence produces the sustained depolarization that initiates and maintains each somatic burst. *Panel D*, SK is responsible for burst termination in the Purkinje soma model. During a burst, the K^+ current conducted by the somatic SK channel builds in magnitude until it ultimately attains enough strength to terminate it. This SK current then resets during the inter-burst interval. *Panel E*, In contrast to the SK current, the BK current (except for an increase at the second spike) declines in magnitude with burst progression and is not responsible for burst termination.

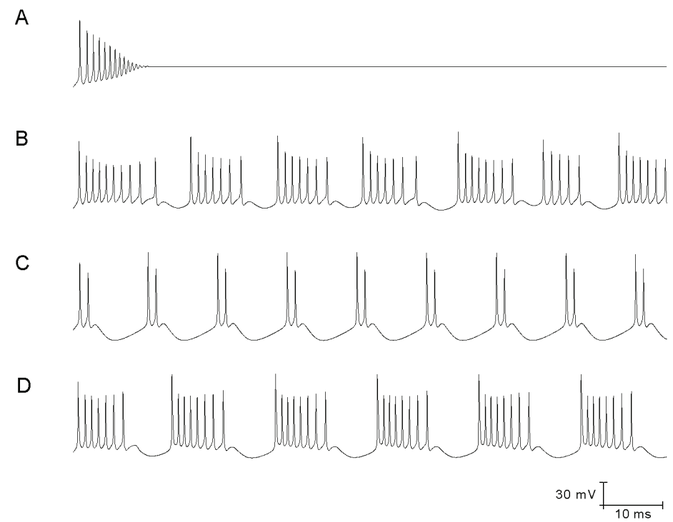

Figure 5.2 **The bursting of the Purkinje soma model is dependent on a number of factors.** *Panel A*, $I_{Na\text{-}p}$ alone is not sufficient for bursting, SK is also required**.** With $I_{Na\text{-}p}$ present (the burst initiator) and SK absent (the burst terminator) a burst initiates but cannot terminate. So, the membrane potential becomes "stuck" mid-burst at a depolarised membrane potential. *Panel B*, Increasing the $I_{Na\text{-}p}$ density (0.004 to 0.005 S/cm^2) increases the number of spikes per burst (4 to 7). *Panel C*, Increasing the SK density (0.004 to 0.008 S/cm^2) decreases the number of spikes per burst (4 to 2). *Panel D*, Increasing the $I_{Na\text{-}r}$ density (0.156 to 0.3 S/cm^2) increases the number of spikes per burst (4 to 7).

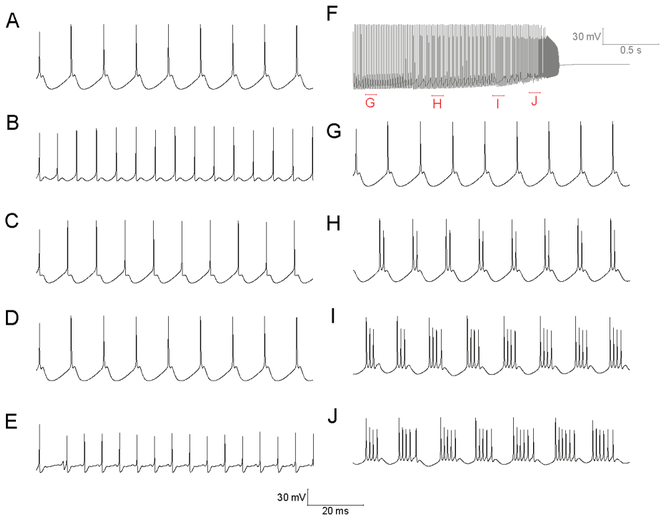

Figure 5.3. **The bursting of the Purkinje soma model is gated by the BK and SK conductances.** *Panel A***,** Increasing the SK density (0.004 to 0.02 S/cm^2) switches the model from bursting to simple spiking. *Panel B***,** Increasing the BK density (0.0728 to 10 S/cm^2) switches the model from bursting to simple spiking. *Panel C*, Increasing both the SK and BK densities (SK from 0.004 to 0.02 S/cm^2. BK from 0.0728 to 10 S/cm^2*)* switches the model from bursting to simple spiking. In this condition bursting is prevented by both BK and SK in a redundancy - removing BK does not permit bursting because the SK block to bursting is still present (*Panel D*); removing SK does not permit bursting because the BK block to bursting is still present (*Panel E*). However, concurrent BK and SK removal does permit bursting - decreasing the BK and SK densities by an empirical function of time (t) [density(t) = density(0)- 0.00001*t] shifts the somatic activity from simple spiking, into bursting and then depolarisation block silence (*Panel F*). This matches the experimental response of real Purkinje cells to concurrent BK and SK block (refer figures 5.6 and 5.7). *Panels G, H, I, J* relate to the labelled parts of *Panel F* and highlight the transition from simple spiking to bursting.

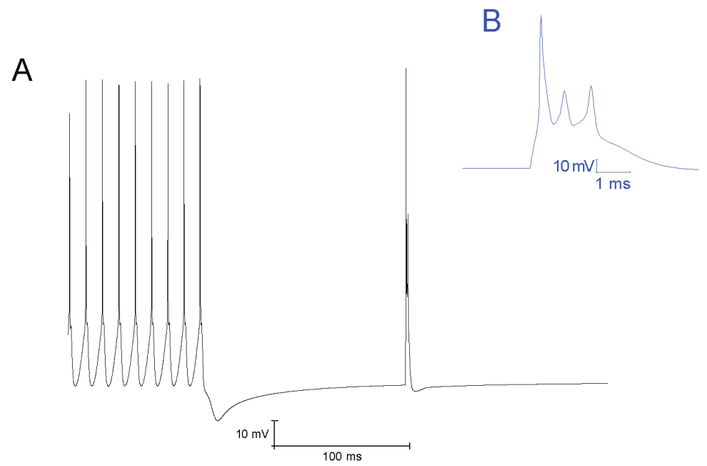

Figure 5.4 **The Purkinje soma model can replicate Swensen and Bean's (2003) elicited burst protocol.** *A,* The model soma spontaneously fires simple spikes because it has an elevated BK and SK density that blocks bursting. At 100 ms it is driven to a hyperpolarised silence, and held there, by a maintained hyperpolarising current injection (-0.5nA). This “held” cell is then driven to fire a single burst by a very short (1 ms) depolarising current injection (2nA). Although the cell intrinsically fires simple spikes, it fires a burst in this protocol. So, the studied burst is elicited rather than spontaneous. *B*, The elicited burst at higher resolution.

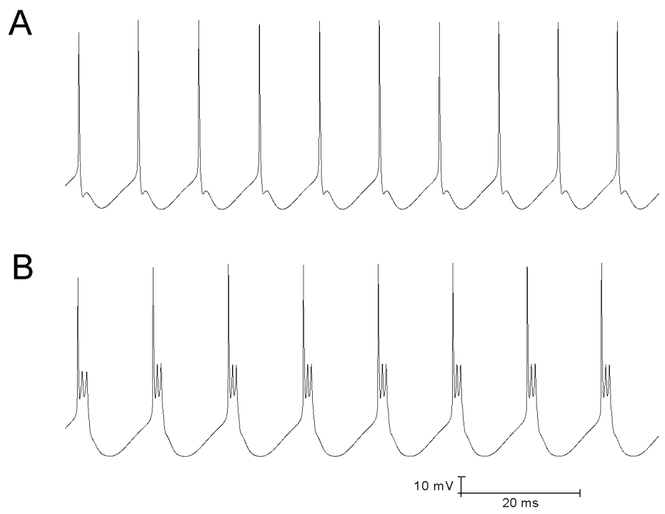

Figure 5.5 **P/Q can initiate somatic bursts in the absence of $I_{Na\text{-}p}$.** Figure 5.1 shows how the Purkinje soma model bursts if the $I_{Na\text{-}p}$ and SK conductances are both set to 0.004 S/cm^2**.** *Panel A*, However, if $I_{Na\text{-}p}$ is then removed the soma model no longer bursts, firing simple spikes instead. *Panel B*, But bursting character can be recaptured, in the absence of $I_{Na\text{-}p}$, by raising the P/Q density from 0.00052 to 0.00092 S/cm^2. In this case, P/Q is the burst initiator in place of $I_{Na\text{-}p}$.

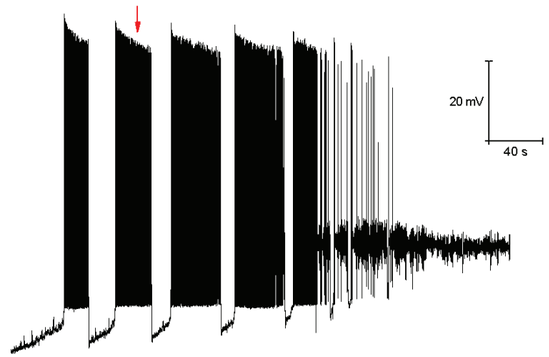

Figure 5.6 Experimental data. **Concurrent BK and SK block switches the Purkinje cell from a repeating bimodal activity pattern (tonic firing and quiescence) to bursting and then depolarisation block.** Whole cell patch clamp recording from a Purkinje cell following the application of Charybdotoxin (100 nM) and Apamin (100 nM) to block the BK and SK currents respectively (recording courtesy of Mark Wall at the University of Warwick, personal communication). Charybdotoxin and Apamin block BK and SK irreversibly and thus, after their application, the proportion of BK and SK molecules blocked increases in time until eventually all BK and SK activity is abolished. The red arrow denotes the time at which the rising BK and SK block starts to modify Purkinje cell firing. The initial firing mode, before any block, is bimodal (tonic firing and quiescence). With time, as an increasing proportion of BK and SK molecules become blocked, the quiescent periods get shorter and there is a switch into bursting and depolarisation block.

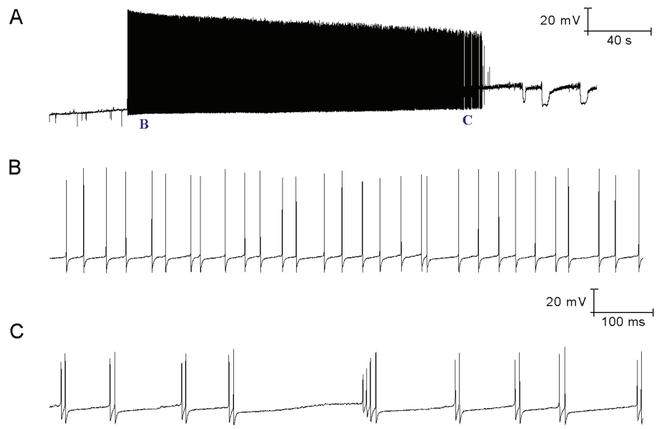

Figure 5.7 Experimental data (2).

A, **Concurrent BK and SK block switches the Purkinje cell from a repeating bimodal activity pattern (tonic firing and quiescence) to bursting and then depolarisation block.** Whole cell patch clamp recording from a Purkinje cell following the application of Charybdotoxin (100 nM) and Apamin (100 nM) to block the BK and SK currents respectively (recording courtesy of Mark Wall at the University of Warwick, personal communication).

B, Component of panel A at higher resolution. Early on, the Purkinje cell fires simple spikes.

C, Component of panel A at higher resolution. Later on, as a greater proportion of BK and SK channels become blocked, the Purkinje cell bursts with waveforms that indicate a somatic drive to bursting.

Chapter 6
Discussion

6.1 Introduction
Our contribution is primarily methodological, with us having built detailed and simplified *in silico* Purkinje cell preparations that other investigators can utilise in their research. We have shown the value of these models by using them ourselves to gain a further insight into Purkinje computation and coding.

6.2 The detailed Purkinje neuron model
Our detailed Purkinje cell model synthesises a lot of disparate electrophysiological and morphological data into a single, compact representation that can serve as an *in silico* experimental preparation. Although not a perfect simulacrum of a Purkinje cell, its detail in place of computationally attractive abstraction confers a good concordance between model and reality.

The Purkinje cell model grants continuous access to all parameters and confers complete control over inputs, which can facilitate investigation of Purkinje cell properties and mechanisms that are presently inaccessible to experimental procedures. For example, studies using the model face no issues with small dendrites, which at this time are impossible to patch experimentally, or incomplete specificity of current/channel blockers.

Modelling cannot provide an absolute answer to experimental questions but can endow a useful narrowing of possible scenarios and can guide the direction of future experiments. Neuroscience research can be highly effective when structured as an iterative back and forth between experimentation and modelling – with experimental data founding models and the investigation of these models prompting new experimental directions and data.

At the time of research, parallelization was **not** feasible for single neuron models. However, this has recently changed (Hines et al., 2008). Running the model on a cluster or grid will permit a faster model run time, which will make it more accessible as an *in silico* experimental preparation. Although at the time of writing there is a practical upper limit of ~16 processors.

6.3 The reduced Purkinje neuron model
Previous theories of cerebellar functioning (Marr, 1969; Albus, 1971) have considered its component neurons to be linear summing devices (integrate and fire), ignoring their complexity, nonlinearity and computations. This is perhaps too abstractive because there is evidence that the richness of biophysical properties on the single neuron scale can supply mechanisms that serve as building blocks for network dynamics (Getting, 1989). We believe that to understand the cerebellar network, researchers should employ network simulations that incorporate more detailed neuron descriptions. Our Purkinje cell model is an intricate *in silico* experimental preparation. It favors detail over abstraction but this

makes it very computationally intensive and unsuitable for use in network simulations. With this in mind, we have used mathematical transforms to produce a simpler, surrogate version with the same electrical properties, but a lower computational overhead, which we hope researchers will deploy in future cerebellar network studies. Indeed, we hope that this model, of intermediate biological fidelity and medium computational complexity, will be used in the future to bridge cellular and network studies and identify how distinctive Purkinje cell behaviours are important to network and system function.

6.4 Our findings

Our detailed biophysical model replicates the Purkinje cell's trimodal and bimodal firing patterns with the mechanisms that we hypothesise to be responsible for their firing in real Purkinje cells. And these predictions are forceful given the model's level of detail, with its faithfully reconstructed morphology and current, synapse and pump equations parameterized to experimental data. The model's methods of generating the trimodal and bimodal firing patterns are validated by endowing the model with the ability to replicate a range of other experimentally observed Purkinje cell operating states. For example, they permit the model to replicate the complex Purkinje cell response to an ouabain block of the Na^+/K^+ pump, both on its own and in combination with a TTX block of Na^+ channels.

Although previous work has reported and characterised different patterns of intrinsic Purkinje firing (Womack and Khodakhah, 2002, 2003, 2004; McKay and Turner, 2005) this thesis is the first study that moves beyond their description and investigates the basis of their generation. The model suggests that the Na^+/K^+ pump fixes the Purkinje cell's intrinsic operating state, dictating whether the cell fires in a trimodal or bimodal pattern and setting the length of their constituent modes (tonic, burst, quiescent). We hence demonstrate that the isolated Purkinje cell's multimodality might be controlled by just a single molecular species.

Our work suggests that the Na^+/K^+ pump can generate quiescent periods in Purkinje cell activity and we propose that their patterning and length is salient to how the Purkinje cell encodes information (especially given that Purkinje output is inhibitory to the downstream deep cerebellar nuclei [DCN] and so quiescence actually conveys downstream disinhibition; Jaeger, 2007; Steuber et al., 2007) We suggest that intracellular Na^+ concentration provides memory in the Purkinje cell, integrating firing history and setting Na^+/K^+ pump activity to dictate silence length and patterning, with potential modulation by signalling cascades convergent on the pump. So, we hypothesise that the Na^+/K^+ pump is more than just a homeostatic mechanism to ionic gradients. We propose that it is a computational element in Purkinje information coding. In support, a mutation in the Na^+/K^+ pump causes rapid-onset dystonia-parkinsonism (RDP), which has symptoms to indicate that it is a pathology of cerebellar computation (Cannon, 2004; de Carvalho et al., 2004).

Climbing fiber (CF) input can *toggle* a Purkinje cell between an up (firing) and down (quiescent) state and can set the *gain* of its response to parallel fiber (PF) input (McKay

et al., 2007). Our Purkinje cell model can perform these toggle and gain computations, with mechanisms that we hypothesise to be responsible in real Purkinje cells. This has a wider importance because there are not many biophysical models of single neuron computation, despite an intense interest in the computational repertoire and power available to individual neurons (Sejnowski et al., 1988; Koch, 1999; Zador, 2000; London and Hausser, 2005; Herz et al., 2006; Mel, 2006). The model incorporates the hypothesis that these computations are a function of an underlying Ca^{2+} computation; that the intracellular Ca^{2+} concentration provides memory, recording the history of firing and inputs, to dictate how the cell responds to future inputs. For example, the model's Ca^{2+} system memorizes a CF input, which causes the model to then respond differently to a PF input than it would otherwise and CF input, in interaction with intracellular Ca^{2+} dynamics, can dictate the timing and duration of quiescent periods. So, again we show the importance of an ion concentration to neural functioning, whilst reconciling biophysics with computation and information processing.

Our modelling indicates that the Purkinje cell has two different bursting modes. One generated by Ca^{2+} spikes in the dendrites and the other by an interaction of somatic conductances. For the latter, we model persistent Na^+ current ($I_{Na\text{-}p}$) to be the burst initiator and SK K^+ current to be the burst terminator. This is a novel bursting form with no previous reports in the literature (for any neuron class). In our model, this bursting is gated by the BK and SK currents in combination/redundancy, and we provide supporting *in vitro* Purkinje cell recordings that affirm the gate is of this character.

6.5 A proposal that reconciles the long temporal dimension of some Purkinje cell behaviours with the much shorter time scale of motor coordination.

Motor coordination is achieved with precise timing signals for augmentation and inhibition of appropriate agonist and antagonist muscles, and this timing information is believed to be encoded in the rate of firing and pattern of activity of Purkinje cells (Ito, 1984). The millisecond time scale of motor coordination in the behaving animal (e.g. average reaction time of normal subjects in a button pressing task is 180 milliseconds; Doyon et al., 1998) is a contrast to the wider spectrum of time scales associated with Purkinje cell behaviour. For example, whilst Purkinje cells can fire fast, millisecond-long sodium action potentials they can also exhibit slow, second-long transitions between the up and down states in CF associated toggling. This raises the question of how the Purkinje cell's slower physiological processes (such as CF toggling) can affect motor behaviour, which has much faster dynamics.

One possibility is spatial averaging. Each DCN neuron receives an input from hundreds of Purkinje cells and so assuming their activity is asynchronous, even slow events in single Purkinje cells will likely affect each DCN neuron many times per second.

However, this asynchronicity assumption is not supported by data showing that the complex spike activity of neighbouring Purkinje cells is synchronized (Lang et al., 1999).

Our view is that these slower processes are relevant and computationally advantageous because, by conferring an access to longer time scales, they permit short-term processing and storage of sensory information in the cerebellar cortex. In essence, the Purkinje cell's slower processes permit a large number of different dynamical states to be sustained in the cerebellar cortex for extended periods. Each of these states is associated with a specific configuration of up (firing; tonic/bursts) and down (quiescent) states in different Purkinje cells. These network states could store information. In our proposal, these hypothesised network computations sit upon the aforementioned, asserted intracellular ion computations (Na^+, Ca^{2+}) that dictate the activity state of individual Purkinje neurons.

In short, as regards function, we venture that these slower, longer processes in the Purkinje cell might be involved in the integration of sensory information, gain modification and motor planning rather than the direct control of fast movements.

6.6 A future research direction

A useful test of our work would be to research how Na^+/K^+ pump block affects behaviour in the intact animal, using intraventricular administration of the Na^+/K^+ pump blocker ouabain. Whilst earlier studies have assayed ouabain's effects on learning tasks (Rogers, 1977; Zhan, 2004) it would be interesting to test ouabain impaired animals in motor co-ordination and motor learning tasks, because these are attributed to the cerebellum where we propose Na^+/K^+ pump function to be especially important.

6.7 Conclusion

In the classical rate coding postulate, the firing rate of neurons is considered to be the significant variable in neural coding. However, it is becoming increasingly clear that this view is overly simplistic. For example, in our work we reach the conclusion that Purkinje neurons encode information not just in their spiking but in the patterning and length of quiescent periods, which are in turn dictated by computations performed by intracellular ion systems (Na^+ and Ca^{2+}). Although we have only studied Purkinje neurons, there is the possibility that this finding might be more general and could relate to the dynamics of other neural units.

APPENDIX

Hodgkin-Huxley equations used

A.1 Hodgkin-Huxley equations for a voltage-dependent current

(This is a brief recap. There is a section of chapter 1 that describes the Hodgkin-Huxley model in detail. Please to refer to this if a fuller explanation is required)

$$I = \bar{g} m^A (V - E_m)$$

Where I is the current, $\bar{g}$ is the maximal conductance of the current, V is the membrane potential, A is a constant, E_m is the reversal potential for this current and m is a voltage dependent "particle":

$$\frac{dm}{dt} = \frac{m_\infty - m}{\tau_m}$$

m is voltage dependent because m_∞ and τ_m are voltage dependent, which are set by:

$$m_\infty = \frac{\alpha_m}{\alpha_m + \beta_m}$$

$$\tau_m = \frac{1}{\alpha_m + \beta_m}$$

m_∞ and τ_m are voltage dependent because α_m and β_m are voltage dependent. α_m and β_m are empirical functions of voltage (or intracellular calcium concentration)

So, to detail a Hodgkin-Huxley current one needs to specify:

1) The maximal conductance/current density ($\bar{g}$)
2) The reversal potential. This depends on which ion the current permeates. Na^+ (+65 mV), K^+ (-88 mV), Ca^{2+} (+135 mV).
3) How many "particles" it has (m^A, h^B, z^C)
4) The equations describing how its alpha and beta functions are dictated by voltage (or intracellular calcium concentration). OR the equations describing how its steady state and time constant are dictated by voltage (or calcium concentration) *

* [α_m , β_m] and [m_∞ , τ_m] are interchangeable through the relations $m_\infty = \alpha_m/(\alpha_m + \beta_m)$, and $\tau_m = 1/(\alpha_m + \beta_m)$. Thus specification of [α_m , β_m] OR [m_∞ , τ_m] are equivalent.

In this section we detail (3) and (4) for each current used in our modelling.
(1) for these currents has been detailed in earlier chapters.

A.2 Hodgkin-Huxley equations for the currents of our Purkinje cell models

In the following equations, *V* represents the membrane potential in mV as a dimensionless quantity.

Kv1.2 K^+ current (Akemann and Knopfel, 2006)

m^4

$$\alpha_m = 0.12889 * \exp\left(\frac{-(V+45)}{-33.90877}\right)$$

$$\beta_m = 0.12889 * \exp\left(\frac{-(V+45)}{12.42101}\right)$$

D-type K^+ current (Miyasho et al., 2001)

$m^1\ h^1$

$$\alpha_m = \frac{8.5}{1+\exp((V+17)/-12.5)}$$

$$\beta_m = \frac{35}{1+\exp((V+99)/14.5)}$$

$$\alpha_h = \frac{0.0015}{1+\exp((V+89)/8)}$$

$$\beta_h = \frac{0.0055}{1+\exp((V+83)/-8)}$$

A-type K^+ current (Miyasho et al., 2001)

$m^4\ h^1$

$$\alpha_m = \frac{1.4}{1+\exp((V+27)/-12)}$$

$$\beta_m = \frac{0.49}{1+\exp((V+30)/4)}$$

$$\alpha_h = \frac{0.00175}{1+\exp((V+50)/8)}$$

$$\beta_h = \frac{0.49}{1+\exp((V+13)/-10)}$$

M-type K^+ current (Miyasho et al., 2001)

m^1

$$\tau_m = \frac{1000}{3.3(e^{+(V+35)/40} + e^{-(V+35)/20})}$$

$$m_\infty = \frac{1}{1+e^{-(V+35)/10}}$$

E-type Ca^{2+} current (Miyasho et al., 2001)

$m^1\ h^1$

$$\alpha_m = \frac{2.6}{1+\exp((V+7)/-8)}$$

$$\beta_m = \frac{0.18}{1+\exp((V+26)/4)}$$

$$\alpha_h = \frac{0.0025}{1+\exp((V+32)/8)}$$

$$\beta_h = \frac{0.19}{1+\exp((V+42)/-10)}$$

T-type Ca^{2+} current (Miyasho et al., 2001)

$m^1\ h^1$

$$\alpha_m = \frac{2.6}{1+\exp((V+21)/-8)}$$

$$\beta_m = \frac{0.18}{1+\exp((V+40)/4)}$$

$$\alpha_h = \frac{0.0025}{1+\exp((V+40)/8)}$$

$$\beta_h = \frac{0.19}{1+\exp((V+50)/-10)}$$

P-type Ca^{2+} current (Miyasho et al., 2001)

m^1

$$\alpha_m = \frac{8.5}{1+\exp((V+-8)/-12.5)}$$

$$\beta_m = \frac{35}{1+\exp((V+74)/14.5)}$$

Delayed rectifier type K$^+$ current (Miyasho et al., 2001)

$$m^2 \quad h^1$$

$$\tau_m = \frac{1}{\left(\frac{-0.0047(V+12)}{e^{-(V+12)/12}-1}\right)+(e^{-(V+147)/30})}$$

$$m_\infty = \frac{\left(\frac{-0.0047(V+12)}{e^{-(V+12)/12}-1}\right)(V-20)}{\left(\left(\frac{-0.0047(V+12)}{e^{-(V+12)/12}-1}\right)(V-20)\right)+\left(\left(e^{-(V+147)/30}\right)(V-20)\right)}$$

$$\tau_h = \begin{cases} 6000 \ldots V < -25mV \\ 50 \ldots\ldots V > -25mV \end{cases}$$

$$h_\infty = \frac{1}{1+e^{+(V+25)/4}}$$

Hyperpolarisation activated cation current (Saraga et al., 2003)

$$m^1$$

$$m_\infty = \frac{1}{1+\exp[(V+84)/10.2]}$$

$$\tau_m = \frac{1}{\exp(-17.9-0.116V)+\exp(-1.84+0.09V)}+100$$

Persistent Na$^+$ current (D'Angelo et al., 2001)

$$m^1$$

$$m_\infty = \frac{1}{1+e^{-(V+40)/5}}$$

$$\tau_m = 5$$

M-type K$^+$ current (Traub et al., 2003)

$$m^1$$

$$\alpha_m = \frac{0.02}{1+\exp[(-V-20)/5]}$$

$$\beta_m = 0.01\exp[(-V-43)/18]$$

Fast Na$^+$ current (Traub et al., 2003)

$$m^3 \quad h^1$$

$$m_\infty = \frac{1}{1+\exp[(-V-34.5)/10]}$$

$$\tau_m = \begin{cases} 0.025+0.14\exp[(V+26.5)/10] \ldots V \le -26.5 \\ 0.02+0.145\exp[(-V-26.5)/10] \ldots V \ge -26.5 \end{cases}$$

$$h_\infty = \frac{1}{1+\exp[(V+59.4/10.7)]}$$

$$\tau_h = 0.15+\frac{1.15}{1+\exp[(V+33.5)/15]}$$

Persistent Na$^+$ current (Traub et al., 2003)

$$m^1$$

$$m_\infty = \frac{1}{1+\exp[(-V-48)/10]}$$

$$\tau_m = \begin{cases} 0.025+0.14\exp[(V+40)/10] \ldots [V \le -40] \\ 0.02+0.145\exp[(-V-40)/10] \ldots [V \ge -40] \end{cases}$$

A-type K$^+$ current (Traub et al., 2003)

$$m^4 \quad h^1$$

$$m_\infty = \frac{1}{1+\exp[(-V-60)/8.5]}$$

$$\tau_m = \frac{0.185+0.5}{\exp[(V+35.8)/19.7]+\exp[(-V-79.7)/12.7]}$$

$$h_\infty = \frac{1}{1+\exp[(V+78)/6]}$$

$$\tau_h = \begin{cases} 9.5 \ldots V \ge -63mV \\ \frac{0.5}{\exp[(V+46)/5]+\exp[(-V-238)/37.5]} \ldots V \le -63mV \end{cases}$$

Delayed rectifier type K$^+$ current (Traub et al., 2003)

$$m^4$$

$$m_\infty = \frac{1}{1+\exp[(-V-29.5)/10]}$$

$$\tau_m = \begin{cases} 0.25 + 4.35\exp[(V+10)/10] \ldots [V \le -10] \\ 0.25 + 4.35\exp[(-V-10)/10] \ldots [V \ge -10] \end{cases}$$

SK type K^+ current (Destexhe et al., 1994)

$$z^2$$

$$z_\infty = \frac{48[Ca^{2+}]^2}{48[Ca^{2+}]^2 + 0.03}$$

$$\tau_z = \frac{1}{48[Ca^{2+}] + 0.03}$$

K2 type K^+ current (Miyasho et al., 2001)

$$m^1 \; z^2$$

$$\alpha_m = 25$$

$$\beta_m = \frac{0.075}{\exp((V+5)/10)}$$

$$z_\infty = 1 \Big/ \left(1 + \frac{20}{[Ca^{2+}]}\right)$$

$$\tau_z = 10$$

BK type K^+ current (Miyasho et al., 2001)

$$m^1 \; z^2$$

$$\alpha_m = 7.5$$

$$\beta_m = \frac{0.11}{\exp((V+-35)/14.9)}$$

$$z_\infty = 1 \Big/ \left(1 + \frac{400}{[Ca^{2+}]}\right)$$

$$\tau_z = 10$$

SK type K^+ current (Komendantov et al., 2004)

$$z^1$$

$$z_\infty = \frac{1}{1 + \left(\frac{0.00019}{[Ca^{2+}]}\right)^4}$$

$$\tau_z = 1$$

Highly TEA sensitive K^+ current (Khaliq et al., 2003)

$$m^3 \; h$$

$$m_\infty = \frac{1}{\exp\left(-\frac{V--24}{15.4}\right)}$$

$$\tau_m = \begin{cases} 0.000103 + 0.0149 * \exp(0.035 * V) \ldots\ldots [V < -35mV] \\ 0.000129 + 1/[\exp(\frac{V+100.7}{12.9}) + \exp(\frac{V-56}{-23.1})] \ldots\ldots [V \ge -35mV] \end{cases}$$

$$h_\infty = 0.31 + \frac{1-0.31}{\exp\left(-\frac{V--5.8}{-11.2}\right)}$$

$$\tau_h = \begin{cases} 1.22 * 10^{-5} + 0.012 * \exp[-(\frac{V+56.3}{49.6})^2] \ldots\ldots [V \le 0mV] \\ 0.0012 + 0.0023 * \exp(-0.141 * V) \ldots\ldots [V > 0mV] \end{cases}$$

Moderately TEA sensitive K^+ current (Khaliq et al., 2003)

$$m^4$$

$$m_\infty = \frac{1}{\exp\left(-\frac{V--24}{20.4}\right)}$$

$$\tau_m = \begin{cases} 0.000688 + 1/[\exp(\frac{V+64.2}{6.5}) + \exp(\frac{V-141.5}{-34.8})] \ldots\ldots [V < -20mV] \\ 0.00016 + 0.0008 * \exp(-0.0267 * V) \ldots\ldots [V \ge -20mV] \end{cases}$$

TEA insensitive K^+ current (Khaliq et al., 2003)

$$m^4$$

$$m_\infty = \frac{1}{\exp\left(-\frac{V--16.5}{18.4}\right)}$$

$$\tau_m = 0.000796 + 1/[\exp(\frac{V+73.2}{11.7}) + \exp(\frac{V-306.7}{-74.2})]$$

P-type Ca^{2+} current (Khaliq et al., 2003)

$$m^1$$

$$m_\infty = \frac{1}{\exp\left(-\frac{V--19}{5.5}\right)}$$

$$\tau_m = \begin{cases} 0.000264 + 0.128 * \exp(0.103 * V) \ldots\ldots\ldots\ldots\ldots\ldots [V \le -50mV] \\ 0.000191 + 0.00376 * \exp[-(\frac{V+11.9}{27.8})^2] \ldots\ldots\ldots [V > -50mV] \end{cases}$$

Hyperpolarisation activated cation current (Khaliq et al., 2003)

$$m^1$$

$$m_\infty = \frac{1}{\exp\left(-\frac{V--90.1}{-9.9}\right)}$$

$$\tau_m = 0.19 + 0.72 * \exp[-(\frac{V+81.5}{11.9})^2]$$

BK type K$^+$ current (Khaliq et al., 2003)

$$m^3 z^2 h^1$$

$$m_\infty = \frac{1}{\exp\left(-\frac{V--28.9}{6.2}\right)}$$

$$h_\infty = 0.085 + \frac{1-0.085}{\exp\left(-\frac{V--32}{-5.8}\right)}$$

$$\tau_m = 0.000505 + 1/[\exp(\frac{V+86.4}{10.1}) + \exp(\frac{V-33.3}{-10})]$$

$$\tau_h = 0.0019 + 1/[\exp(\frac{V+48.5}{5.2}) + \exp(\frac{V-54.2}{-12.9})]$$

$$z_\infty = \frac{1}{1 + \frac{0.001}{[Ca^{2+}]}}$$

$$\tau_z = 1$$

Intracellular calcium dynamics (Miyasho et al., 2001)

$$\frac{d[Ca^{2+}]_i}{dt} = \left(\frac{1000 * I_{Ca^{2+}}}{2 * F * depth}\right) + \left(\frac{-kt * [Ca^{2+}]_i}{[Ca^{2+}]_i + kd}\right) + \left(\frac{y - [Ca^{2+}]_i}{tau_r}\right)$$

Where $[Ca^{2+}]_i$ is the intracellular Ca^{2+} concentration in a supra-membrane shell of *depth* = 0.1 µm, *F* is the Faraday constant, $I_{Ca^{2+}}$ is the Ca^{2+} membrane current, *kt* = 1e^{-4} mM/ms, *kd* = 1e^{-4} mM, tau$_r$ = 1e^{10} ms and y = 2.4e^{-4} mM.

Resurgent Na$^+$ current (Khaliq et al., 2003)

This current is not described by a Hodgkin-Huxley formalism but by the following Markov scheme:

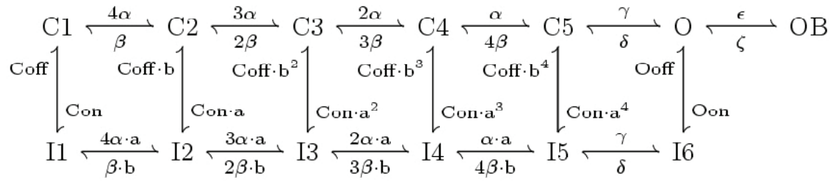

C, I, O, and OB represent closed, inactivated, open, and blocked states, respectively. The rate constants are α, β, γ, δ, ε, ζ, Con, Coff, Oon, and Ooff. For their values refer to Khaliq et al. (2003).

REFERENCES

Abeles M (1991) Corticonics: Neural Circuits of the Cerebral Cortex. Cambridge University Press.

Akemann W, Knopfel T (2006) Interaction of Kv3 potassium channels and resurgent sodium current influences the rate of spontaneous firing of Purkinje neurons. J. Neurosci. 26:4602-4612.

Alberts B, Johnson A, Lewis J, Raff M, Roberts K, Walter P (1994) Molecular Biology Of The Cell. 3rd Ed. Garland Publishing, NY.

Albus JS (1971) A theory of cerebellar function. Math Biosci 10:25-61.

Alroy G, Su H, Yaari Y (1999) Protein kinase C mediates muscarinic block of intrinsic bursting in rat hippocampal neurons. J Physiol (Lond) 517:71-79.

Amzica F, Massimini M, Manfridi (2002) A spatial buffering during slow and paroxysmal sleep oscillations in cortical networks of glial cells in vivo. J Neurosci 22:1042–1053.

Arganda S, Guantes R, de Polavieja GG (2007) Sodium pumps adapt spike bursting to stimulus statistics. Nat Neurosci 11:1467-73.

Armstrong CM, Bezanilla F (1973) Currents related to movement of the gating particles of the sodium channels. Nature 242:459-461.

Baccus SA (1998) Synaptic facilitation by reflected action potentials: enhancement of transmission when nerve impulses reverse direction at axon branch points. Proc Natl Acad Sci USA 95:8345-50.

Baker MD (2005) Protein kinase C mediates up-regulation of tetrodotoxin-resistant, persistent Na+ current in rat and mouse sensory neurones. J Physiol 567:851-67.

Barbour B (1993) Synaptic currents evoked in Purkinje cells by stimulating individual granule cells. Neuron 11(4):759–769.

Barlow JB (2002) The Cerebellum and Adaptive Control. Cambridge University Press.

Baylor DA, Nicholls JG (1969) After-effects of nerve impulses on signalling in the central nervous system of the leech. J Physiol 203:571-589.

Bazhenov M, Timofeev I, Steriade M, Sejnowski TJ (2004) Potassium Model for Slow (2-3 Hz) In Vivo Neocortical Paroxysmal Oscillations. J Neurophysiol 92:1116–1132.

Bezanilla (2000) The voltage sensor in voltage-dependent ion channels. Physiol Rev 80:555-592.

Blakemore SJ, Wolpert DM, Frith CD (1998) Central cancellation of self-produced tickle sensation. Nat Neurosci 1:635-640.

Blaustein MP, Lederer WJ (1999) Sodium/Calcium Exchange: Its Physiological Implications. Physiol Rev 79:763-854.

Blaustein MP, Wier WG (2007) Local sodium, global reach: filling the gap between salt and hypertension. Circ Res. 101(10):959-61.

Bower JM (1997) Is the cerebellum sensory for motor's sake, or motor for sensory's sake: the view from the whiskers of a rat? Prog Brain Res 114:463-496.

Braitenberg V, Atwood RP (1958) Morphological observations on the cerebellar cortex. J Comp Neurol 109:1-33.

Burke RE (2000) Comparison of alternative designs for reducing complex neurons to equivalent cables. J Comput Neurosci 9(1):31-47.

Bush PC, Sejnowski TJ (1993) Reduced compartmental models of neocortical pyramidal cells. J Neurosci Methods 46:159-166.

Canavier CC (1999) Sodium dynamics underlying burst firing and putative mechanisms for the regulation of the firing pattern in midbrain dopamine neurons: a computational approach. J Comput Neurosci 6:49-69.

Cannon C (2004) Paying the Price at the Pump: Dystonia from Mutations in a Na+/K+-ATPase. Neuron 43(2):153-154.

Carafoli E (1991) Calcium pump of the plasma membrane. Physiol Rev 71(1):129–153.

Carlin KP, Jones KE, Jiang Z, Jordan LM, Brownstone RM (2000) Dendritic L-type calcium currents in mouse spinal motoneurons: implications for bistability. Eur J Neurosci 12:1635-46.

Castagna M, Takai Y, Kaibuchi K, Sano K, Kikkawa U, Nishizuka Y (1982) Direct activation of calcium-activated, phospholipid-dependent protein kinase by tumor-promoting phorbol esters. J Biol Chem 257:7847-7851.

Cataldo E, Brunelli M, Byrne JH, Av-Ron E, Cai Y, Baxter DA (2005) Computational model of touch sensory cells (T Cells) of the leech: role of the afterhyperpolarization (AHP) in activity-dependent conduction failure. J Comput Neurosci 18(1):5-24.

Catarsi S, Scuri R, Brunelli M (1993) Cyclic AMP mediates inhibition of the Na+/K+ electrogenic pump by serotonin in tactile sensory neurons of the leech. J Physiol 462:229–242.

Chang W, Strahlendorf JC, Strahlendorf HK (1993) Ionic contributions to the oscillatory firing activity of rat Purkinje cells in vitro. Brain Res 614(1-2):335-41.

Chono K, Takagi H, Koyama S, Suzuki H, Ito E (2003) A cell model study of calcium influx mechanism regulated by calcium dependent potassium channels in Purkinje cell dendrites. J Neurosci Methods 129:115-127.

Cole KS, Curtis HJ (1939) Electrical impedance of the squid giant axon during activity. J. Gen Physiol 22:649-670.

Colley B, Tucker K, Fadool DA (2004) Comparison of modulation of Kv1.3 channel by two receptor tyrosine kinases in olfactory bulb neurons of rodents. Receptors Channels 10:25–36.

Connors (2002) Neuroscience: Single-neuron mnemonics. Nature 420:133-134.

Courtemanche M, Ramirez RJ, Nattel S (1998) Ionic mechanisms underlying human atrial action potential properties: insights from a mathematical model. Am J Physiol 275:301-21.

D'Angelo E, Nieus T, Maffei A, Armano S, Rossi P, Taglietti V, Fontana A, Naldi G (2001) Theta-frequency bursting and resonance in cerebellar granule cells: experimental evidence and modeling of a slow k+-dependent mechanism. J Neurosci 21:759-70.

de Carvalho A, Sweadner KJ, Penniston JT, Zaremba J, Liu L, Caton M, Linazasoro G, Borg M, Tijssen M, Bressman SB, Dobyns WB, Brashear A, Ozelius LJ (2004) Mutations in the Na+/K+-ATPase [alpha]3 Gene ATP1A3 Are Associated with Rapid-Onset Dystonia Parkinsonism. Neuron 43(2):169-175.

Delmas P, Brown DA (2002) Junctional Signaling Microdomains: Bridging the Gap between the Neuronal Cell Surface and Ca2+ Stores. Neuron 36(5):787-790.

De Schutter E (1992) A consumer guide to neuronal modeling software. Trends Neurosci 15:462-464.

De Schutter E, Bower JM (1994a) An active membrane model of the cerebellar Purkinje cell. I. Simulation of current clamps in slice. J Neurophysiol 71:375-400.

De Schutter E, Bower JM (1994b) An active membrane model of the cerebellar Purkinje cell. II. Simulation of synaptic responses. J Neurophysiol 71:401-419.

De Schutter E, Bower JM (1994c) Simulated responses of cerebellar Purkinje cells are independent of the dendritic location of granule cell synaptic inputs. Proc Natl Acad Sci USA 91:4736-4740.

De Schutter E (1998) Dendritic voltage and calcium-gated channels amplify the variability of postsynaptic responses in a Purkinje cell model. J Neurophysiol 80:504-519.

Destexhe A, Contreras D, Sejnowski TJ, Steriade M (1994) A model of spindle rhythmicity in the isolated thalamic reticular nucleus. J Neurophysiol 72:803-18.

Destexhe A, Mainen ZF, Sejnowski TJ (1995) Synaptic currents, neuromodulation and kinetic models. Chapter (pp 956 – 959) in: The Handbook of Brain Theory and Neural Networks (Arbib M, Ed). MIT Press, Cambridge, MA.

Destexhe A, Neubig M, Ulrich D, Huguenard J (1998) Dendritic low-threshold calcium currents in thalamic relay cells. J Neurosci 18:3574–3588.

Destexhe A, Huguenard JR (2000) Which formalism to use for modelling voltage-dependent conductances? Chapter (pp 129 – 157) in: Computational Neuroscience: Realistic Modelling For Experimentalists (DeSchutter E, Ed). CRC Press, Boca Raton, FL.

Despa S, Bers DM (2003) Na/K Pump Current and [Na]i in Rabbit Ventricular Myocytes: Local [Na]i Depletion and Na Buffering. Biophys J 84:4157–4166.

Devor A (2000) Is the cerebellum like cerebellar-like structures? Brain Res Rev 34:149-156.

Doyon J, Laforce R, Jr., Bouchard G, Gaudreau D, Roy J, Poirier M, Bedard PJ, Bedard F, Bouchard JP (1998) Role of the striatum, cerebellum and frontal lobes in the automatization of a repeated visuomotor sequence of movements. Neuropsychologia 36:625-641.

Dudman JT, Siegelbaum SA (2006) Making the Grade with Models of Persistent Activity. Neuron 49(5):649-651.

Durstewitz D, Seamans JK, Sejnowski TJ (2000) Neurocomputational models of working memory. Nat Neurosci 3:1184-91.

Durstewitz D, Seamans JK, Sejnowski TJ (2000) Dopamine-mediated stabilization of delay-period activity in a network model of prefrontal cortex. J Neurophysiol 83:1733--1750.

Eccles JC, Ito M, Szentagothai J (1967) The Cerebellum as a Neuronal Machine. Springer Verlag, Berlin.

Egorov AV, Hamam BN, Fransén E, Hasselmo ME, Alonso AA (2002) Graded persistent activity in entorhinal cortex neurons. Nature 420: 173-178.

Engel J, Schultens HA, Schild D (1999) Small conductance potassium channels cause an activity-dependent spike frequency adaptation and make the transfer function of neurons logarithmic. Biophys J 76:1310-1319.

Falcke M, Malchow D (2003) Understanding Calcium Dynamics: Experiments and Theory. Springer, Berlin.

Fall CP, Rinzel J (2006) An intracellular Ca2+ subsystem as a biologically plausible source of intrinsic conditional bistability in a network model of working memory. J Comput Neurosci 20(1):97-107.

Feng JF (2003) Computational Neuroscience: A Comprehensive Approach. Chapman and Hall/CRC Press, Boca Raton, FL.

Fierro L, DiPolo R, Llano I (1998) Intracellular calcium clearance in Purkinje cell somata from rat cerebellar slices. J Physiol 510:499-512.

Forrest MD (2008) The Biophysics of Purkinje Computation. Ph.D. Thesis. University of Warwick: U.K.

Fransen E, Tahvildari B, Egorov AV, Hasselmo ME and Alonso AA (2006) Mechanism of Graded Persistent Cellular Activity of Entorhinal Cortex Layer V Neurons. Neuron 49(5):735-746.

Frohlich F, Bazhenov M, Timofeev I, Steriade M, Sejnowski TJ (2006) Slow State Transitions of Sustained Neural Oscillations by Activity-Dependent Modulation of Intrinsic Excitability. J Neurosci 26(23):6153–6162.

Gadsby DC, Cranefield PF (1979) Electrogenic sodium extrusion in cardiac Purkinje fibers. J Gen Physiol 73:819-837.

Gaillard S, Dupont JL (1990) Ionic control of intracellular pH in rat cerebellar Purkinje cells maintained in culture. J Physiol (Lond) 425:71–83.

Genet S, Kado RT (1997) Hyperpolarizing current of the Na/K ATPase contributes to the membrane polarization of the Purkinje cell in rat cerebellum. Pflügers Arch – Eur J Physiol 434:559–567.

Getting PA (1989) Emerging principles governing the operation of neural networks. Annu Rev Neurosci 12:185– 204.

Gilbert PFC (1974) A theory of memory that explains the structure and function of the cerebellum. Brain Res 128:1-18.

Gilbert PFC (1975) How the cerebellum could memorise movements. Nature 254:688-689.

Gillies A, Willshaw D (2006) Membrane channel interactions underlying rat subthalamic projection neuron rhythmic and bursting activity. J Neurophysiol 95:2352-65.

Glickstein M (1997) Mossy-fibre sensory input to the cerebellum. Prog Brain Res 114:251-259.

Glitsch HG (2001) Electrophysiology of the sodium-potassium-ATPase in cardiac cells. Physiol Rev 81:1791–2826.

Gruol DL, Netzeband JG, Schneeloch J, Gullette CE (2006) L-type Ca2+ channels contribute to current-evoked spike firing and associated Ca2+ signals in cerebellar Purkinje neurons. Cerebellum 5:146.

Gustafsson B, Wigstom H (1983) Hyperpolarization following long-lasting tetanus activation of pyramidal hippocampal cells. Brain Res 275:159–163.

Gutfreund Y, Yarom Y, Segev I (1995) Subthreshold oscillations and resonant frequency in guinea-pig cortical neurons: physiology and modeling. J Physiol (Lond) 483:621– 640.

Hamlyn JM, Blaustein MP, Bova S, DuCharme DW, Harris DW, Mandel F, Mathews WR, Ludnes JH (1991) Identification and characterization of an ouabain-like compound from human plasma. Proc Natl Acad Sci USA 88(14):6259-63.

Hammarstrom AK, Gage PW (1999) Nitric oxide increases persistent sodium current in rat hippocampal neurons. J Physiol (Lond) 520:451–461.

Hausser M, Clark BA (1997) Tonic synaptic inhibition modulates neuronal output pattern and spatiotemporal synaptic integration. Neuron 19:665–678.

Hebb DO (1949) The Organization of Behaviour. Wiley, NY.

Heinemann U, Lux HD, Gutnick MJ (1977) Extracellular free calcium and potassium during paroxsmal activity in the cerebral cortex of the cat. Exp Brain Res 27:237–243.

Heinemann U, Lux HD (1977) “Ceiling” of stimulus induced rises in extracellular potassium concentration in cerebral cortex of cats. Brain Res 120:231–250.

Henkart M, Landis DMD, Reese TS (1976) Similarity of junctions between plasma membranes and endoplasmic reticulum in muscle and neurons. J Cell Biol 70:338–347.

Hernandez R-J (1992) Na+/K+-ATPase regulation by neurotransmitters. Neurochem Int 20:1–10.

Herz AV, Gollisch T, Machens CK, Jaeger D (2006) Modelling single-neuron dynamics and computations: a balance of detail and abstraction. Science 314(5796):80-5.

Herzog RI, Cummins TR, Waxman SG (2001) Persistent TTX-resistant Na+ current affects resting potential and response to depolarization in simulated spinal sensory neurons. J Neurophysiol 86:1351-64.

Hille B (2001) Ion Channels of Excitable Membranes. 3rd Ed. Sinauer Associates, Sunderland, MA.

Hines ML, Carnevale NT (1997) The NEURON simulation environment. Neural Comput 9:1179–1209.

Hines ML, Markram H, Schuermann F (2008) Fully Implicit Parallel Simulation of Single Neurons. J Comp Neurosci 25:439-448.

Hodgkin AL, Huxley AF (1952) A quantitative description of membrane current and its application to conduction and excitation in nerve. J Physiol (Lond) 117:500–544.

Holmes G (1939) The cerebellum of man. Brain 62:1-30.

Holmes W, Ambros-Ingerson J, Grover L (2006) Fitting experimental data to models that use morphological data from public databases. J Comput Neurosci 20(3):349-365.

Horn R (1996) Counting charges. J Gen Physiol 108:129-132.

Huang XY, Morielli AD, Peralta EG (1993) Tyrosine kinase-dependent suppression of a potassium channel by the G protein-coupled m1 muscarinic acetylcholine receptor. Cell 75:1145–1156.

Irvine LA, Jafri MS, Winslow RL (1999) Cardiac sodium channel Markov model with temperature dependence and recovery from inactivation. Biophys J 76:1868-1885.

Ito M, Sakurai M, Tongroach P (1982) Climbing fiber induced depression of both mossy fibre responsiveness and glutamate sensitivity of cerebellar Purkinje cells. J Physiol 324:133–134.

Ito M (1989) Long-term depression. Annu Rev Neurosci 12:85–102.

Ito M (1984) The Cerebellum and Neural Control. Raven Press, NY.

Ito M (1998) Book review of: The cerebellum: from structure to control. Trends Neurosci 21:419.

Ito M (2001) Cerebellar long-term depression: Characterization, signal transduction, and functional roles. Physiol Rev 81:1143–1195.

Jaeger D, De Schutter E and Bower JM (1997) The role of synaptic and voltage-gated currents in the control of Purkinje cell spiking: a modeling study. J Neurosci 17:91-106.

Jaeger D (2007) Pauses as Neural Code in the Cerebellum. Neuron 54(1):9-10.

Jansen JKS, Nicholls JG (1973) Conductance changes, an electrogenic pump and the hyperpolarization of leech neurones following impulses. J. Physiol. (Lond.) 229:635-655.

Jansonius NM (1990) Properties of the sodium pump in the blowfly photoreceptor cell. J Comp Physiol 167:461–467.

Jiang YX, Ruta V, Chen JY, Lee A, MacKinnon R (2003) The principle of gating charge movement in a voltage-dependent K^+ channel. Nature 423:42-48.

Johnston D, Wu S (1995) Foundations of cellular neurophysiology. MIT Press, Cambridge, MA.

Kager H, Wadman WJ, Somjen GG (2007) Seizure-like afterdischarges simulated in a model neuron. J Comput Neurosci 22:105–128.

Kandel ER, Schwartz JH, Jessell TM (2000) Principles of Neural Science. 4th Ed. McGraw-Hill, NY.

Kelvin, Lord (1855) On the theory of the electric telegraph. Proc. Roy. Soc. (London) 7:382.

Keynes RD, Elinder F (1999) The screw helical voltage gating of ion channels. Proc R Soc Lond B Biol Sci 266(1421):843-52.

Khaliq ZM, Gouwens NW, Raman IM (2003) The contribution of resurgent sodium current to high-frequency firing in Purkinje neurons: an experimental and modeling study. J Neurosci 23:4899–4912.

Khavandgar S, Walter JT, Sageser K, Khodakhah K (2005) Kv1 channels selectively prevent dendritic hyperexcitability in Purkinje cells. J Physiol (Lond) 569:545–557

Kiernan MC, Lin CS-Y & Burke D (2004). Differences in activity-dependent hyperpolarization in human sensory and motor axons. J Physiol 558, 341–349.

Koch C (1999) Biophysics of Computation: Information Processing in Single Neurons. Oxford University Press.

Koch C, Segev I (1998) Methods in Neuronal Modeling: From Ions to Networks. 2nd Ed. MIT press, Cambridge, MA.

Komendantov AO, Komendantova OG, Johnson SW, Canavier CC (2004) A modeling study suggests complementary roles for GABAA and NMDA receptors and the SK channel in regulating the firing pattern in midbrain dopamine neurons. J Neurophysiol 91:346-57.

Kofuji P, Newman EA (2004) Potassium buffering in the central nervous system. Neurosci 129:1045–1056.

Kuffler SW, Nicholls JG, Orkand RK (1966) Physiological properties of glial cells in the central nervous system of amphibia. J Neurophysiol 29:768 –787.

Lang EJ, Sugihara I, Welsh JP, Llinas R (1999) Patterns of spontaneous Purkinje cell complex spike activity in the awake rat. J Neurosci 19:2728–2739.

Laughlin SB, de Ruyter van Steveninck, RR, Anderson JC (1998) The metabolic cost of neural information. Nat Neurosci 1:36-41.

Lederer WJ, Niggli E, Hadley RW (1990) Sodium calcium exchange in excitable cells: fuzzy space. Science 248:283.

Lester HA, Cao Y, Mager S (1996) Listening to neurotransmitter transporters. Neuron 17:807–810.

Lindblad DS, Murphey CR, Clark JW, Giles WR (1996) A model of the action potential and underlying membrane currents in a rabbit atrial cell. Am J Physiol Heart Circ Physiol 271:1666-1696.

Lisman JE, Fellous JM, Wang XJ (1998) A role for NMDA-receptor channels in working memory. Nat Neurosci 1:273–275.

Llinas RR, Sugimori M (1980a) Electrophysiological properties of in vitro Purkinje cell somata in mammalian cerebellar slices. J Physiol 305:171-195.

Llinas R, Sugimori M (1980b) Electrophysiological properties of in vitro Purkinje cell dendrites in mammalian cerebellar slices. J Physiol 305:197-213.

Loewenstein Y, Sompolinsky H (2003) Temporal integration by calcium dynamics in a model neuron. Nat Neurosci 6:961–967.

Loewenstein Y, Mahon S, Chadderton P, Kitamura K, Sompolinsky H, Yarom Y, Hausser M (2005) Bistability of cerebellar Purkinje cells modulated by sensory stimulation. Nat Neurosci 8(2):202-211.

Loewenstein Y, Mahon S, Chadderton P, Kitamura K, Sompolinsky H, Yarom Y, Hausser M (2006) Purkinje cells in awake behaving animals operate at the upstate membrane potential - Reply, Nat Neurosci 9(2):461.

London M, Häusser M (2005). Dendritic computation. Ann Rev Neurosci 28:503-32.

Luo C, Rudy Y (1994) A dynamic model of the cardiac ventricular action potential. Circ Res 74:1071-1096.

Luthi A, Bal T, McCormickDA (1998) Periodicity of thalamic spindle waves

is abolished by ZD7288, a blocker of *I*h. J Neurophysiol 79:3284–3289.

Major G, Larkman AU, Jonas P, Sakmann B, Jack JJB (1994) Detailed passive cable models of whole-cell recorded CA3 pyramidal neurons in rat hippocampal slices. J Neurosci 14:4613–4638.

Marder E, Abbott LF, Turrigiano GG, Liu Z, Golowasch J (1996) Memory from the dynamics of intrinsic membrane currents. Proc Natl Acad Sci USA 93:13481–13486.

Marr D (1969) A theory of cerebellar cortex. J Physiol (Lond) 202:437– 470.

Mannuzzu LM, Moronne MM, Isacoff EY (1996) Direct physical measure of conformational rearrangement underlying potassium channel gating. Science 271:213-216.

McKay BE, Turner RW (2004) Kv3 K channels enable burst output in rat cerebellar Purkinje cells. Eur J Neurosci 20:729 –739.

McKay BE, Turner RW (2005) Physiological and morphological development of the rat cerebellar Purkinje cell. J Physiol 567: 829-850.

McKay BE, Molineux ML, Mehaffey WH, Turner RW (2005) Kv1 K+ channels control Purkinje cell output to facilitate postsynaptic rebound discharge in deep cerebellar neurons. J Neurosci 25:1481–1492.

McKay BE, Engbers JDT, Mehaffey WH, Gordon G, Molineux ML, Bains J, Turner RW (2007) Climbing fiber discharge regulates cerebellar functions by controlling the intrinsic characteristics of Purkinje cell output. J Neurophysiol 97:2590-2604.

McKee M, Scavone C, Nathanson JA (1994) Nitric oxide, cGMP and hormone regulation of active sodium transport. Proc Natl Acad Sci USA 91:12056–12060.

McGrail KM, Phillips JM, Sweadner KJ (1991) Immunofluorescent localization of three Na,K-ATPase isozymes in the rat central nervous system: both neurons and glia can express more than one Na,K-ATPase. J Neurosci 11:381–391.

Mel BW (2006) Why have dendrites? A computational perspective. Chapter (pp 421 – 441) in: Dendrites (Stuart, G; Spruston N; Hausser, M; Eds.). Oxford University Press.

Meunier C, Segev I (2002) Playing the devil's advocate: is the Hodgkin-Huxley model useful? Trends Neurosci 25(11):558-63.

Miyasho T, Takagi H, Suzuki H, Watanabe S, Inoue M, Kudo Y, Miyakawa H (2001) Low-threshold potassium channels and a low-threshold calcium channel regulate Ca2+ spike firing in the dendrites of cerebellar Purkinje neurons: a modeling study. Brain Res 891:106-15.

Moczydlowski E, Latorre R (1983) Gating kinetics of Ca2+-activated K+ channels from rat muscle incorporated into planar lipid bilayers. Evidence for two voltage-dependent Ca2+ binding reactions. J Gen Physiol 82:511-4.

Moody WJ, Futamachi KJ, Prince DA (1974) Extracellular potassium activity during epileptogenesis. Exp Neurol 42:248 –263.

Nakao M, Gadsby DC (1989) [Na] and [K] dependence of the Na/K pump current-voltage relationship in guinea-pig ventricular myocytes. J Gen Physiol 94:539-565.

Nam SC, Hockberger PE (1997) Analysis of spontaneous electrical activity in cerebellar Purkinje cells acutely isolated from postnatal rats. J Neurobiol 33:18–32.

Nathanson JA, Scavone C, Scanlon C, McKee M (1995) The cellular Na+ pump as a site of action for carbon monoxide and glutamate: a mechanism for long-term modulation of cellular activity. Neuron 14:791–794.

Nauta JHW, Feirtag M (1986) Fundamental Neuroanatomy. Freeman, NY.

Nelson R, Bender AM, Connaughton VP (2003) Stimulation of sodium pump restores membrane potential to neurons excited by glutamate in zebrafish distal retina. J Physiol (Lond) 549:787-800.

Oka Y (1996) Characterization of TTX-resistant persistent Na+ current underlying pacemaker potentials of fish gonadotrophin-releasing hormone neurons (GnRH). J Neurophysiol 75:2397–2404.

Orkand RK, Nicholls JG, Kuffler SW (1966) Effect of nerve impulses on the membrane potential of glial cells in the central nervous system of amphibia. J Neurophysiol 29:788–806.

Palay SL, Chan-Palay V (1982) The Cerebellum: New Vistas. Springer Verlag, Berlin.

Pape HC (1996) Queer current and pacemaker: the hyperpolarization activated cation current in neurons. Annu Rev Physiol 58:299–327.

Pape H-C, Driesang RB (1998) Ionic mechanisms of intrinsic oscillations in neurons of the basolateral amygdaloid complex. J Neurophysiol 79:217–226.

Patlak J (1991) Molecular kinetics of voltage dependent Na^+ channels. Physiol Rev 71:1047-1076.

Philipson KD (1985) Sodium-Calcium Exchange in Plasma Membrane Vesicles. Ann Rev Physiol 47:561-571.

Rall W (1959) Branching dendritic trees and motoneuron membrane resistivity. Exp Neurol 1:491–527.

Rall W (1962) Electrophysiology of a dendritic neuron model. Biophys J 2:145–167.

Rall W (1967) Distinguishing theoretical synaptic potentials computed for different some-dendritic distributions of synaptic inputs. J Neurophysiol 30:1138-1168.

Rall W (1989) Cable theory for dendritic neurons. Chapter (pp 9-92) in: Methods in Neuronal Modelling: From Synapses to Networks. (Koch C, Segev I, Eds). MIT Press, Cambridge, MA.

Rapp M, Yarom Y, Segev I (1992) The impact of parallel fiber background activity on the cable properties of cerebellar Purkinje cells. Neural Comput 4:18-533.

Rapp M, Segav I, Yarom Y (1994) Physiology, morphology and detailed passive models of guinea-pig cerebellar Purkinje cells. J Physiol 474:101–108.

Rogers LJ, Oettinger R, Szer J, Mark RF (1977) Separate chemical inhibitors of long-term and short-term memory: contrasting effects of cycloheximide, ouabain and ethacrynic acid on various learning tasks in chickens. Proc R Soc Lond B Biol Sci 196:171–195.

Rothman JS, Manis PB (2003) The roles potassium currents play in regulating the electrical activity of ventral cochlear nucleus neurons. J Neurophysiol 89:3097-113.

Rutecki PA, Lebeda FJ, Johnston D (1985) Epileptiform activity induced by changes in extracellular potassium in hippocampus. J Neurophysiol 54:1363–1374.

Sakmann B, Neher E (1995) Single-Channel Recording. Plenum Press, NY.

Sanguinetti MC, Curran ME, Zou A, Shen J, Spector PS, Atkinson DL, Keating MT (1996) Coassembly of KvLQT1 and minK (IsK) proteins to form cardiac I_{Ks} potassium channel. Nature 384:80-83.

Santamaria F, Jaeger D, De Schutter E, Bower JM (2002) Modulatory effects of parallel fiber and molecular layer interneuron synaptic activity on Purkinje cell responses to ascending segment input: a modeling study. J Comput Neurosci 13:217-235.

Saraga F, Wu CP, Zhang L, Skinner FK (2003) Active Dendrites and Spike Propagation in Multi-compartment Models of Oriens-Lacunosum/Moleculare Hippocampal Interneurons. J Physiol 552:502-504.

Sausbier M, Hu H, Arntz C, Feil S, Kamm S, Adelsberger H, Sausbier U, Sailer CA, Feil R, Hofmann F, Korth M, Shipston MJ, Knaus HG, Wolfer DP, Pedroarena CM, Storm JF, Ruth P (2004) Cerebellar ataxia and Purkinje cell dysfunction caused by Ca^{2+}-activated K^{+} channel deficiency. Proc Natl Acad Sci USA 101:9474–9478.

Schmahmann JD, Sherman JC (1998) The cerebellar cognitive affective syndrome. Brain 121:561-579.

Schonewille M, Khosrovani S, Winkelman BHJ , Hoebeek FE, De Jeu MTG, Larsen IM, Van Der Burg J, Schmolesky MT, Frens MA, De Zeeuw CI (2006) Purkinje cells in awake behaving animals operate at the upstate membrane potential. Nat Neurosci 9 (4):459-61.

Segev I, Rinzel J, Shepherd G (1995) The Theoretical Foundation of Dendritic Function. MIT Press, Cambridge, MA.

Semb SO, Sejersted OM (1996) Fuzzy space and control of Na+, K+-pump rate in heart and skeletal muscle. Acta Physiologica Scandinavica 156(3):213–225.

Scuri R, Lombardo P, Cataldo E, Ristori C, Brunelli M (2007) Inhibition of Na+/K+ ATPase potentiates synaptic transmission in tactile sensory neurons of the leech. Eur J Neurosci 25(1):159-67.

Segal MM, Douglas AF (1997) Late sodium channel openings underlying epileptiform activity are preferentially diminished by the anticonvulsant phenytoin. J Neurophysiol 77:3021-3304.

Sejnowski TJ, Koch C, Churchland PS (1988) Computational neuroscience. Science 241(4871):1299-1306.

Seutin V, Shen KZ, North RA, Johnson SW (1996) Sulfonylurea-sensitive potassium current evoked by sodium-loading in rat midbrain dopamine neurons. Neuroscience 71(3):709–719.

Shelton DP (1985) Membrane resistivity estimates for the Purkinje neuron by means of a passive computer model. Neuroscience 14:111–131.

Shen W, Hernandez-Lopez S, Tkatch T, Held JE, Surmeier DJ (2004) Kv1.2-containing K+ channels regulate subthreshold excitability of striatal medium spiny neurons. J Neurophysiol 91:1337–1349.

Shen WX, Hernandez-Lopez S, Tkatch T, Held JE, Surmeier DJ (2004) Kv1.2-containing K+ channels regulate subthreshold excitability of striatal medium spiny neurons. J Neurophysiol 91:1337-1349.

Silverman BDZ, Warley A, Miller JIA, James AF, Shattock MJ (2003) Is there a transient rise in sub-sarcolemmal Na and activation of Na/K pump current following activation of INa in ventricular myocardium? Cardiovascular Research 57(4):1025-1034.

Sneyd J (2007), Scholarpedia, 2(3):1576.

Solinas SMG, Maex R, De Schutter E (2006) Dendritic Amplification of Inhibitory Postsynaptic Potentials in a Model Purkinje Cell. Eur J Neurosci 23:1207-1218.

Sonders MS, Amara SG (1996) Channels in transporters. Curr Opin Neurobiol 6:294–302.

Staub C, De Schutter E and Knöpfel T (1994) Voltage-imaging and simulation of effects of voltage and agonist activated conductances on soma-dendritic voltage coupling in cerebellar Purkinje cells. J Comput Neurosci 1:301-311.

Steuber V, De Schutter E (2002) Rank order decoding of temporal parallel fibre input patterns in a complex Purkinje cell model. Neurocomputing 44:183-188.

Steuber V, Mittmann W, Freek E, Hoebeek R, Silver A, De Zeeuw CI, Hausser M, De Schutter E (2007) Cerebellar LTD and Pattern Recognition by Purkinje Cells. Neuron 54(1): 121-136.

Stuart G, Hausser M (1994) Initiation and spread of sodium action potentials in cerebellar Purkinje cells. Neuron 13:703–712.

Su H, Alroy G, Kirson ED, Yaari Y (2001) Extracellular calcium modulates persistent sodium current-dependent burst-firing in hippocampal pyramidal neurons. J Neurosci 21:4173–4182.

Su Z, Zou A, Nonaka A, Zubair I, Sanguinetti MC, Barry WH (1998) Influence of prior Na+ pump activity on pump and Na+/Ca2+ exchange currents in mouse ventricular myocytes. Am J Physiol Heart Circ Physiol 275:1808-1817.

Swensen AM, Bean BP (2003) Ionic mechanisms of burst firing in dissociated Purkinje neurons. J Neurosci 23:9650-9663.

Swensen AM and Bean BP (2005) Robustness of Burst Firing in Dissociated Purkinje Neurons with Acute or Long-Term Reductions in Sodium Conductance. J Neurosci 25:3509–3520.

Teramae JN, Fukai T (2005) A cellular mechanism for graded persistent activity in a model neuron and its implications in working memory. J Comput Neurosci 18:105-121.

Thach WT (1996) On the specific role of the cerebellum in motor learning and cognition: Clues from PET activation and lesion studies in man. Behavioral and Brain Sciences 19:411-431.

Therien AG, Blostein R (2000) Mechanisms of sodium pump regulation. Am J Physiol Cell Physiol 279:541-566.

Thompson SM, Prince DA (1986) Activation of electrogenic sodium pump in hippocampal CA1 neurons following glutamate-induced depolarization. J Neurophysiol 56:507–522.

Timofeev I, Grenier F, Bazhenov M, Sejnowski TJ, Steriade M (2000) Origin of slow cortical oscillations in deafferented cortical slabs. Cereb Cortex 10:1185–1199.

Tokimasa T, Shirasaki T, Yoshida M, Ito M, Tanaka E, Mitsumoto T, Akasu T, Tanaka M, Higashi M, Nakano T (1996) Calcium-dependent potentiation of M-current in bullfrog sympathetic neurons. Neurosci Lett 214:79-82.

Traub RD, Buhl EH, Gloveli T, Whittington MA (2003) Fast Rhythmic Bursting Can Be Induced in Layer 2/3 Cortical Neurons by Enhancing Persistent Na(+) Conductance or by Blocking BK Channels. J Neurophysiol 89:909-21.

Traynelis SF, Dingledine R (1988) Potassium-induced spontaneous electrographic seizures in the rat hippocampal slice. J Neurophysiol 59:259 –276.

Vandenberg CA, Bezanilla F (1991) A sodium channel gating model based on single channel, macroscopic ionic, and gating currents in squid giant axon. Biophys J 60:1511-1533.

Verdonck F, Mubagwa K, Sipido KR (2004) [Na+] in the subsarcolemmal `fuzzy' space and modulation of [Ca2+]i and contraction in cardiac myocytes, Cell Calcium 35(6):603-612.

Vetter P, Roth A, Hausser M (2001) Propagation of action potentials in dendrites depends on dendritic morphology. J Neurophysiol 85(2): 926-37.

Wang YC, Huang RC (2006) Effects of Sodium Pump Activity on Spontaneous Firing in Neurons of the Rat Suprachiasmatic Nucleus. J Neurophysiol 96:109-118.

Wang SSH, Major G (2003) Integrating over time with dendritic wave-fronts. Nat Neurosci 6:906 – 908.

Walker MS, Bower JM, Parsons LM (2000) A brief history of cerebellar theories. Soc. Neurosci. Abstr. 26:30.

Wall MJ, Usowicz MM (1997) Development of action potential-dependent and independent spontaneous GABAA receptor-mediated currents in granule cells of postnatal rat cerebellum. Eur J Neurosci 9:533-48.

Wendt-Gallitelli F, Voigt T, Isenberg G (1993) Microheterogeneity of subsarcolemmal sodium gradients. Electron probe microanalysis in guinea-pig ventricular mycytes. J Physiol (Lond.) 472:33–44.

Wilson MA, Bhalla US, Uhley JD, Bower JM (1989) GENESIS: A system for simulating neural networks. Chapter (pp 485 – 492) in: Advances in Neural Information Processing Systems (Touretzky D, Ed.). Morgan Kaufmann, San Mateo, CA.

Winklhofer M, Matthias K, Seifert G, Stocker M, Sewing S, Herget T, Steinhauser C, Sealer-Reinhardt S (2003) Analysis of phosphorylationdependent modulation of Kv1.1 potassium channels. Neuropharmacology 44:829–842.

Wit AL, Cranefield PF, Gadsby DC (1981) Electrogenic sodium extrusion can stop triggered activity in the canine coronary sinus. Circ Res 49:1029-1042.

Womack M, Khodakhah K (2002) Active contribution of dendrites to the tonic and trimodal patterns of activity in cerebellar Purkinje neurons. J Neurosci 22:10603-10612.

Womack MD, Chevez C, Khodakhah K (2004a) Calcium-activated potassium channels are selectively coupled to P/Q-type calcium channels in cerebellar Purkinje neurons. J Neurosci 24(40):8818-22.

Womack MD, Khodakhah K (2004b) Dendritic control of spontaneous bursting in cerebellar Purkinje cells. J Neurosci 24:3511-3521.

Womack MD, Khodakhah K (2003) Somatic and dendritic small conductance calcium-activated potassium channels regulate the output of cerebellar Purkinje neurons. J Neurosci 23:2600–2607.

Zador M (2000) The basic unit of computation. Nat Neurosci 3:1167.

Zahler R, Brines M, Kashgarian M, Benz EJ Jr, Gilmore-Hebert M (1992) The cardiac conduction system in the rat expresses the 2 and 3 isoforms of the Na,K-ATPase. Proc Natl Acad Sci USA 89:99-103.

Zerangue N, Kavanaugh MP (1996) Flux coupling in a neuronal glutamate transporter. Nature 383:634–637.

Zhan H, Tada T, Nakazato F, Tanaka Y, Hongo K (2004) Spatial learning transiently disturbed by intraventricular administration of ouabain. Neurol Res 26:35-40.

ADDENDUM

Some of the research presented in this book, and related research, has been published in international peer-reviewed journals:

1) Forrest MD, Wall MJ, Press DA, Feng J (2012) The Sodium-Potassium Pump Controls the Intrinsic Firing of the Cerebellar Purkinje Neuron. *PLoS ONE* 7(12): e51169. http://dx.doi.org/10.1371%2Fjournal.pone.0051169
2) Forrest MD (2014) Intracellular Calcium Dynamics Permit a Purkinje Neuron Model to Perform Toggle and Gain Computations Upon its Inputs. *Frontiers in Computational Neuroscience* 8:86. http://journal.frontiersin.org/Journal/10.3389/fncom.2014.00086/full
3) Forrest MD (2013) Mathematical Model of Bursting in Dissociated Purkinje Neurons. *PLoS ONE* 8(8): e68765. http://dx.doi.org/10.1371/journal.pone.0068765

These publications are freely available on the internet. Indeed - arguably - the research is much better presented in these journal publications than in this book. The book gives more context but the papers are tight with clarity. In addition, the research of this book was presented at a conference in 2009 - the abstract of which is in its conference proceedings:

4) Forrest MD, Wall MJ, Press DA (2009) The Sodium-Potassium Pump Controls the Intrinsic Firing of the Cerebellar Purkinje Neuron. Poster session presented at: 16th International Conference on Neural Information Processing (ICONIP 09); Bangkok, Thailand

Readers may also be interested to read a journal paper derivative of Dr. Forrest's Master degree thesis:

5) Forrest MD (2014) Can the Thermodynamic Hodgkin-Huxley Model of Voltage-Dependent Conductance Extrapolate for Temperature? *Computation* 2(2):47-60. http://www.mdpi.com/2079-3197/2/2/47

N.B. The cover picture of this book/thesis is largely a composite of pictures found in its body. Where a picture has been sourced from an outside party, the relevant permission is stated at its point of use in the main body. The Purkinje morphology component of the cover image is sourced from: Coop AD, Cornelis H, Santamaria F (2010) Dendritic excitability modulates dendritic information processing in a Purkinje cell model. Front Comput Neurosci 4:6. doi: 10.3389/fncom.2010.00006

Proof

Printed By Createspace

createspace™
an Amazon.com company

Digital Proofer